

©[2012]

Jean-Pierre Dollé

ALL RIGHTS RESERVED

DEVELOPMENT OF AN ORGANOTYPIC MODEL FOR CHARACTERIZING
AXONAL RESPONSES TO IN VITRO UNIAXIAL STRAIN INJURIES

by

JEAN-PIERRE DOLLÉ

A Dissertation submitted to the

Graduate School-New Brunswick

Rutgers, The State University of New Jersey

And

The Graduate School of Biomedical Sciences

University of Medicine and Dentistry of New Jersey

In partial fulfillment of the requirements

For the degree of

Doctor of Philosophy

Graduate Program in Biomedical Engineering

Written under the direction of

Dr. Martin L. Yarmush

And approved by

New Brunswick, New Jersey

May, 2012

ABSTRACT OF THE DISSERTATION

Development of an Organotypic Model for Characterizing Axonal Responses to *In Vitro*

Strain Injuries

By JEAN-PIERRE DOLLÉ

Dissertation Director:
Dr. Martin L. Yarmush, M.D., Ph.D.

Traumatic brain injuries are the leading cause of disability each year in the US. The most common and devastating consequence is the stretching of axons caused by shear deformation that occurs during rotational acceleration of the brain during injury. These injuries often lead to unconsciousness and long-term impairment and unfortunately the effects on axonal molecular and functional events are not fully characterized. We have developed a strain injury model that maintains the three dimensional cell architecture and neuronal networks found *in vivo* with the ability to visualize individual axons and their response to a mechanical injury. The advantage of this model is that it can apply uniaxial strain injuries to axons that make functional connections between two organotypic slices and injury responses can be observed in real-time and over long term. This is accomplished using microfabrication techniques to produce micron-sized channels that direct axon growth originating from the periphery of organotypic hippocampal slices. This guidance of axonal growth allows for two organotypic slices to connect to each other. The dimension of these channels can be manipulated to control the number of entering axons allowing for observation of injury effects on both individual axons and axon bundles in real-time and long term following injury. These injury effects are assessed through the use of morphology, molecular, biochemical, and cellular techniques.

This uniaxial strain injury model was designed to be capable of applying an array of mechanical strains at various rates of strain, thus replicating a range of modes of axonal injury. These applied uniaxial strains are reproducible and verified through finite element analysis. Long term culture, preservation of slice and cell orientation, and slice-slice connection on the device was demonstrated. The fidelity of the model was verified by observing characteristic responses to various strain injuries which included axonal beading, delayed elastic effects, microtubule degeneration, axonal transport, axonal degeneration and mitochondrial membrane potential. The axonal beading and delayed elastic effect responses to a strain injury are dependent on both the applied strain and the bundle diameter. As the diameter increases the number of beads that form decreases and the delayed elastic effect increases. Axonal bundle unraveling and primary axotomy at lower applied strains than previously reported are observed. The induced strain injury leads to a breakdown in axonal cytoskeleton resulting in a failure in axonal transport of essential proteins as seen by accumulations of amyloid precursor protein along the length of the axon. Both of these responses result in axonal degradation and are proportional to the degree of applied strain and time following injury. We observe an applied strain injury threshold with respect to mitochondrial membrane potential response, below which there is a delayed hyperpolarization and above which immediate depolarization. Using EIPA, a sodium / hydrogen exchanger inhibitor, we were able to attenuate both mitochondrial membrane hyperpolarization and depolarization, resulting in a decrease in axonal degeneration following injury. This model could prove to be a powerful tool in assessing strain injury effects on functional axon-axon connections by further characterizing axonal responses to controlled uniaxial strain injuries and the testing of additional potential traumatic brain injury therapeutics.

ACKNOWLEDGEMENTS

I would like to thank my mentors Martin Yarmush and Rene Schloss, and my committee members Barclay Morrison III, Dave Shreiber and Bonnie Firestein for their continued support and guidance throughout my time at Rutgers. Their knowledge and expertise allowed me to successfully develop the traumatic brain injury model that is described in this thesis. I would also like to thank Eugene Berdichevsky and Bhaskar Mitra for their technical support over the years.

I am grateful to the members of the Yarmush lab both past and present for their day to day support and for making life in the lab a fun place to do science.

Finally I would like to thank my wife Christine for her support, love and patience during these years, and my family back in South Africa for their continued support and encouragement.

TABLE OF CONTENTS

Abstract	ii
Acknowledgements	iv
Table of Contents	v
List of Tables	viii
List of Illustrations	ix
Chapter 1.....	1
1.1 Introduction	1
Chapter 2: Characterization Of An Organotypic Uniaxial Strain Injury Model.	6
2.1 Abstract.....	6
2.2 Introduction	7
2.3 Materials and Methods	9
2.3.1 Organotypic Slice Isolation	9
2.3.2 Making / assembling device.....	10
2.3.3 Testing OPDMS material properties	12
2.3.4 FEA – Abaqus.....	13
2.3.5 Applying Strain.....	13
2.3.6 Slice viability.....	14
2.3.7 Dil Staining.....	14
2.3.8 Immunohistochemical staining.....	15
2.4 Results	17
2.4.1 Device – PDMS material properties.....	17
2.4.2 Abaqus results	18
2.4.3 Dynamic pressure effects	21
2.4.4 Monitoring hippocampus slice health on the device over time	23
2.4.5 Characterization of axon extension	24
2.4.6 Microchannel dimensions	27

2.4.7 Application of strain injury	28
2.4.8 Cytoskeletal effects following strain injury	30
2.5 Discussion.....	32
2.6 References:.....	42
Chapter 3 Characterizing and Quantifying Axonal Responses to In Vitro Uniaxial Strain Injuries	47
3.1 Introduction	47
3.2 Materials and Methods	50
3.2.1 Organotypic hippocampus slice isolation.....	50
3.2.2 Strain device	50
3.2.3 Axonal beading analysis	52
3.2.4 Delayed elasticity analysis	52
3.2.5 Axonal degradation analysis	52
3.2.6 Monitoring changes in mitochondrial membrane potential	53
3.2.7 EIPA and CsA treated conditions.....	54
3.2.8 Immunohistochemical staining.....	55
3.2.9 Data Analysis	56
3.3 Results	57
3.3.1 Axonal beading	57
3.3.2 Delayed Elasticity.....	60
3.3.3 Cytoskeletal effects following strain injury	63
3.3.4 Axonal transport effects following strain injury.....	65
3.3.5 Degradation.....	67
3.3.6 Changes in mitochondrial membrane potential	68
3.3.7 Mitochondrial numbers.....	71
3.3.8 Addition of EIPA and CsA	72
3.4 Discussion.....	80
3.5 References:.....	96
Chapter 4	107

4.1 Conclusions	107
4.2 Future Studies.....	108

LIST OF TABLES

Table 1 Strain rates that correspond to chosen peak deflection times	22
Table 2. Increase in the number of mitochondria by 24hrs after 25% applied strain as compared to before injury.	71
Table 3. Summary of axonal response to 10%, 25% and 45% applied strain injuries.	79

LIST OF ILLUSTRATIONS

Figure 2.1 Organotypic uniaxial axonal strain injury device.	12
Figure 2.2 Tensile test results - Stress vs. Strain curve for PDMS	18
Figure 2.3 Abaqus displacement and strain predictions	19
Figure 2.4 PDMS deflection profiles	21
Figure 2.5 Dynamic pressure effects within the system	22
Figure 2.6 Hippocampus slices on the strain device stained with Propidium Iodide over time.....	23
Figure 2.7 MAP-2 staining of organotypic slices on the strain device	24
Figure 2.8 Axons in microchannels stained for Tau	25
Figure 2.9 Hippocampus slice-to-slice connection verification	26
Figure 2.10 PDMS microchannel dimensions control the number of entering axons.....	27
Figure 2.11 Time progression of delayed elastic effect on axon bundle after application of 42% strain, 20s-1	29
Figure 2.12 Examples of axonal bundle unraveling and primary axotomy	30
Figure 2.13 Applied strain distribution across pressure cavity and axons stained for β -tubulin 4hours after 42% strain injury	31
Figure 3.1 Axonal beading after uniaxial strain injury.	58
Figure 3.2 Diameter dependence of axonal beading after uniaxial strain injury	59
Figure 3.3 Delayed Elastic effects on axons that are strain injured	61
Figure 3.4 Diameter dependence for delayed elastic effects after strain injury	63
Figure 3.5 Axons stained for β -tubulin.....	65
Figure 3.6 Axons stained for Amyloid- β Precursor Protein	66
Figure 3.7 Axonal degradation assessed at 24hrs following strain injury with respect to applied strain	67
Figure 3.8 Monitoring mitochondrial membrane potential changes over a 24hr period through the use of the JC-1 dye	70

Figure 3.9 Monitoring mitochondrial membrane potential changes over a 24hr period after applying the NHE-1 inhibitor EIPA and a uniaxial strain injury	74
Figure 3.10 Monitoring mitochondrial membrane potential changes over a 24hr period after applying the mPTP inhibitor Cyclosporin A and a uniaxial strain injury.....	77
Figure 3.11 Axonal degradation assessed at 24hrs post injury after treatment with EIPA and cyclosporine A.....	78
Figure 4.1 Schematic of a device incorporating multiple electrode arrays.....	110
Figure 4.2 Schematic of a potential device that allows for the incorporation of oligodendrocytes	111

Chapter 1

1.1 Introduction

The incidence of traumatic brain injury (TBI) makes it the leading cause of death and disability in the United States (Coronado, Xu et al. 2011). Inertial forces that occur during acceleration / deceleration of the brain can lead to the generation of shearing or straining forces being exerted on axons (Smith, Meaney et al. 2003). These injuries are sustained primarily due to the viscoelastic nature of brain tissue, where during normal brain accelerations the tissue behaves elastically whereas at high accelerations it resists being strained in a viscous manner. The dynamic nature of these injuries is when forces are applied in less than 50 milliseconds (Gennarelli and Meaney 1996). Axons that traverse large distances in the brain are particularly susceptible to this type of injury and can have devastating results. The resultant axonal damage is commonly referred to as diffuse axonal injury (DAI) and is the most common type of pathology in TBI occurring in approximately 40-50% of reported cases (Meythaler, Peduzzi et al. 2001; Iwata, Stys et al. 2004).

One result of the primary mechanical injury is the breakdown in axonal cytoskeleton, in particular microtubules (Tang-Schomer, Patel et al. 2010). Since the majority of axonal transport occurs along microtubules, this results in the interruption of the transport of vital proteins and organelles to distal sections of the axon. This interruption results in an accumulation of transport products that produces a swelling of the axon commonly referred to as an axonal bead. Axonal beads and the accumulation of fast axonally transported proteins such as amyloid precursor protein (APP) within these beads are hallmarks of DAI (Povlishock and Christman 1995; Smith, Chen et al. 1999). Another response of axons to the initial primary strain injury is the prolonged time it takes for certain axons to return to their original length after injury (Smith, Wolf et al. 1999). This delayed response is termed “delayed elastic effect” and can be clearly observed in *in vitro* models of DAI where the dynamic nature of the response is observed in real-time.

Following the initial primary trauma, the release of glutamate from neurons and glia and the activation of mechanosensitive channels result in the influx of ions into the cell (Wolf, Stys et al. 2001; Morrison, Elkin et al. 2011). A large proportion of the secondary effects is an influx in calcium that if large enough, initiate signaling cascades eventually resulting in cell death (Weber 2004). High calcium levels can among others, lead to the generation of reactive oxygen species (ROS), activate calpain (calcium dependant proteases with papain-like activity), and lead to mitochondrial dysfunction. Mitochondrial dysfunction is widely observed in DAI and TBI resulting in neurodegeneration (Mazzeo, Beat et al. 2009). The mitochondrial membrane potential (MMP) that exists across the mitochondrial inner-membrane controls ATP synthesis, mitochondrial calcium buffering and the generation of ROS, all fundamental processes during normal mitochondrial function (Nicholls and Budd 2000). Disrupting any one of these functions can lead to cell death. Low ATP levels can initiate necrosis, excessive mitochondrial calcium can among others lead to disruption in MMP generation and activate the mitochondrial permeability transition pore (mPTP) and excessive ROS generation leads to damage of lipids, proteins, DNA and membranes. Opening of the mPTP results in mitochondrial swelling and outer membrane rupture that releases pro-apoptotic molecules that can lead to cell death (Mazzeo, Beat et al. 2009). Disruptions in the MMP could result in either a decrease (depolarization – reduction in ATP) or increase (hyperpolarization – generation of ROS) in potential both of which can lead to detrimental effects on the cell (Sullivan, Thompson et al. 1999; Poppe, Reimertz et al. 2001). Thus monitoring MMP is a key indicator of mitochondrial function and can be used to assess potential mechanisms that play a role in axonal degradation (Perry, Norman et al. 2011).

There is currently no “standard treatment” protocol for patients suffering from TBI and with almost one third of all injury related deaths in the US being attributed to a TBI related incident, finding relevant therapies is of utmost importance (Coronado, Xu et al. 2011). In order to develop appropriate interventions, reliable and accurate models that can simulate an applied injury need to be developed. These models need to be capable of being able to apply physiological levels of injury and assessing the extent of injury. Numerous strain induced injury models have been developed both *in vivo* and *in vitro* (Morrison, Elkin et al. 2011). Animal models are both costly

and inherently variable, and even though injuries can be precisely applied, it is particularly difficult to know how these forces and strains are translated from the point of application to the cellular level. *In vitro* models vary from using dissociated cells to organotypic tissue slices and from applying uniaxial to biaxial strains. While organotypic slices maintain the cellular cytoarchitecture and functional connections, there are issues with slice attachment, knowing exactly how the applied strain is translated through the thickness of the slice and imaging injury effects at the cellular level in real time (Morrison, Cater et al. 2006). Dissociated cells however are easily cultured and precise strains can be applied but they unfortunately lack the natural connectivity and interaction with surrounding extracellular matrix (ECM) and glial cells (Smith, Wolf et al. 1999; Pfister, Weihs et al. 2003).

A model that is capable of incorporating both organotypic and cellular level cultures will thus be able to overcome multiple issues. It will maintain the tissue structure found *in vivo* while being able to, in real-time, monitor cellular level changes following injury. This is accomplished by incorporating microfluidics with organotypic slice cultures. Organotypic slices have the inherent capacity for axons to extend from their periphery. These axons thus originate from cell bodies that are deep within the tissue surrounded by natural extracellular matrix proteins and support cells. Two organotypic slices are placed in close proximity to each other but separated by micron sized channels that guide the growth / extension of these axons to each other thereby allowing for functional connections to be made (Berdichevsky, Sabolek et al. 2009; Berdichevsky, Staley et al. 2010). Depending on the slices placed in culture, specific physiologically relevant networks can be tested. The hippocampus is the ideal organotypic tissue to use in TBI injury models since they are frequently injured during TBI events and maintain their structure and functional networks in culture over extended periods of time.

(Stoppini, Buchs et al. 1991; Tate and Bigler 2000; Berdichevsky, Sabolek et al. 2009).

The microfluidic channels extend over a pressure cavity, that when inflated exerts a strain injury to axons within the channel. This model thus incorporates the advantages of organotypic slice

cultures and the ability to observe in real-time and over long-term morphological, molecular and functional changes in axons following a strain injury.

We have developed and characterized a uniaxial strain injury device that is capable of applying precise levels of strain to individual and/or bundles of axons that extend from an organotypic hippocampus slice and connect to an adjacent organotypic slice. These organotypic slices are cultured on an elastic substrate manufactured from polydimethylsiloxane (PDMS) and remain healthy for over three weeks in culture. With this device we demonstrated characteristic phenotypic responses to strain injury which included axonal beading and delayed elastic effects (Smith, Wolf et al. 1999; Kilinc, Gallo et al. 2008).

Although these responses are common to DAI, we feel that there is a need to better understand the response of axons to the dynamic nature of the injury by quantifying how they vary according to different applied strain injuries. In this study we will also look at the molecular events, i.e. changes in cytoskeleton and axonal transport, which may be occurring that account for the morphological changes observed. These events are all trademarks of axonal degradation (Koike, Yang et al. 2008). Mitochondrial membrane potential (MMP) is a key indicator of mitochondrial function and can be used to assess potential mechanisms that play a role in axonal degradation (Mazzeo, Beat et al. 2009; Perry, Norman et al. 2011). We will thus assess the effects of strain injury on MMP at the axonal level.

The relationship between degree of strain and microtubule integrity following injury and responses typically seen in vivo are observed using this device. These responses vary according to the degree of applied strain injury with respect to axonal bead formation, delayed elasticity and microtubule degradation. We report how their response to injury is further dependant on axonal diameter. These injury responses correspond to the extent of axonal degradation observed at the various strain injuries. We also reveal a threshold that exists in applied strain injury on axonal MMP response, where at lower applied strains hyperpolarization occurs whereas at higher

applied strains depolarization occurs. We show that CsA significantly attenuates these changes in MMP and resultant axonal degradation and that the NHE-1 inhibitor EIPA has similar effects demonstrating a potential new DAI therapeutic.

Chapter 2: Characterization Of An Organotypic Uniaxial Strain Injury Model.

2.1 Abstract

Traumatic brain injuries are the leading cause of disability each year in the US. The most common and devastating consequence is the stretching of axons caused by shear deformation that occurs during rotational acceleration of the brain during injury. The injury effects on axonal molecular and functional events are not fully characterized. We have developed a strain injury model that maintains the three dimensional cell architecture and neuronal networks found *in vivo* with the ability to visualize individual axons and their response to a mechanical injury. The advantage of this model is that it can apply uniaxial strain injuries to axons that make functional connections between two organotypic slices and injury responses can be observed in real-time and over long term. This uniaxial strain injury model was designed to be capable of applying an array of mechanical strains at various rates of strain, thus replicating a range of modes of axonal injury. Long term culture, preservation of slice and cell orientation, and slice-slice connection on the device was demonstrated. The device has the ability to strain either individual axons or bundles of axons through the control of microchannel dimensions. The fidelity of the model was verified by observing characteristic responses to various strain injuries which included axonal beading, delayed elastic effects and breakdown in microtubules. Axonal bundle unraveling and primary axotomy at lower applied strains than previously reported are observed. Microtubule breakdown is dependent on the degree of the applied strain field, where maximal breakdown is observed at peak strain and minimal breakdown is observed at low strain. This strain injury model could be a powerful tool in assessing strain injury effects on functional axon-axon connections.

2.2 Introduction

Traumatic brain injury (TBI) is the leading cause of death and disability in the United States (US) (Coronado, Xu et al. 2011). Inertial forces that occur during acceleration / deceleration of the brain can lead to the generation of shearing or straining forces exerted on axons (Smith, Meaney et al. 2003). The consequence of these physical forces is that axons are injured and the resultant damage is commonly referred to as diffuse axonal injury (DAI). DAI is the most common type of pathology in TBI occurring in approximately 40-50% of reported cases (Meythaler, Peduzzi et al. 2001; Iwata, Stys et al. 2004). After the initial mechanical trauma, secondary injury cascades are initiated which include among others, cytoskeletal damage, calcium influx, neurotransmitter release, and mitochondrial dysfunction. (Andriessen, Jacobs et al. 2010). There is currently no “standard treatment” protocol for these secondary effects of TBI and with almost one third of all injury related deaths in the US attributed to a TBI related incident, finding relevant therapies is of utmost importance (Coronado, Xu et al. 2011).

In order to develop appropriate interventions, reliable and accurate models that can simulate an applied injury need to be developed. These models need to be able to apply physiological levels of injury and assess the extent of injury. Numerous strain induced injury models have been developed both *in vivo* and *in vitro* (Morrison, Elkin et al. 2011). Animal models are unfortunately both costly and inherently variable, and even though injuries can be precisely applied; it is particularly difficult to know how these forces and strains are translated from the point of application to the cellular level. *In vitro* models vary from using dissociated cells to organotypic tissue slices and from applying uniaxial to biaxial strains. While organotypic slices maintain the cellular cytoarchitecture and functional connections, knowing exactly how the applied strain is translated through the thickness of the slice and imaging injury effects in real time (Morrison, Cater et al. 2006) limits the imaging access of this approach. Dissociated cells however, are easily cultured and precise strains can be applied, but they unfortunately lack the natural connectivity and interaction with surrounding extracellular matrix (ECM) and glial cells (Smith,

Wolf et al. 1999; Pfister, Weihs et al. 2003). Both biaxial and uniaxial applied strains are equally important since both are physically found to occur during TBI events (Strich 1961).

A model that can incorporate the benefits of both organotypic and cellular level cultures will thus be able to overcome multiple issues. It will maintain the tissue structure found *in vivo* while being able to, in real time, monitor cellular level changes following injury. This is accomplished by incorporating microfluidics with organotypic slice cultures. Two organotypic slices are placed in close proximity to each other but separated by micron sized channels. These microchannels allow for axons that extend from the periphery of the slice to be guided from one slice to the other, thereby allowing functional connections to be made (Berdichevsky, Sabolek et al. 2009; Berdichevsky, Staley et al. 2010). Depending on the slices placed in culture, specific physiologically relevant networks can be tested. Hippocampus slices are the ideal organotypic tissue to use in TBI injury models since they are frequently injured during TBI events and maintain their structure and functional networks in culture over extended periods of time. (Stoppini, Buchs et al. 1991; Tate and Bigler 2000; Berdichevsky, Sabolek et al. 2009).

We have thus developed and characterized a uniaxial strain injury device that can apply precise levels of strain to individual and/or bundles of axons that extend from an organotypic hippocampus slice and connect to an adjacent organotypic slice. These organotypic slices are cultured on an elastic substrate manufactured from polydimethylsiloxane (PDMS) and remain healthy for over three weeks in culture. The strain injury is applied to the connecting axons by pressurizing a cavity beneath the microchannels. The relationship between degree of strain and microtubule integrity following injury and responses typically seen *in vivo* are observed using this device.

2.3 Materials and Methods

2.3.1 Organotypic Slice Isolation

The brains of Sprague-Dawley rat pups (Taconic, Hudson, NY, USA) between the ages of 4 to 6 days old were removed and placed in ice cold Gey's Balanced Salt Solution (Sigma-Aldrich Corp, MO) supplemented with 10mM D-glucose (Sigma-Aldrich Corp, St. Louis, MO, USA) and 3 μ M Kynurenic Acid (Sigma-Aldrich Corp, St. Louis, MO, USA). In our hands, we have found that axon extension from the periphery of organotypic hippocampal slices is very dependent on the age of the rat pup they have been excised from with axon extension decreasing significantly after day 6 (data not shown). The hippocampi are separated from the surrounding cortex and sliced into 400 μ m thick slices using a McIlwain Tissue Chopper (Stoelting Co, Wood Dale IL, USA). The slices were carefully placed into PDMS (Sylgard 184, Fischer Scientific, Pittsburgh, PA, USA) mini-wells and orientated such that the dentate gyrus (DG) region was facing the CA1 region of the adjacent slice, i.e. these regions were facing the microchannels. The PDMS was precoated with poly-d-lysine (1mg/ml, Sigma-Aldrich Corp, St. Louis, MO, USA) and laminin (25 μ g/ml, Sigma-Aldrich Corp, St. Louis, MO, USA). The device was filled with 450 μ l of serum containing media (1:1:2 of heat inactivated horse serum, Hanks Balanced Salt Solution, Basal Medium Eagle, supplemented with 0.5mM L-Glutamine, 30 μ g/ml gentamycin and 10mM HEPES, all from Invitrogen, Carlsbad, CA, USA), i.e. enough media to just cover the exposed basement PDMS area. The cultures were placed on a rocker (~1 revolution/60s) in a humidified 5% CO₂ incubator. Glial cell proliferation was reduced by changing from serum containing media to a serum free media after 24hours (Neurobasal A, 1X B27, 0.5mM L-glutamine, 30 μ g/ml gentamycin and 10mM HEPES, all from Invitrogen, Carlsbad, CA, USA). Thereafter, half of the media was changed every 48hours. Media evaporation was reduced by applying a semi-permeable membrane, i.e. permeable to O₂ and CO₂ but not permeable to H₂O, (ALA Scientific Instruments, Farmingdale, NY, USA) over the PDMS outer well and sealed with an O-ring. The small mini-well that the organotypic slice is placed in provides a buffering against shear forces that occur during device movement and media changes to both the organotypic slice as well as to delicate axons

extending from the slice (Berdichevsky, Sabolek et al. 2009). A small opening in the PDMS is critical for allowing sufficient nutrient exchange for long term slice cultures. All animal experiments were approved by the Animal Care and Use Committee of Rutgers, The State University of New Jersey.

2.3.2 Making/assembling device

A schematic representation of the device is shown in Figure 2.1A and a more detailed assembled device is shown in Figure 2.1B. The device consists of two layers of PDMS. The first layer (referred to as the basement PDMS layer) is the layer on which the organotypic slices are placed and axons extend, and the second layer is the microchannel layer in which axons extending from the periphery of the organotypic hippocampal slices are guided to grow between the two slices. Both PDMS layers were fabricated by mixing PDMS to its crosslinker (Sylgard 184, Dow Corning Corporation, auburn, MI, USA) in a 10:1 ratio followed by 40mins of degassing in a desiccant chamber (Nalgene, Rochester, NY, USA). The basement PDMS layer was produced by spincoating PDMS onto a blank silicon wafer (EI-Cat Inc, Waldwick, NJ, USA) at 1000rpm for 30s resulting in a thickness of $75\pm 5\mu\text{m}$. The microchannel PDMS layer was produced using a modified soft-lithography method. Silicon mold masters were prepared by using a negative chrome mask (Fine Line Imaging, Colorado Springs, CO, USA) and SU-8 (2002) photoresist (Microchem, Newton, MA, USA). Two SU-8 patterns were produced: $50\mu\text{m}$ (microchannel width) x $6\mu\text{m}$ (microchannel height) x $50\mu\text{m}$ (microchannel spacing) and $25\mu\text{m}$ (microchannel width) x $3\mu\text{m}$ (microchannel height) x $50\mu\text{m}$ (microchannel spacing). These dimensions were confirmed using a profilometer (Dektak 3030, Veeco, Plainview, NY, USA). The microchannel PDMS layer was produced by spincoating PDMS onto a SU-8 master at 1000rpm for 30s resulting in a thickness of $71\pm 5\mu\text{m}$. Both layers of PDMS were cross-linked at 65°C overnight. The manufacturing protocol for both PDMS layers was strictly followed so as to ensure that the material thicknesses and resulting material properties were consistent from batch to batch. The cured PDMS was then removed from the silicon master (blank or microchannels) and cut into

appropriate shapes. The basement PDMS layers are cut into strips of 40mm x 45mm. The microchannel PDMS is cut into 22mm diameter circles with 3mm mini-wells punched at a spacing of ~2mm from each other with a media access channel leading to each of the mini-wells. Before irreversibly bonding PDMS to either glass or PDMS, all surfaces were cleaned. This is important since these layers will experience large pressures and are susceptible to delamination. The glass was cleaned by boiling in 0.5M Hydrochloric Acid (HCL) for 10mins, rinsed in deionized water (diH_2O) for 10mins and then dehydrated by placing in an oven at 65°C overnight. The basement and microchannel PDMS were cleaned by first applying scotch tape to both surfaces to remove any large adherent debris, placed in methanol and sonicated for 10mins, boiled in 0.5M HCL for 10mins, rinsed in diH_2O for 10mins and then dehydrated by placing in an oven at 65°C overnight. The basement PDMS layer was first bonded to the glass substrate. Both surfaces were oxygen plasma treated (ENI, Rochester, NY, USA) at 100W for 30s at 60% O_2 . The exposed surfaces were immediately placed into contact with each other and then placed on a hotplate at 100°C for 30mins with a 0.5kg weight applied on top. The microchannel PDMS was bonded to the basement PDMS layer by treating both surfaces with oxygen plasma at 100W for 30s at 60% O_2 . The exposed surfaces were immediately placed into contact with each other. To contain the media for the organotypic slices, a PDMS well was manufactured with an outer diameter of 38.1mm and inner diameter of 31.8mm. This was bonded to the basement PDMS by exposing both surfaces to oxygen plasma at 100W for 30s at 60% O_2 . To ensure that this outer well was leak tight, it was epoxy sealed using EPO-TEK 353ND (Epoxy Technology Inc, Billerica, MA, USA). Media evaporation was reduced by placing a semi-permeable membrane, i.e. permeable to O_2 and CO_2 but not permeable to H_2O , (ALA Scientific Instruments, Farmingdale, NY, USA) over the PDMS outer well and sealed with an O-ring.

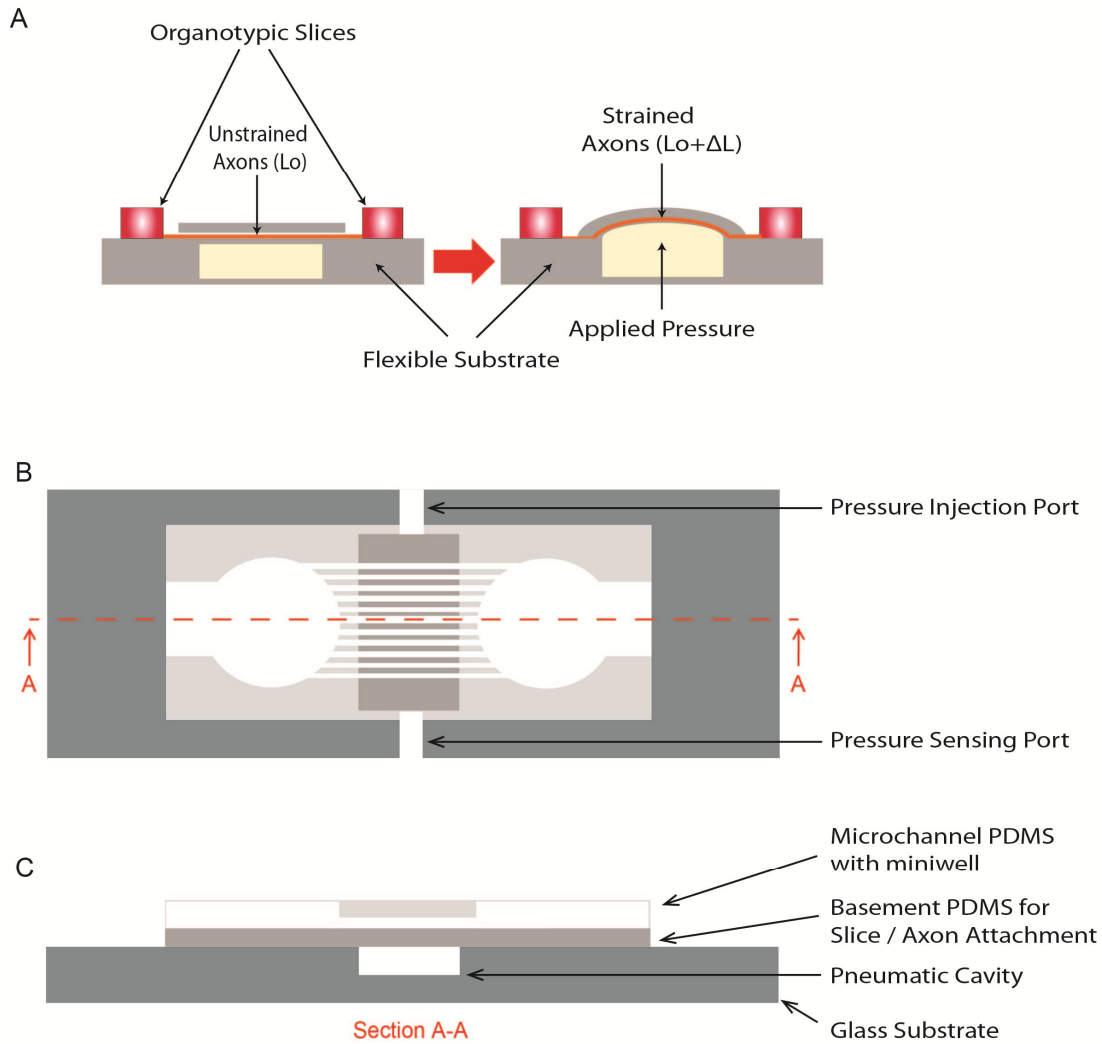


Figure 2.1 Organotypic uniaxial axonal strain injury device. A) Schematic of device before and after strain application. B) Detailed top view of assembled device. C) Detailed sectioned view (A-A) of assembled device. All figures are not to scale.

2.3.3 Testing PDMS material properties

The tensile material properties of the PDMS were measured using a Bose/*EnduraTEC ELF 3200* mechanical testing machine (EnduraTEC, Eden Prairie, MN, USA). These tests were done according to ASTM D 412 standards. The size of the test specimens were scaled down to one fourth of those specified within the standard (Mata, Fleischman et al. 2005). A “dumbbell” shaped

die was cast using rapid prototyping (Viper, 3D Systems, Overview Drive, SC, USA) and used to cut out samples of PDMS for testing (8.25mm-length by 2.5mm-width). These samples were securely placed in the jaws of the mechanical testing machine and tensile strained at a rate of 3.75mm/s. The force and displacement readings were recorded at a rate of 80HZ. Markings were applied to the PDMS around the jaws to assess for slippage during loading.

2.3.4 FEA – Abaqus

The finite element analysis software Abaqus (Dassault Systemes, Waltham, MA, USA) was used to assess the degree of PDMS strain that occurs when applying a pressure and to ensure that uniaxial strain is applied across all relevant microchannels. Material properties obtained from tensile material tests were input into the software. A second order Ogden hyperelastic material model was used to calculate strains. An 8-node linear brick, hybrid, constant pressure model was used with a seed size of 0.035mm. No slippage between the PDMS and glass substrate (if the bonding wasn't absolutely ideal at the edge of the pressure cavity, with the range of pressures applied, complete delamination occurred) or between the PDMS layers (the bonding was tested before and after testing and no slippage was ever observed) was assumed, i.e. no translation or rotation boundary conditions were applied.

2.3.5 Applying Strain

In order to produce a uniaxial strain field a pneumatic pressure is applied to a cavity beneath the microchannels (Figure 2.1A). This pneumatic pressure is produced by coupling to a pressure injection system that consists of a linear actuator (PS01-23x80, Lin Mot Inc, Elkhorn, WI, USA), controller (E100-MT - Lin Mot Inc, Elkhorn, WI, USA), a pressure sensor (Honeywell International, Morristown, NJ, USA) and a high speed sampling system (USB-5132, National Instruments Corporation, Austin, TX, USA). The linear actuator and controller are coupled to the inlet port on the device and controlled by a visual basic program. A pressure sensor is coupled to the pneumatic cavity and attached to a high speed digitizer that is controlled by a Labview program

(National Instruments Corporation, Austin, TX, USA). The injected volume and rate of injection are varied to produce a variety of strains and rate of strain. To verify that the Abaqus model accurately describes the system, PDMS deflections were monitored at various cavity pressures. This was done by slowly increasing the cavity pressure using a syringe pump (PHD 2000 – Harvard Apparatus, Holliston, MA, USA) and measuring the corresponding deflection of the PDMS at the center of the pressure cavity using an Olympus IX81 DSU microscope (Olympus, Center Valley, PA, USA). This microscope has a high-resolution Z-axis motor capable of 0.01 μm step sizes.

2.3.6 Slice viability

The viability of slices was determined using Propidium Iodide (PI, Invitrogen, Carlsbad, CA, USA). PI is used to assess for cell death since it is membrane impermeant and thus excluded from viable cells. When cells are injured or dead, PI enters the cell and binds to nuclear DNA which enhances its fluorescence (Cy5). Cultures were incubated at 37°C for 30mins with 5 $\mu\text{g}/\text{ml}$ of PI in serum free media, then washed twice for 10mins with serum free media and imaged using an Olympus IX-81 DSU microscope. The extent of cell death was assessed by completely killing control cultures by incubating in artificial cerebrospinal fluid (120 mM NaCl, 3.3 mM KCl, 1.25 mM NaH_2PO_4 , 1.3 mM CaCl_2 , 0.9 mM MgCl_2 , 10 mM HEPES, and 10 mM glucose, pH 7.4) for 48hrs at 4°C and then PI staining (Frantseva, Kokarovtseva et al. 2002). The relevant fluorescence intensity was then normalized according to the fluorescence intensity of the completely dead hippocampus slice.

2.3.7 Dil Staining

Axons traversing the distance from one organotypic slice and connecting to the adjacent slice was visualized by applying the lipophilic carbocyanine dye, Dil (1,1',di-octadecyl-3,3,3'-tetramethylindocarbocyanine perchlorate – Invitrogen, Carlsbad, CA, USA) to one organotypic slice. Dil is a fluorescent probe that is nontoxic and allows for the labeling of cell plasma

membranes with high specificity. Since it is lipophilic it inserts itself freely into the plasma membrane where it either diffuses freely or is trafficked through intracellular vesicles. This probe thus allows for the tracing of axons through the uptake of the dye in the cell body and via anterograde transport, labels the axons through to its axon terminal. One small Dil crystal was carefully placed on top of one slice (in the center). The device was carefully handled making sure to not dislodge the crystal. Within 24-48 hours later the culture was imaged using a 540nm fluorescent filter on an Olympus IX81 DSU microscope. Dil labeling proved to be quite difficult due to the fact that the device is an open system, i.e. the media that supports one slice is the same that supports the adjacent slice. Thus if the Dil crystal that is placed on top of one slice comes into direct contact with the media, there is a potential for it to diffuse to the adjacent slice through the media thus bypassing the connecting axons. For this reason the cultures were not placed on a rocker like other devices that were injured.

2.3.8 Immunohistochemical staining

Cultures were fixed before immunofluorescent staining for specific protein markers. This was done by washing three times in phosphate buffered saline (PBS) followed by incubating in 4% paraformaldehyde (Sigma–Aldrich Corp, MO) for 25mins at room temperature. The cultures were again washed three times in PBS for 5mins each at room temperature. For primary conjugated MAP2 and Tau staining, the following protocol was followed: non-specific binding of antibodies to proteins on/within the cells was reduced by first blocking for 45mins at room temperature by incubating with Tris Buffered Saline (TBS), 10% mouse serum (Invitrogen, Carlsbad, CA, USA), 1% Bovine Serum Albumin (BSA) (Sigma-Aldrich Corp, St. Louis, MO, USA) and 0.1% Triton X-100 (Sigma-Aldrich Corp, St. Louis, MO, USA). The cultures were then incubated for 45mins with the respective primary conjugated antibody in TBS and 1% mouse serum. The antibodies used were: 1.2 µg/ml mouse anti-MAP2B IgG₁ conjugated with Alexa Fluor 647 (BD Pharmingen, San Diego, CA, USA) and 1.5 µg/ml mouse anti-Tau IgG_{2b} conjugated with Alexa Fluor 488 (BD Pharmingen, San Diego, CA, USA). To account for non-specific binding, isotype controls were

used for each antibody: for MAP2 - mouse IgG₁ conjugated with Alexa Fluor 647 (BD Pharmingen, San Diego, CA, USA), and for Tau – mouse IgG_{2b} conjugated with Alexa Fluor 488. The cultures were washed three times for 15mins in PBS. For indirect immunostaining for beta III tubulin, the following protocol was followed: non-specific binding was reduced by first blocking for 45mins at room temperature by incubating with TBS, 10% goat serum (Invitrogen, Carlsbad, CA, USA), 1% BSA and 0.1% Triton X-100. The cultures were then incubated overnight at 4°C with 2µg/ml beta III tubulin rabbit IgG (Abcam, Cambridge, MA, USA) in TBS and 1% goat serum. To account for non-specific binding, isotype control cultures were incubated at 4°C overnight with 2µg/ml rabbit IgG (BD Pharmingen, San Diego, CA, USA) in TBS and 1% goat serum. Both beta II tubulin and isotype control cultures were then incubated for 1 hour with 2µg/ml Alexa Fluor 647 goat-anti-rabbit IgG (Invitrogen, Carlsbad, CA, USA) secondary antibody. The cultures were then washed three times for 15mins in PBS. Fluorescent images were acquired using a computer interfaced inverted Olympus IX81 DSU microscope. Specimens were excited using either 488nm or 647nm filters. Fluorescent intensity values were determined using SlidebookTM software (Olympus, Center Valley, PA, USA) and control values were subtracted from experimental values.

2.4 Results

2.4.1 Device – PDMS material properties

In order to apply a strain to cells, they need to be cultured on a flexible substrate. The substrate of choice for the device designed for the current studies was PDMS since it is transparent, permeable to gases, non-toxic to cells, highly elastic, can be bonded to other surfaces, and can rapidly produce micron-sized structures using soft lithography methods (Sia and Whitesides 2003). In order to produce the required thicknesses for the basement and microchannel layers, PDMS was spincoated at 1000rpm for 30s. This speed resulted in material thicknesses of $75 \pm 5 \mu\text{m}$ for the basement PDMS layer and $71 \pm 5 \mu\text{m}$ for the microchannel PDMS layer. The finite element analysis software, Abaqus, was used to predict the strain produced when the device is pressurized. Since this software requires material properties to calculate these predictions, PDMS layers were tensile tested for stress strain properties (Figure 2.2). The best material model that fits the stress strain behavior of the PDMS thicknesses produced is the 2nd order Ogden hyperelastic material model ($\mu_1=107.6 \text{ kPa}$, $\alpha_1=6.1$, $\mu_2=535.2 \text{ kPa}$, $\alpha_2=-3.96$). The fit of the model to the PDMS material is shown in the inset of Figure 2.2 demonstrating how well it models the material behavior.

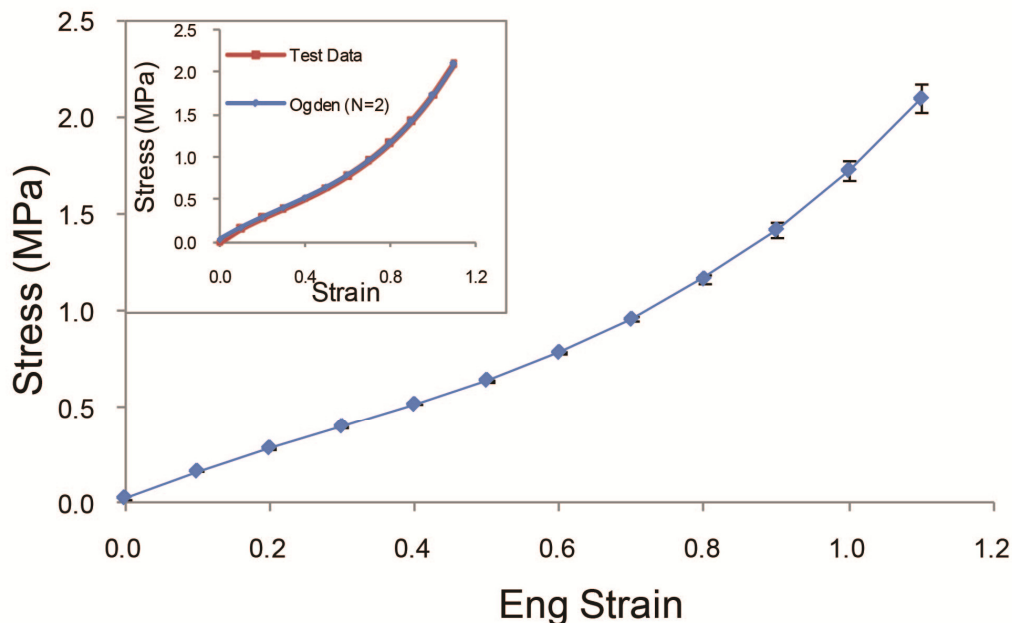


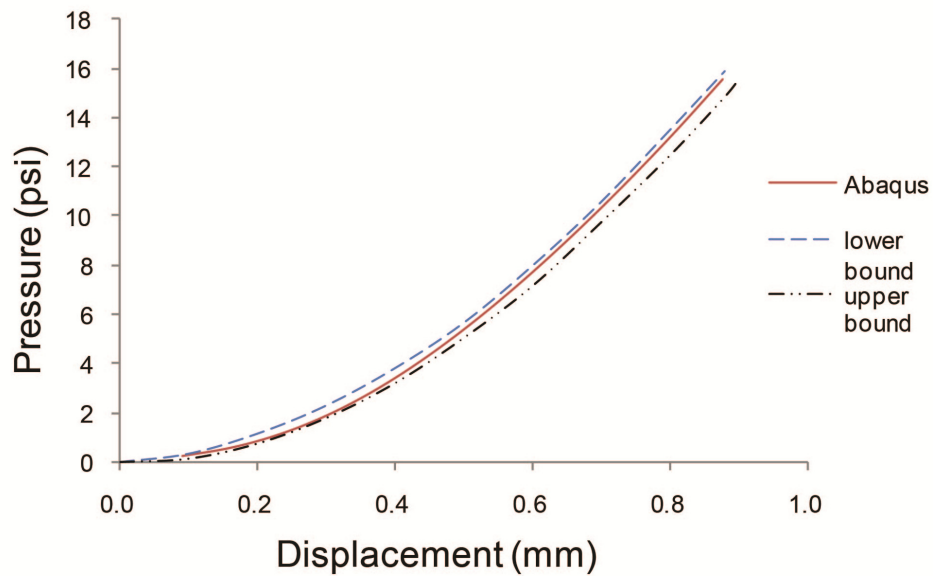
Figure 2.2 Tensile test results - Stress vs. Strain curve for PDMS. (1.0 strain = 100% elongation). Inset: Curve fit using 2nd order Ogden hyperelastic model.

2.4.2 Abaqus results

The material properties obtained from the tensile testing were input into the finite element software Abaqus and the following were calculated: 1) the strain experienced by the PDMS when applying specific pressures to the device, and 2) confirmation that the area in which the axons extend and connect with the adjacent slice experiences uniform uniaxial strain. The fidelity of the Abaqus simulations was confirmed by initially applying discrete static pressures to the device and the amount of PDMS deflection measured and compared to simulation results (Figure 2.3A). As the graph indicates, the simulations correlate well to experimental deflections staying within the upper and lower bounds of deflection. In the region below 5psi, Abaqus is closer to the upper bounds of displacement, whereas above 5psi Abaqus is closer to the lower bounds of displacement. The corresponding strain experienced by the PDMS as calculated by Abaqus is shown in Figure 2.3B. These strains have almost a linear relationship with respect to the applied pressure ($R^2=0.9998$). The strain injury device was characterized using three cavity pressures selected on the basis of a range of resulting strains, namely: 3.5psi ($\pm 11\%$ strain), 8.5psi ($\pm 25\%$

strain), and 14.5psi ($\pm 42\%$ strain). These strains span the range believed to cause damage in TBI events, i.e. 10%-50% strain (Margulies, Thibault et al. 1990; Meaney and Thibault 1990; Morrison, Meaney et al. 1998).

A



B

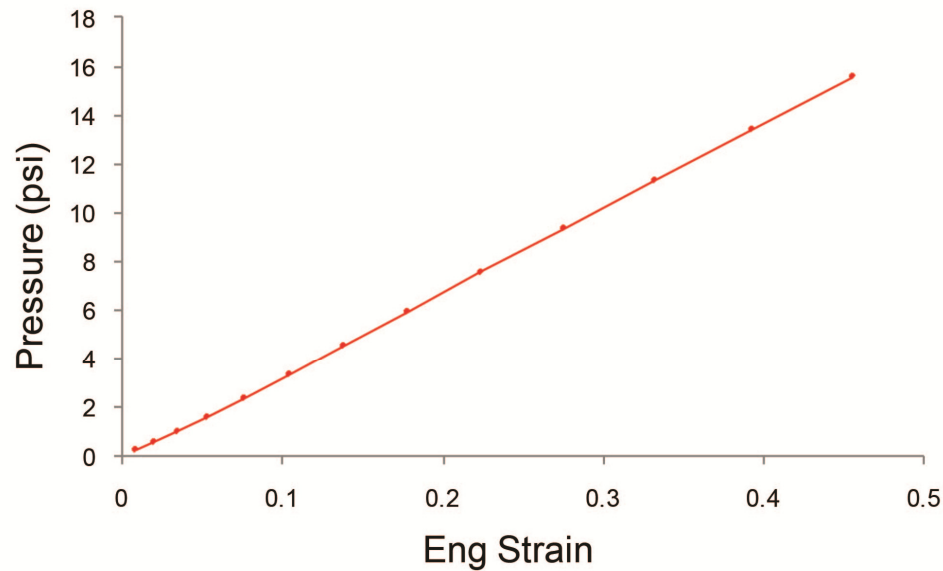


Figure 2.3 Abaqus displacement and strain predictions. A) PDMS deflections – Abaqus vs. experimental, and B) resulting strain from different applied pressures, as determined from Abaqus.

Deflection profiles across the length and width of the pressure cavity were determined (Figure 2.4A defines pressure cavity length and width). A uniform deflection along the length indicates a uniform strain field along the width of the cavity. When a width to length ratio of 1:16 is used, a uniform deflection profile occurs in the region in which axons traverse the microchannels (Figure 2.4B shows cavity length deflection profile). We observe that in the region in which the axons extend (indicated on the 14.5psi deflection profile curve, i.e. between 45% and 55% along the length) the deflection is uniform for all applied pressures. Biaxial strain, i.e. strain along the length of the pressure cavity, was verified using Abaqus. At an applied pressure of 15.5psi (i.e. above our maximum applied pressure), there is a maximum of $0.11\mu\text{m}$ deflection along the length of the channel (i.e. 90° to the applied strain) equating to a biaxial strain of 0.006% (essentially zero). The PDMS deflection profile across the width of the pressure cavity can be seen in Figure 2.4C. As expected, the maximal deflection occurs at the midpoint of the cavity and is consistent for all applied pressures. The corresponding strain (E_{xx}) profile across the pressure cavity width for the three applied pressures is shown in Figure 2.4D.

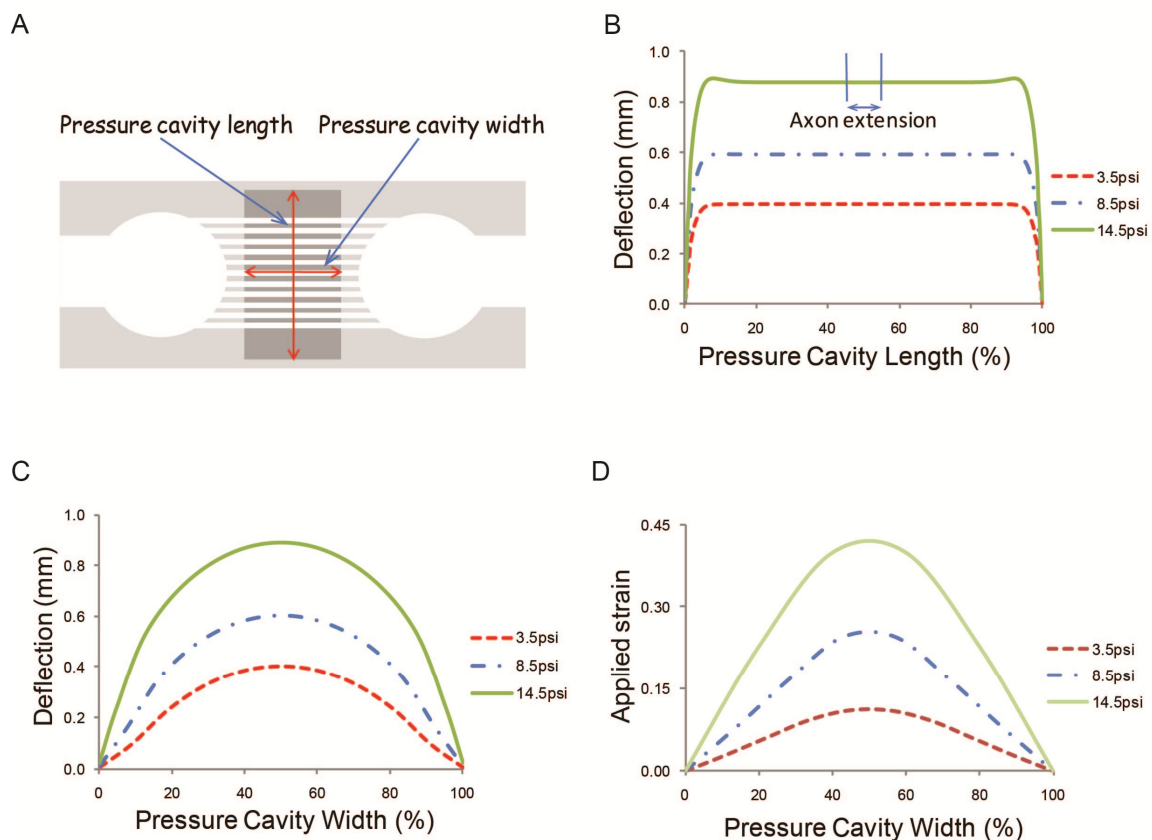


Figure 2.4 PDMS deflection profiles. A) Definition of deflection profiles. B) PDMS deflection profile along the pressure cavity length. Area in which axons extend is indicated on the top curve (i.e. between 45%-55%). C) PDMS deflection profile along the pressure cavity width. D) Strain (E_{xx}) profiles across the pressure cavity width.

2.4.3 Dynamic pressure effects

This device is capable of applying strains at various strain rates. Figure 2.5 shows three different times to reach peak deflection, i.e. 260ms, 50ms, and 22ms, for the three different applied pressures, i.e. 3.5psi / 11% strain (Fig 2.5A), 8.5psi / 25% strain (Fig 2.5B), and 14.5psi / 42% strain (Fig 2.5C). Table 1 reflects the strain rates that equate to the three different deflection times. These strain rates fall within the range shown to produce damage during TBI. In Figure 2.5A all three curves have a maximum pressure of 3.5psi showing no dynamic effects on the

applied strain. In Figure 2.5B and C, it may be difficult to observe, but at the highest applied rate, the maximum pressure is approximately 0.9% and 1.2% higher respectively, than at the lowest applied rate. These dynamic effects equate to an increase in <0.5% strain.

Table 1. Strain rates that correspond to chosen peak deflection times.

Applied pressure / Time to peak deflection / strain	3.5 psi / 11% strain	8.5 psi / 25% strain	14.5 psi / 42% strain
260ms	0.4s^{-1}	1.0s^{-1}	1.6s^{-1}
50ms	2.2s^{-1}	5.0s^{-1}	8.4s^{-1}
22ms	5.0s^{-1}	11.4s^{-1}	19.1s^{-1}

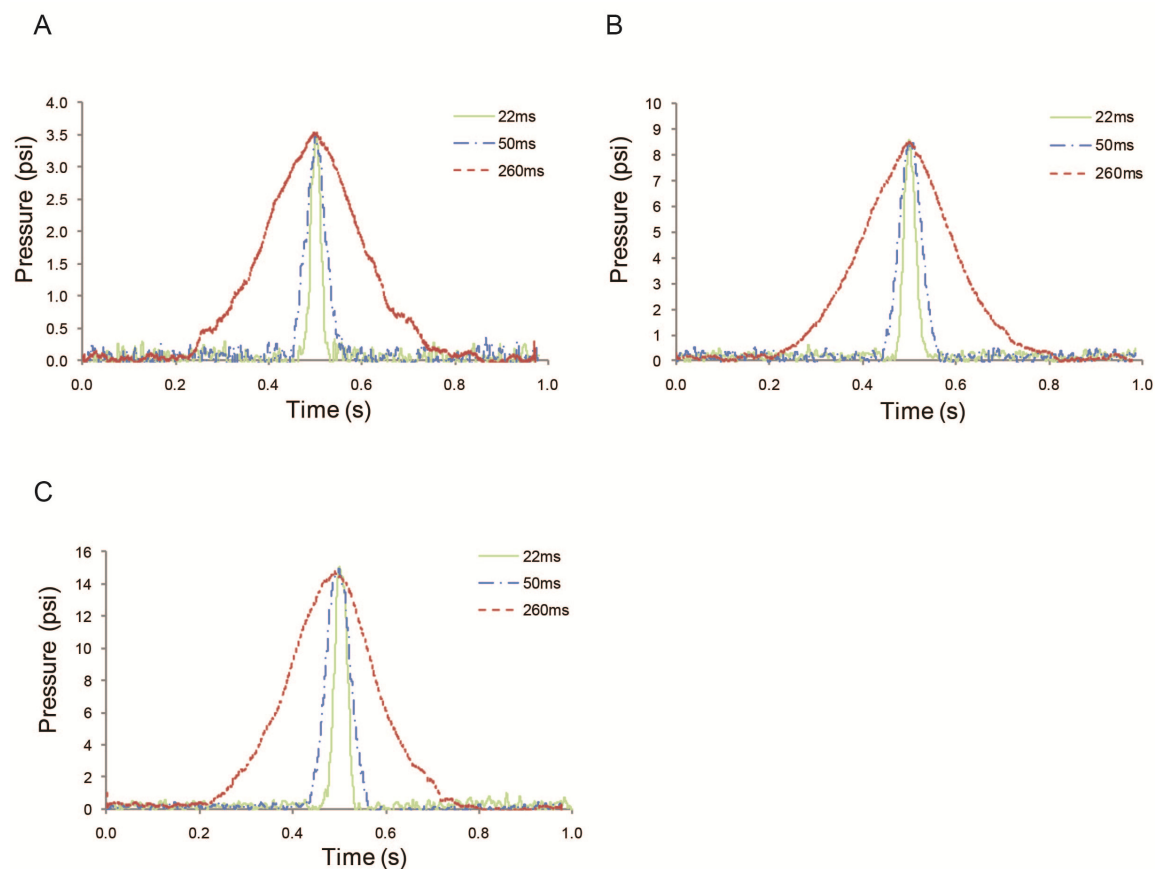


Figure 2. 5. Dynamic pressure effects within the system. Representative graphs of the pressures measured within the device for various times to peak deflection (22ms, 50ms, and 260ms). A) 3.5psi applied pressure, B) 8.5psi applied pressure, and C) 14.5psi applied pressure.

2.4.4 Monitoring hippocampus slice health on the device over time

Cell death within the organotypic slices was assessed to confirm that the slices remain healthy throughout the course of the expected experiment. This was done using the fluorescent molecule Propidium Iodide (PI). Figure 2.6 (A-H) shows a time progression of slices stained with PI. The images show that after the initial cell death observed on Day 0 (Fig 2.6A, due to initial trauma of slicing of the hippocampus with the tissue chopper), cell death steadily decreases over time till Day 14 (Fig 2.6F) and is maintained that way until Day 22 (Fig 2.6H).

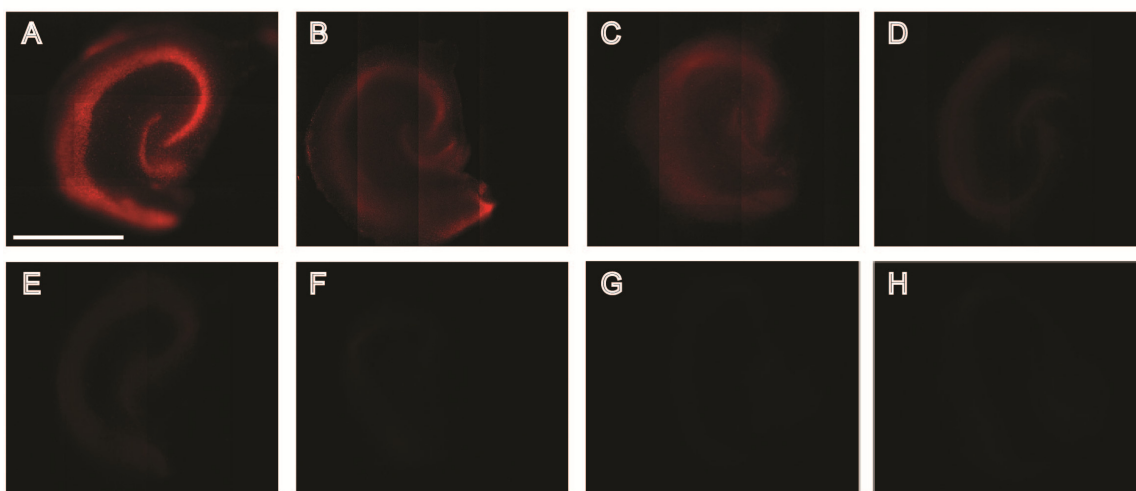


Figure 2.6. Hippocampus slices on the strain device stained with Propidium Iodide over time. A) Day 0, B) Day 1, C) Day 4, D) Day 7, E) Day 11, F) Day 14, G) Day 18, H) Day 22. Scale, 1mm.

Organotypic slice health was not only assessed by cell death but also by observing the integrity of the different neuronal cell layers that are so distinct to the hippocampus over time. Figure 2.7 shows hippocampal slices stained with the neuronal cell marker MAP2 (microtubule associated protein) on Day 7 (Fig 2.7A), 14 (Fig 2.7B) and 22 (Fig 2.7C) on the device. The three distinct neuronal cell layers of the dentate gyrus (DG), CA3 and

CA1 are clearly seen. Not only are the distinct regions of the hippocampus visible, but the specific cell orientation within the slice is maintained over the same time period (Fig 2.7D), where the characteristic apical and basal branching of a CA1 pyramidal neuron can be seen.

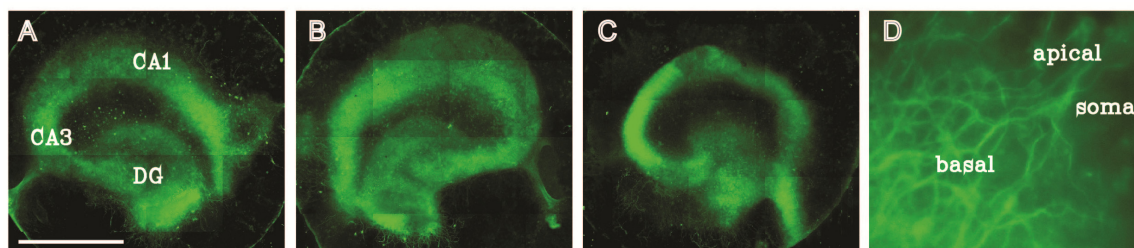


Figure 2.7. MAP-2 staining of organotypic slices on the strain device. A) Day 7, B) Day 14, C) Day22, (DG – dentate gyrus), and D) CA1 neuron on Day22, showing apical and basal branching. Scale, 1mm.

2.4.5 Characterization of axon extension

Axons are observed to extend from the periphery of hippocampal slices in early postnatal slices (P4-P6). These extending axons generally enter microchannels that are closest to them. The axons extend down the length of the microchannels and connect with the adjacent slice. These extensions within the microchannels were confirmed to be axons and not dendrites by immunostaining for the axon specific marker Tau (stabilizes microtubules in axons) (Figure 2.8). In this particular example, we see both individual axons as well as bundles of axons (thicker more intense stained axons).

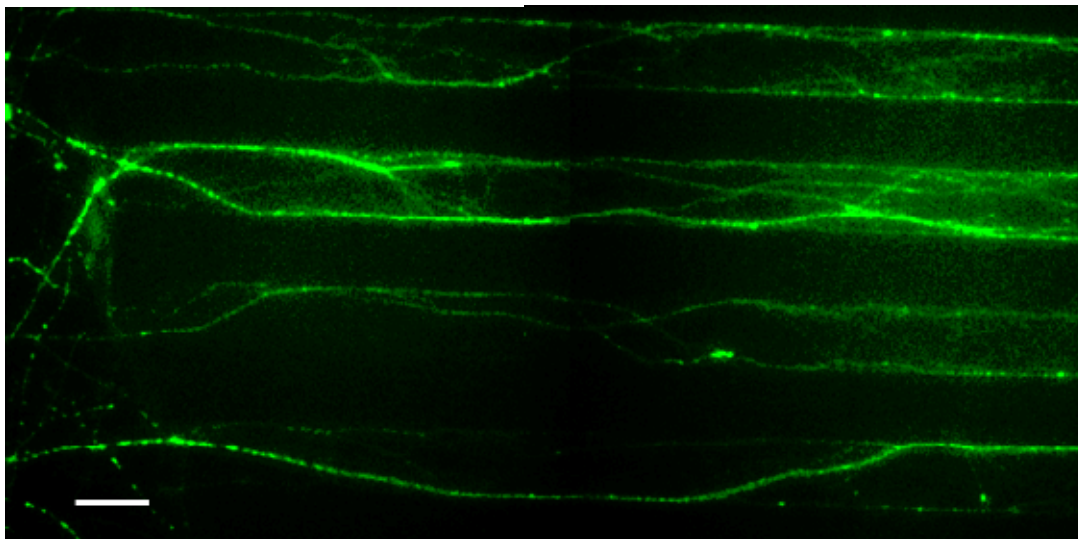


Figure 2.8. Axons in microchannels stained for Tau (axonal marker). Scale, 50 μ m.

In order to confirm that axons from one organotypic slice do indeed extend the full distance and connect to the adjacent slice, axons were traced using the lipophilic plasma membrane dye, Dil. Dil labels the cell / axon plasma membranes by diffusing freely along its length and allows for tracing of axons both *in vivo* and *in vitro* (Murphy and Fox 2007). One small Dil crystal was carefully placed upon one slice and within 48 hours the culture was imaged (Figure 2.9). The slice on which the Dil crystal was placed (top slice) is very brightly fluorescent due to the very high concentration of Dil on that slice. The Dil has diffused along the plasma membrane of axons that extend from the periphery of the slice. This diffusion proceeds along their length where we observe axons entering a particular microchannel and extending down the full length (the section over the pressure cavity is not shown for conciseness) and emerging from the other end. In this particular example, one axon that has exited the microchannel clearly makes its way to the adjacent slice. Along the way it has transferred the dye to three connecting cells. A few axons that exit the microchannel have not quite made it to the adjacent slice by the time these images were taken.

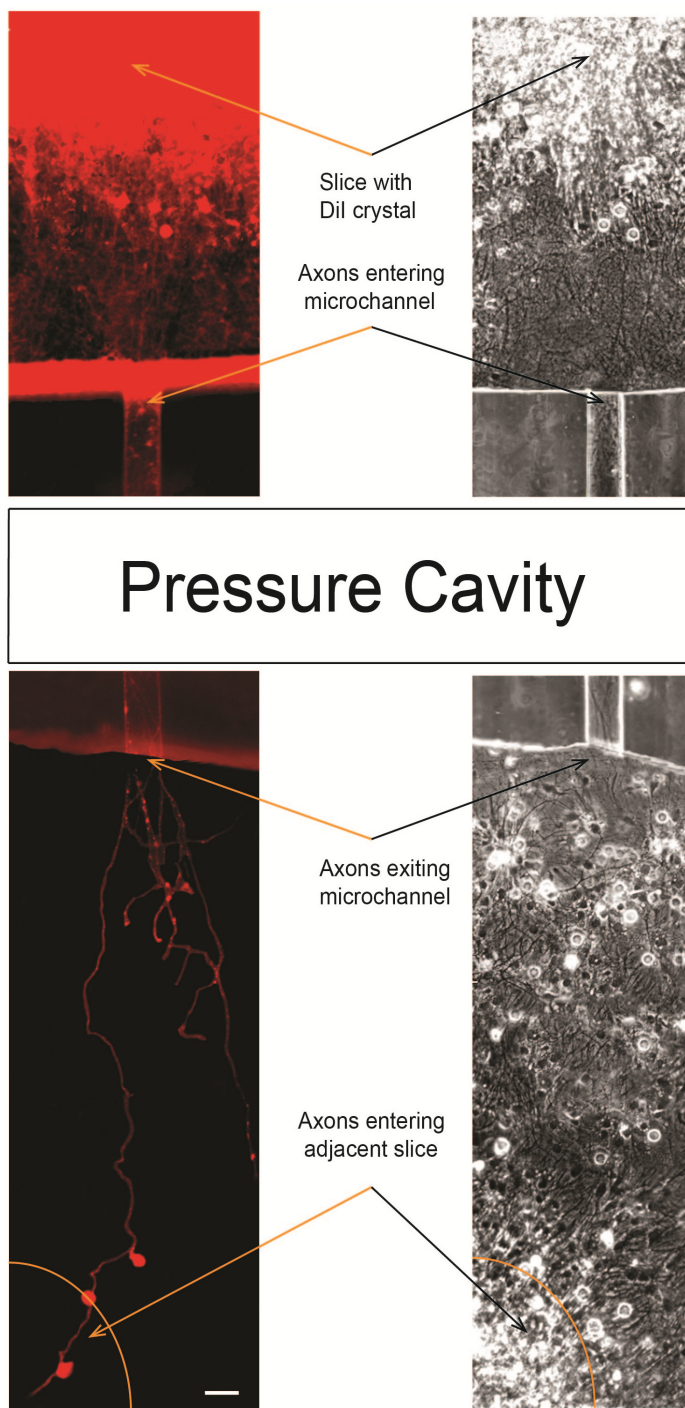


Figure 2.9. Hippocampus slice-to-slice connection verification. Dil staining of axons extending from one slice (top) and connecting to adjacent slice (bottom). Scale, 50 μ m.

2.4.6 Microchannel dimensions

The microchannel height was optimized to $6\mu\text{m}$ in order to minimize cell migration down the channel (data not shown). This is important since a large number of glial cells migrate out from the organotypic slice and if they enter a microchannel, may obstruct the progression of axons and interfere with the way in which axons experience the applied strain. The number of axons entering a given microchannel can be manipulated by changing its dimensions. Reducing the microchannel width not only controls the number of axons that enter a microchannel, but also reduces the tortuous path that the axon may take. By reducing the microchannel width from $50\mu\text{m}$ to $25\mu\text{m}$ we are able to reduce the number of axons entering a given microchannel (Figure 2.10). Thus the effect of uniaxial strain on single axons could be investigated.

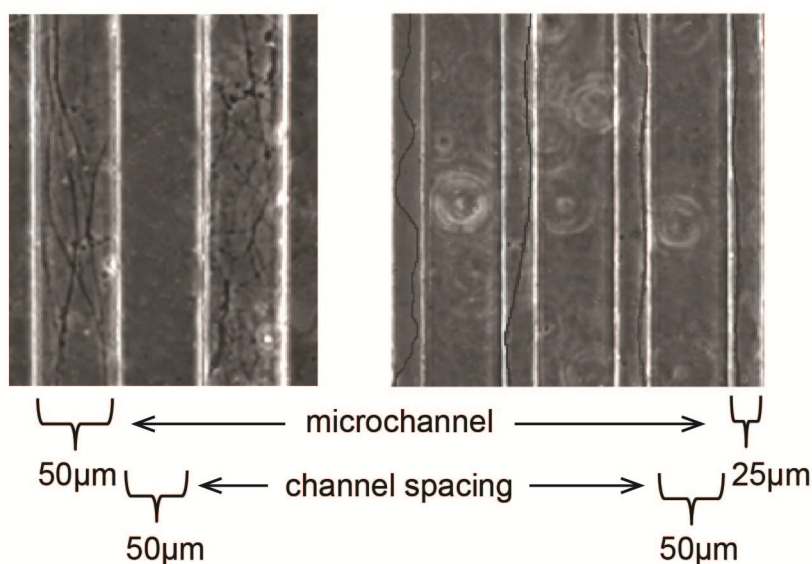


Figure 2.10. PDMS microchannel dimensions control the number of entering axons. A) $50\mu\text{m}$ wide microchannels = large number of entering axons, and B) $25\mu\text{m}$ wide microchannels = single axons / small number of entering axons.

2.4.7 Application of strain injury

One way to confirm that our device does indeed simulate what is experienced *in vivo*, is to look for characteristic responses. Two of the more common axonal responses to strain injuries include axonal beading and delayed elastic effects (Gennarelli, Thibault et al. 1989; Tomei, Spagnoli et al. 1990; Tang-Schomer, Patel et al. 2010). Axonal beading is believed to occur due to the breakdown in the axon cytoskeleton that affects axonal transport, ultimately leading to a buildup of transported organelles and proteins. The delayed elastic effect is the response that occurs at high strain rates where axons temporarily retain their elongated length even when the applied strain is removed. When a uniaxial strain is applied to axons on our device we observe these typical responses, thus demonstrating that our device is capable of applying uniaxial strains. Figure 2.11 shows the response to a 42% strain (strain rate of 19s^{-1}) applied to axons connecting hippocampal slices. This strain injury is applied approximately 14 days after initially plating the slices onto the device. Figure 2.11 i-vii, shows a time progression of an axon bundle before and after a strain injury. Immediately following injury, distinct delayed elastic effects can be seen along the axon bundle length in the form of waves / oscillations (arrows) (Fig 2.11 ii). This effect typically disappears within 50minutes after injury (Fig 2.11 iv). In this particular example, partial degradation of the axon has occurred by 210minutes (Fig 2.11 vi) after injury and complete degradation by 24 hours (Fig 2.11 vii).

Axonal beading is also observed after strain injury. Interestingly, in the particular example shown in Figure 2.11, around the time that the delayed elastic effect is no longer visible, i.e. when the axon has returned to its original length, axonal beading starts to be visible (Fig 2.11 v – arrowheads). Thus in this example axonal beading

coincides with regions that have undergone delayed elasticity, however this is not always the case as axonal beading can and does occur outside of these regions (Fig 2.11B i,ii).

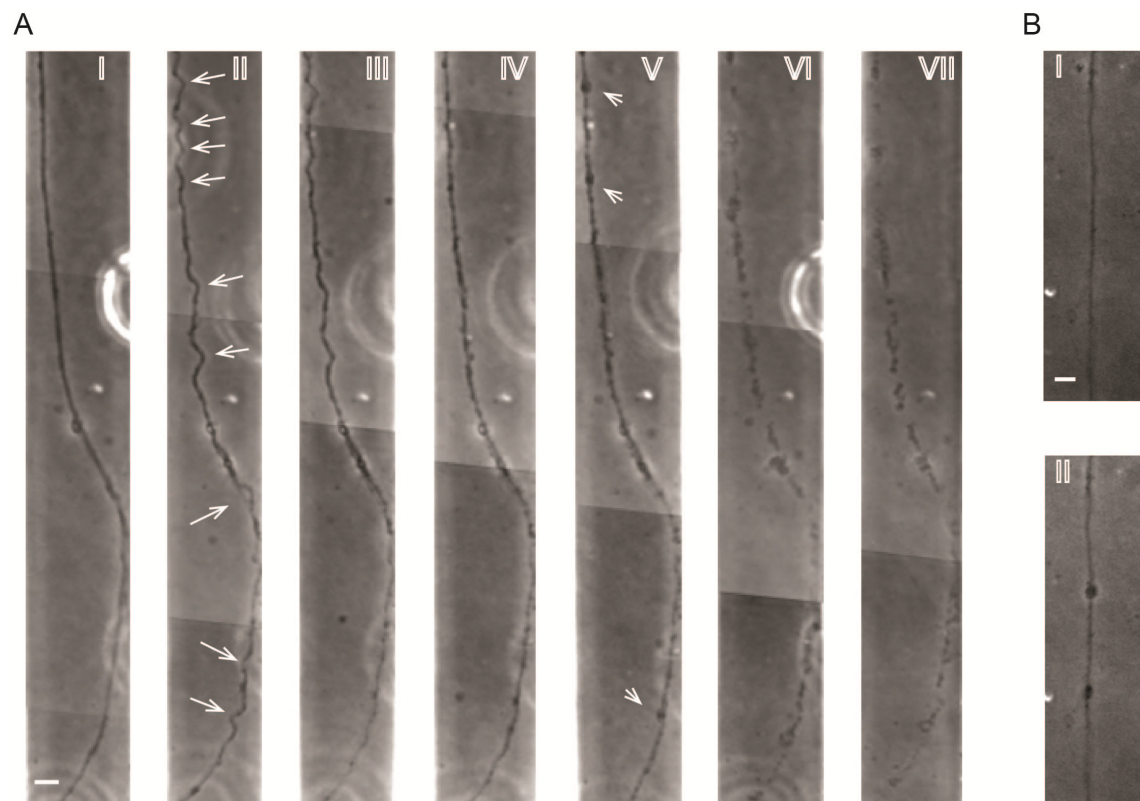


Figure 2.11. Time progression of delayed elastic effect on axon bundle after application of 42% strain, 20s⁻¹. A) i) before injury, ii) immediately after injury, iii) 20mins after injury, iv) 50mins after injury, v) 75mins after injury, vi) 210mins after injury, vii) 24hours after injury. B) i) Axon before injury, ii) axon after injury. Arrows show individual “waves”, arrow heads show beading. Scale, 10μm.

Not all axons within a particular bundle experience this delayed elastic effect demonstrating that not all axons have the same adhesion to the rest of the bundle. We observe on occasion at the higher applied strain and strain rate (42% applied strain and 19s⁻¹ strain rate), one or more axons may locally return to its original length (as soon as

the applied strain is removed) while the rest of the axons within the bundle undergo the temporary increase in length associated with delayed elastic effects (Figure 2.12A). Another effect that is occasionally observed is primary axotomy of an axon or axon bundle following strain injury, i.e. total severing (Figure 2.12B). Again, this seems to only occur at the higher applied strain and strain rate, and typically occurs in larger diameter bundles.

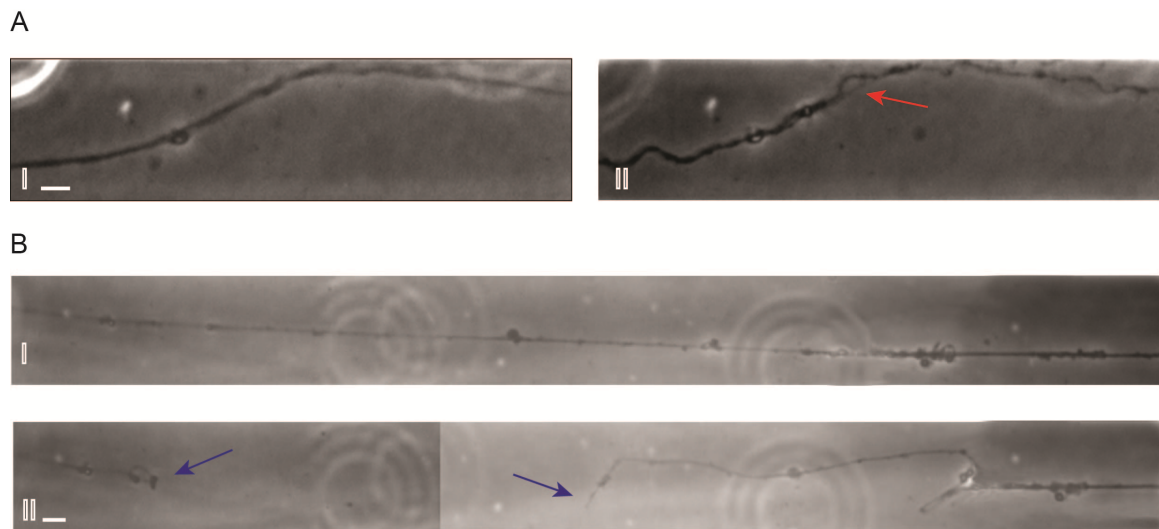


Figure 2.12. Examples of axonal bundle unraveling and primary axotomy. A) Axon bundle unraveling when a 42% strain is applied, i) before injury, ii) after injury, red arrow shows point of unraveling. B) Axon primary axotomy after a 42% strain is applied, i) before injury, ii) after injury, blue arrows show free ends of axon. Scale, 10 μ m.

2.4.8 Cytoskeletal effects following strain injury

Cytoskeletal components actin and microtubules form the basis for the structural integrity of the axon. When an axon is subjected to a strain injury, these are the components that will thus resist the force. Since microtubules are the stiffer of the two, they will oppose the majority of the force (Gittes, Mickey et al. 1993; Tang-Schomer, Patel et al. 2010). If the applied force is above what the microtubules can withstand, then

there is a mechanical breaking that can lead to further disassembly of surrounding microtubules (Tang-Schomer, Patel et al. 2010). Figure 2.4D depicts the PDMS strain profile across the pressure cavity width, thus axons within the microchannels will experience a peak strain in the center decreasing towards the two pressure cavity walls. An example of how this varying applied strain affects microtubules within the axon can be seen in Figure 2.13. The figure shows axons that have been subjected to a 42% strain injury at a strain rate of $19s^{-1}$ immunostained for β -tubulin (microtubule marker). In this figure we see that in regions of low applied strain, i.e. at the pressure cavity walls (Fig 2.13 i, ii), there is a continuous flow of microtubules as seen by uninterrupted β -tubulin staining in both small (Fig 2.13 i) and large diameter (Fig 2.13 ii) axon bundles. However, at the center of the cavity, i.e. at peak applied strain (Fig 2.13 iii, iv), we see a breakdown in microtubules (gaps in staining) occurring in both smaller (Fig 2.13 iii) and larger diameter (Fig 2.13 iv) axon bundles. We also observe brighter fluorescence intensity with punctuate staining at specific regions along the length, denoting areas of axonal beading on single axons within the bundle. The results observed in Figure 2.13 for the applied strain of 42% were also observed at the lower applied strains, just to lesser extents.

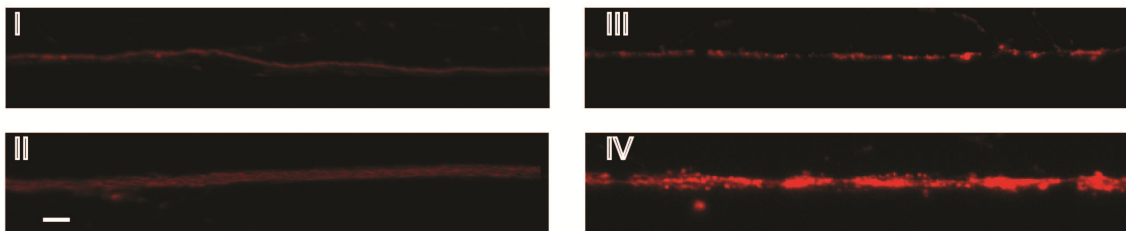


Figure 2.13. Applied strain distribution across pressure cavity and axons stained for β -tubulin 4hours after 42% strain injury. β -tubulin staining of axons at pressure cavity walls, i.e. regions of low applied strain, i) small diameter axon, ii) larger diameter bundle, and at the center of the pressure cavity, i.e. region of peak applied strain, iii) small diameter axon, iv) larger diameter bundle. Scale, $10\mu m$.

2.5 Discussion

We have successfully designed and evaluated a device that can apply accurate uniaxial strains to an elastic substrate on which axons extend from one organotypic hippocampus slice and connect to an adjacent hippocampus slice. These axons are guided to the adjacent slice by microchannels that allow for the most direct route between the slices. The dimensions of these microchannels can be manipulated to control the number of axons entering a given channel. The application of precise strains and strain rates believed to be within those experienced during TBI has been demonstrated and characteristic injury responses observed. These axonal responses to uniaxial strain injury demonstrate device fidelity and microtubule responses to injury along the length of the axon vary according to the applied strain field.

In vivo models of TBI have the advantage of being able to measure electrophysiological and behavioral outcomes that are based on quantitative and semi-quantitative observations (Cernak 2005). It is however, very difficult to assess the degree of the stresses and strains being applied at the cellular level given the complex geometry, boundary conditions and material properties of brain tissue. On the other hand, *in vitro* models offer precise control over the environment, amount of injury that is imposed and allow for dynamic measurements of injury responses (Morrison, Saatman et al. 1998; Wolf, Stys et al. 2001). Various dissociated cell culture injury models have been developed over the years that have provided very useful information on neuronal cell and axonal injury responses (Ellis, McKinney et al. 1995; Cargill and Thibault 1996; Smith, Wolf et al. 1999; Geddes and Cargill 2001; Wolf, Stys et al. 2001; Pfister, Weihs et al. 2003). However dissociated cell culture models lack the three dimensional nature of *in vivo* tissue where cell morphology, viability, ECM synthesis and cytokine production

can affect injury responses. Thus the use of organotypic slices is an ideal compromise between *in vivo* and *in vitro* models (Sundstrom, Morrison et al. 2005). Organotypic slices retain their tissue and cellular architecture that are specific to that brain region, as demonstrated in this study and others where the layers and relative arrangement of pyramidal and granule neurons in hippocampal slices are maintained for relatively long periods (Morrison, Cater et al. 2006; Berdichevsky, Sabolek et al. 2009). The use of organotypic slice cultures in strain injury is valuable for monitoring overall slice health and electrophysiological changes (Cater, Gitterman et al. 2007). However it is difficult to observe changes on the axonal level, since they are not easily accessible to microscopic techniques unless injection methods are used which prohibits the long-term study of axonal changes following injury. These organotypic slices do extend axons, if placed on an extension permissive substrate, and our lab has shown that these axons make functional connections to an adjacent organotypic slice (Berdichevsky, Sabolek et al. 2009; Berdichevsky, Staley et al. 2010). This demonstrates that these extending axons are healthy and fully functional and may represent a more physiologically relevant DAI model than pure dissociated cell culture models. Having a fully functional connection between two organotypic slices before injury will allow researchers to investigate the effects of strain injury on slice-to-slice communication. For the purpose of this study, i.e. characterizing the strain injury device, we chose hippocampus-hippocampus connections, however by incorporating different organotypic slices, the effects of strain injury could be tested on various functional pathways found to be affected during TBI events *in vivo*. Some other pathways that could be included are the entorhinal cortex-hippocampal pathway (Del Turco and Deller 2007), septo-hippocampal projections (Fischer, Gahwiler et al. 1999) and thalamocortical pathways (Molnar and Blakemore 1999). Another reason for incorporating different organotypic slices is due to the fact that various brain regions have different material properties which may significantly affect

their response to injury (Elkin and Morrison III 2007). Thus to combine the advantages of an organotypic slice culture system that maintains the *in vivo* tissue structure with the capability of monitoring single axon molecular and functional responses to strain injury in real-time could prove to be a powerful tool for studying TBI responses.

TBI is generally divided into the broad categories of mild, moderate or severe (Saatman, Duhaime et al. 2008) with DAI being the most common mechanism of injury in all three of these categories, occurring in up to 50% of TBI cases (Smith 2000; Meythaler, Peduzzi et al. 2001). It is believed that during non-contact inertial TBI events, brain tissue is subjected to strains in the order of 10-50% and at strain rates as high as 50s⁻¹ (Margulies, Thibault et al. 1990; Morrison, Meaney et al. 1998). These wide ranging boundaries are most likely one of the reasons why we see DAI being manifested at all levels of TBI. We have designed our device such that our applied strains span those believed to produce damage during these events, i.e. a low (11%), an intermediate (25%) and a high applied strain (42%). Our device could be modified to generate higher strains with a slight modification, i.e. a linear actuator capable of producing higher pressures. Our strain rates that are applied in this study fall within the lower half of the range shown to produce damage. However, in a comprehensive study conducted by Morrison and colleagues that applied varying strains (5-50%) and strain rates (0.1-50s⁻¹) to organotypic hippocampus slices, they showed that injury response was more dependent on strain than on strain rate (Cater, Sundstrom et al. 2006).

The strain applied by this device matches very well with the geometric relationship equation used by Smith and colleagues. This relationship is quite robust given the fact that the material stiffness's and thickness' are different between the two models. In our

strain device, this relationship predicts strain within 1% at the higher end and within 3% at the lower applied strain. In the longitudinal deflection profile seen in Figure 2.4B small ridges are seen in the two opposing ends of the 14.5psi profile. These seem to be edge effects due to the radius at the end of the pressure cavity, however these effects only reflect a 1.6% increase in deflection over the central stabilized portion of the device and within 7% of the length of the pressure cavity has stabilized to the maximum deflection observed in the region in which the axons extend. These edge effects are only observed at the higher pressures.

One critical comment of other uniaxial strain injury models is the verification of adhesion of cells and axonal processes to the substrate. This in part, is due to the fact that some models apply a downward deflection to the substrate on which the axons have extended (Ellis, McKinney et al. 1995; Morrison, Meaney et al. 1998; Smith, Wolf et al. 1999). Our device applies a positive pressure to a pressure cavity located beneath the basement PDMS and microchannel PDMS layers, resulting in the PDMS being deflected upwards. We do not observe any movement of axons due to the application of a strain (apart from the obvious “delayed elastic effects” observed), i.e. the axon is in the same exact position after injury as it was before injury implying that they are firmly attached to the PDMS substrate. Thus axons that are adhered to the top surface of the PDMS basement layer will be forced upwards and experience similar strains as that of the PDMS on which they have adhered.

The mechanical stiffness / properties of the PDMS are of utmost importance due to the fact that this is what dictates the strain that is experienced when exposed to a positive pressure. Thus the manufacture of the PDMS basement and microchannel layers is a

very important and controlled step in the assembly of the strain device. In our hands, it was very important to be as accurate as possible with the mixing of the PDMS to crosslinker and consistent with both the degassing time and time to spincoat the PDMS since these parameters have a large influence on the viscosity of the PDMS and ultimately the final thickness of the PDMS.

The device utilizes the inherent capability of organotypic hippocampal slices to extend axons from the periphery of the slice (Berdichevsky, Sabolek et al. 2009). This extension is likely to be due to the spontaneous response to the elimination of axonal projections during the dissection procedure. The axons that extend from the periphery of the organotypic slice are unmyelinated. *In vivo* studies using a fluid percussion injury model have shown that small caliber and unmyelinated axons can be even more susceptible to TBI, particularly from a functional point of view, i.e. electrophysiologically, than larger caliber and myelinated axons (Reeves, Phillips et al. 2005). One of the advantages of our device is the ability to control the dimensions of the microchannels and thus control the number of axons entering a particular channel. We have observed that the larger the channel width the higher the probability of axons aggregating together and forming bundles. Thus this device has the capability of investigating strain injury effects on various caliber axons.

The common methods for culturing hippocampus slices incorporate either a permeable membrane on which the slices are placed or in roller tubes (Gahwiler 1984; Stoppini, Buchs et al. 1991). More recently hippocampal slices have been cultured on glass substrates (with enough media to just cover the substrate on which they are cultured) (Berdichevsky, Sabolek et al. 2009) or on elastic substrates such as PDMS (Morrison,

Meaney et al. 1998; Morrison, Cater et al. 2006; Bottlang, Sommers et al. 2007). This method has been adapted for the culture of hippocampal slices on our device with the addition of placing our strain device on a rocker in order to ensure an adequate oxygen supply to the organotypic slice (Morrison, Cater et al. 2003). This culture method allows for organotypic slices to remain healthy over a period of 22 days *in vitro* as demonstrated by the reduction in cell death over time. As expected, the highest amount of cell death (as measured using PI) is observed on day 0 immediately after slicing. This steadily decreases over time until day 11 where we observe almost no cell death. The initial decrease in cell death is consistent with the removal of dead cells by resident microglia / macrophage cells (Stence, Waite et al. 2001). The health of slices on this device is also consistent with other organotypic slice injury models that wait until slices are cultured for 14 days *in vitro* and then either mechanically or chemically injure the slices (Morrison, Cater et al. 2006; Kawalec, Kowalczyk et al. 2011). Over this initial 14 day period, the slice not only stabilizes, i.e. we observe a decrease in cell death, but also matures. This 14 day slice stabilizing period is convenient since it takes between 7-10 days for the axons to traverse the distance from one slice to the other, which can be between 2.5-3.0mm depending on how close the organotypic slice is placed to the entrance of the microchannels.

When confirming axons from one slice connecting to the adjacent slice through Dil labeling, we observed what appeared to be a number of cells to which the Dil had transferred. This was unexpected due to the fact that the dye should not have crossed over synaptic clefts since it should only diffuse down continuous membranes. However, Dil transfer has been shown to occur in immature synaptic clefts possibly due to the fact

that immature synapses come into very close contact and only upon maturity, does this gap increase (Bruce, Christensen et al. 1997).

In contrast to other uniaxial strain injury models, we observe primary axotomy occurring at peak strains of 42%. Smith and colleagues report that on their strain injury device they observe primary axotomy occurring at strains only above 65% (Smith, Wolf et al. 1999). This disparity in results could be attributed to a number of different reasons, one of them being the fact that the Smith model stretches their membrane downwards which may result in their axons not experiencing the full applied strain since they have the potential to delaminate from the substrate. Our model however applies a positive pressure beneath the axons thus stretching the axons to the full extent of the substrate strain. Another reason could be due to the fact that our device utilizes axons that extend from organotypic slices whereas their model uses dissociated cells from the NTera-2 cell line. The neuronal cell bodies from which our axons originate have a fairly rigid anchoring within the tissue being firmly embedded in extracellular matrices and surrounded by other cell bodies. Once axons have traversed the full distance and connected to the adjacent slice, a few of them seem to slightly straighten along their length. Organotypic slices have been shown to mature *in vitro* (Buchs, Stoppini et al. 1993), and with the fact that CNS tissue has also been shown to become stiffer with increasing age (Thibault and Margulies 1998), what we may be observing is a slight stiffening of axons extending from the organotypic slice (Buchs, Stoppini et al. 1993). If the axons are slightly more stiff when a strain injury is applied, slightly higher forces would be experienced that might result in primary axotomy occurring at lower applied strains. This may demonstrate that some of the axons extending within this model may be physiologically closer to those found *in vivo*. Another possible source of the difference is that they stretch the

membrane down, so the axons may not experience the full strain due to potential delamination from the substrate, however in our device, since we push against the axons, they will be stretched to the full extent of the substrate strain.

The delayed elastic effect observed on our device is similar to what has been observed in other *in vitro* uniaxial strain injury models (Smith, Wolf et al. 1999). This response is due to a breakdown in microtubules following high rates of strain injury that lead to misalignment of individual microtubules within the bundle resulting in them not being able to slide freely over one another (Tang-Schomer, Patel et al. 2010). This delay in the axon returning to its original length once the applied strain has been removed results in the oscillations observed along the axon length. This strain induced microtubule damage correlates to the observation of an increase in the number of axonal beads occurring in areas of delayed elasticity. This increase in axonal beading also correlates to more rapid axonal degradation occurring in these areas as seen by the amount of degradation occurring within four hours (Figure 2.11A vi). The return to the original axonal length within 50minutes is comparable to that seen in other *in vitro* models (Smith, Wolf et al. 1999; Tang-Schomer, Patel et al. 2010).

Kilinc and colleagues have suggested that mechanoporation (axonal plasma membrane permeability) may be an initiating event that results in axonal beading and the influx of calcium (Kilinc, Gallo et al. 2008). Their model uses a fluid shear stress to induce injury where they observe significant amounts of Lucifer Yellow (480Da) entering axons following injury. In our model, we observed no axonal plasma membrane permeability to molecules 622Da (calcein) and larger following injury, i.e. to all three applied strains (data not shown). However we demonstrate that there is indeed a breakdown in

microtubules. The effect of strain injury on microtubules appears to be dependent on the degree of strain that is applied. In the region in which peak strain is experienced, i.e. in the central portion of the pressure cavity, we observe significant microtubule breakdown as compared to regions of low strain, i.e. at the edges of the pressure cavity, where little to no microtubule breakdown is seen. This was confirmed by β - tubulin staining of cultures within 4 hours following strain injury. In low strain regions we observe constant intensity fluorescent staining along the length of both single axons and larger axon bundles. Whereas in regions of peak strain we observe sections of either no fluorescence, indicating a breakdown in microtubules, or pockets of high fluorescence, indicating an accumulation of microtubules typically found in axonal beads.

In regions where delayed elasticity occurs, we observe some unraveling of axon bundles at specific locations along the bundle. In these sections one or more axons return to their original length while surrounding axons undergo delayed elasticity. It appears that axonal bundles that form either do not completely bind along the full length of the bundle or the elastic recoil force inherent to the axon exceeds the binding force of the axon to the rest of the bundle. This unraveling is however only occasionally seen at the higher applied strain.

One potential application of this model is to assess how various strain injuries affect action potential propagation between two organotypic slices. This would be accomplished through the incorporation of multiple electrode arrays into the device (Berdichevsky, Sabolek et al. 2009; Yu, Graudejus et al. 2009). This strain injury device could prove to be particularly useful in elucidating mechanisms involved in TBI induced alterations in axonal action potential propagation, since TBI induced epilepsy is the most

common form of acquired epilepsy with almost half of people experiencing a severe TBI event succumbing to bouts of epilepsy (Lowenstein 2009).

2.6 References

- Alberts, B., A. Johnson, et al. (2002). "Molecular Biology of the Cell, 4th Edition."
- Andriessen, T. M., B. Jacobs, et al. (2010). "Clinical characteristics and pathophysiological mechanisms of focal and diffuse traumatic brain injury." J Cell Mol Med **14**(10): 2381-2392.
- Berdichevsky, Y., H. Sabolek, et al. (2009). "Microfluidics and multielectrode array-compatible organotypic slice culture method." J Neurosci Methods **178**(1): 59-64.
- Berdichevsky, Y., K. J. Staley, et al. (2010). "Building and manipulating neural pathways with microfluidics." Lab Chip **10**(8): 999-1004.
- Bottlang, M., M. B. Sommers, et al. (2007). "Modeling neural injury in organotypic cultures by application of inertia-driven shear strain." J Neurotrauma **24**(6): 1068-1077.
- Bruce, L. L., M. A. Christensen, et al. (1997). "Electron microscopic differentiation of directly and transneuronally transported Dil and applications for studies of synaptogenesis." J Neurosci Methods **73**(1): 107-112.
- Buchs, P. A., L. Stoppini, et al. (1993). "Structural modifications associated with synaptic development in area CA1 of rat hippocampal organotypic cultures." Brain Res Dev Brain Res **71**(1): 81-91.
- Cargill, R. S., 2nd and L. E. Thibault (1996). "Acute alterations in $[Ca^{2+}]_i$ in NG108-15 cells subjected to high strain rate deformation and chemical hypoxia: an in vitro model for neural trauma." J Neurotrauma **13**(7): 395-407.
- Cater, H. L., D. Gitterman, et al. (2007). "Stretch-induced injury in organotypic hippocampal slice cultures reproduces in vivo post-traumatic neurodegeneration: role of glutamate receptors and voltage-dependent calcium channels." J Neurochem **101**(2): 434-447.
- Cater, H. L., L. E. Sundstrom, et al. (2006). "Temporal development of hippocampal cell death is dependent on tissue strain but not strain rate." J Biomech **39**(15): 2810-2818.
- Cernak, I. (2005). "Animal models of head trauma." NeuroRx **2**(3): 410-422.

- Coronado, V. G., L. Xu, et al. (2011). "Surveillance for traumatic brain injury-related deaths--United States, 1997-2007." MMWR Surveill Summ **60**(5): 1-32.
- Del Turco, D. and T. Deller (2007). "Organotypic entorhino-hippocampal slice cultures--a tool to study the molecular and cellular regulation of axonal regeneration and collateral sprouting in vitro." Methods Mol Biol **399**: 55-66.
- Elkin, B. S. and B. Morrison III (2007). "Region-specific tolerance criteria for the living brain." Stapp Car Crash Journal **51**: 127-138.
- Ellis, E. F., J. S. McKinney, et al. (1995). "A new model for rapid stretch-induced injury of cells in culture: characterization of the model using astrocytes." J Neurotrauma **12**(3): 325-339.
- Fischer, Y., B. H. Gahwiler, et al. (1999). "Activation of intrinsic hippocampal theta oscillations by acetylcholine in rat septo-hippocampal cocultures." J Physiol **519 Pt 2**: 405-413.
- Frantseva, M. V., L. Kokarovtseva, et al. (2002). "Ischemia-induced brain damage depends on specific gap-junctional coupling." J Cereb Blood Flow Metab **22**(4): 453-462.
- Gahwiler, B. H. (1984). "Slice cultures of cerebellar, hippocampal and hypothalamic tissue." Experientia **40**(3): 235-243.
- Geddes, D. M. and R. S. Cargill, 2nd (2001). "An in vitro model of neural trauma: device characterization and calcium response to mechanical stretch." J Biomech Eng **123**(3): 247-255.
- Gennarelli, T. A., L. E. Thibault, et al. (1989). "Axonal injury in the optic nerve: a model simulating diffuse axonal injury in the brain." J Neurosurg **71**(2): 244-253.
- Gittes, F., B. Mickey, et al. (1993). "Flexural rigidity of microtubules and actin filaments measured from thermal fluctuations in shape." J Cell Biol **120**(4): 923-934.
- Iwata, A., P. K. Stys, et al. (2004). "Traumatic axonal injury induces proteolytic cleavage of the voltage-gated sodium channels modulated by tetrodotoxin and protease inhibitors." J Neurosci **24**(19): 4605-4613.

- Kawalec, M., J. E. Kowalczyk, et al. (2011). "Neuroprotective potential of biphalin, multireceptor opioid peptide, against excitotoxic injury in hippocampal organotypic culture." Neurochem Res **36**(11): 2091-2095.
- Kilinc, D., G. Gallo, et al. (2008). "Mechanically-induced membrane poration causes axonal beading and localized cytoskeletal damage." Exp Neurol **212**(2): 422-430.
- Lowenstein, D. H. (2009). "Epilepsy after head injury: an overview." Epilepsia **50 Suppl 2**: 4-9.
- Margulies, S. S., L. E. Thibault, et al. (1990). "Physical model simulations of brain injury in the primate." J Biomech **23**(8): 823-836.
- Mata, A., A. J. Fleischman, et al. (2005). "Characterization of polydimethylsiloxane (PDMS) properties for biomedical micro/nanosystems." Biomed Microdevices **7**(4): 281-293.
- Meaney, D. F. and L. E. Thibault (1990). "Physical model studies of cortical brain deformation in response to high strain rate inertial loading." In: International Conference on the Biomechanics of Impacts. Lyon, France: IRCOBI: 215- 224.
- Meythaler, J. M., J. D. Peduzzi, et al. (2001). "Current concepts: diffuse axonal injury-associated traumatic brain injury." Arch Phys Med Rehabil **82**(10): 1461-1471.
- Molnar, Z. and C. Blakemore (1999). "Development of signals influencing the growth and termination of thalamocortical axons in organotypic culture." Exp Neurol **156**(2): 363-393.
- Morrison, B., 3rd, H. L. Cater, et al. (2006). "An in vitro model of traumatic brain injury utilising two-dimensional stretch of organotypic hippocampal slice cultures." J Neurosci Methods **150**(2): 192-201.
- Morrison, B., 3rd, H. L. Cater, et al. (2003). "A tissue level tolerance criterion for living brain developed with an in vitro model of traumatic mechanical loading." Stapp Car Crash J **47**: 93-105.
- Morrison, B., 3rd, B. S. Elkin, et al. (2011). "In vitro models of traumatic brain injury." Annu Rev Biomed Eng **13**: 91-126.
- Morrison, B., 3rd, D. F. Meaney, et al. (1998). "Mechanical characterization of an in vitro device designed to quantitatively injure living brain tissue." Ann Biomed Eng **26**(3): 381-390.

- Morrison, B., 3rd, K. E. Saatman, et al. (1998). "In vitro central nervous system models of mechanically induced trauma: a review." J Neurotrauma **15**(11): 911-928.
- Murphy, M. C. and E. A. Fox (2007). "Anterograde tracing method using Dil to label vagal innervation of the embryonic and early postnatal mouse gastrointestinal tract." J Neurosci Methods **163**(2): 213-225.
- Pfister, B. J., T. P. Weihs, et al. (2003). "An in vitro uniaxial stretch model for axonal injury." Ann Biomed Eng **31**(5): 589-598.
- Povlishock, J. T. and D. P. Becker (1985). "Fate of reactive axonal swellings induced by head injury." Lab Invest **52**(5): 540-552.
- Reeves, T. M., L. L. Phillips, et al. (2005). "Myelinated and unmyelinated axons of the corpus callosum differ in vulnerability and functional recovery following traumatic brain injury." Exp Neurol **196**(1): 126-137.
- Saatman, K. E., A. C. Duhaime, et al. (2008). "Classification of traumatic brain injury for targeted therapies." J Neurotrauma **25**(7): 719-738.
- Sia, S. K. and G. M. Whitesides (2003). "Microfluidic devices fabricated in poly(dimethylsiloxane) for biological studies." Electrophoresis **24**(21): 3563-3576.
- Smith, D. H., D. F. Meaney, et al. (2003). "Diffuse axonal injury in head trauma." J Head Trauma Rehabil **18**(4): 307-316.
- Smith, D. H., Meaney, D.F (2000). "Axonal Damage in Traumatic Brain Injury." Neuroscientist **6**(6): 483-495.
- Smith, D. H., J. A. Wolf, et al. (1999). "High tolerance and delayed elastic response of cultured axons to dynamic stretch injury." J Neurosci **19**(11): 4263-4269.
- Stence, N., M. Waite, et al. (2001). "Dynamics of microglial activation: a confocal time-lapse analysis in hippocampal slices." Glia **33**(3): 256-266.
- Stoppini, L., P. A. Buchs, et al. (1991). "A simple method for organotypic cultures of nervous tissue." J Neurosci Methods **37**(2): 173-182.

- Strich, S. J. (1961). "Shearing of nerve fibers as a cause of brain damage due to head injury." Langmuir **1**: 443-448.
- Sundstrom, L., B. Morrison, 3rd, et al. (2005). "Organotypic cultures as tools for functional screening in the CNS." Drug Discov Today **10**(14): 993-1000.
- Tang-Schomer, M. D., A. R. Patel, et al. (2010). "Mechanical breaking of microtubules in axons during dynamic stretch injury underlies delayed elasticity, microtubule disassembly, and axon degeneration." FASEB J **24**(5): 1401-1410.
- Tate, D. F. and E. D. Bigler (2000). "Fornix and hippocampal atrophy in traumatic brain injury." Learn Mem **7**(6): 442-446.
- Thibault, K. L. and S. S. Margulies (1998). "Age-dependent material properties of the porcine cerebrum: effect on pediatric inertial head injury criteria." J Biomech **31**(12): 1119-1126.
- Tomei, G., D. Spagnoli, et al. (1990). "Morphology and neurophysiology of focal axonal injury experimentally induced in the guinea pig optic nerve." Acta Neuropathol **80**(5): 506-513.
- Wolf, J. A., P. K. Stys, et al. (2001). "Traumatic axonal injury induces calcium influx modulated by tetrodotoxin-sensitive sodium channels." J Neurosci **21**(6): 1923-1930.
- Yu, Z., O. Graudejus, et al. (2009). "Monitoring hippocampus electrical activity in vitro on an elastically deformable microelectrode array." J Neurotrauma **26**(7): 1135-1145.

Chapter 3 Characterizing and Quantifying Axonal Responses to In Vitro Uniaxial Strain Injuries

3.1 Introduction

As many as half of hospital-admitted traumatic brain injury (TBI) patients experience events associated with diffuse axonal injury (DAI), making it the most common form of TBI (Meythaler, Peduzzi et al. 2001). This form of injury is primarily due to axons being strained due to inertial forces experienced during rapid rotation of the brain (Smith 2000). These injuries are sustained primarily due to the viscoelastic nature of brain tissue, where during non-injurious brain accelerations the tissue behaves elastically, whereas at high accelerations it resists being strained in a viscous manner. The dynamic nature of these injuries occurs when forces are applied in less than 50 milliseconds (Gennarelli and Meaney 1996). The initial physical trauma results in a primary injury that is physical, but in addition to this secondary injury responses are initiated.

The result of the primary injury is a breakdown in axonal cytoskeleton, in particular microtubules (Tang-Schomer, Patel et al. 2010). Since the majority of axonal transport occurs along microtubules, this results in the interruption of the transport of vital proteins and organelles to distal sections of the axon. This interruption results in an accumulation of transport products that produces a swelling of the axon commonly referred to as an axonal bead. These beads are observed both *in vivo* and *in vitro* (Gennarelli, Thibault et al. 1989; Kilinc, Gallo et al. 2008; Tang-Schomer, Patel et al. 2010). The accumulation of fast axonally transported proteins, such as amyloid precursor protein (APP), within these beads are hallmarks of DAI (Povlishock and Christman 1995; Smith, Chen et al. 1999). Excitotoxicity and the activation of mechanosensitive channels are some of the secondary injury effects that are initiated following injury (Wolf, Stys et al. 2001; Morrison, Elkin et al. 2011). These effects can result in a number of molecular changes that can ultimately lead to cell death.

It is generally accepted that the primary trauma is irreversible, but the secondary mechanisms that occur subsequent can be minimized through the intervention of therapeutics. However there is currently no “standard treatment” protocol for these secondary effects of TBI and with almost one third of all injury related deaths in the US attributed to a TBI related incident, finding relevant therapies is of utmost importance (Coronado, Xu et al. 2011).

What are needed are more physiologically relevant injury models that will allow for appropriate therapeutics to be tested. In previous work done by our lab, we developed a strain injury model that allows researchers to observe and investigate the effects of injury at the axonal level while remaining part of a more physiological tissue structure (Dolle, Morrison et al. 2012). This model incorporates the use of organotypic hippocampal slices that extend axons from their periphery. These axons thus originate from cell bodies that are deep within the tissue surrounded by natural extracellular matrix proteins and support cells. The growth / extension of these axons are guided through the use of microfluidic channels to extend over a pressure cavity, that when inflated exerts a strain injury. These axons are directed towards an adjacent organotypic slice to allow for slice-to-slice communication (Berdichevsky, Sabolek et al. 2009). This model thus incorporates the advantages of organotypic slice cultures and the ability to observe in real-time and over long-term morphological, molecular and functional changes in axons following a strain injury. With this device we demonstrated characteristic phenotypic responses to strain injury which included axonal beading and delayed elastic effects (Smith, Wolf et al. 1999; Kilinc, Gallo et al. 2008). Although these responses are common to DAI, we feel that there is a need to better understand the response of axons to the dynamic nature of the injury by quantifying how they vary according to different applied strain injuries. In this study we will also look at the molecular events, i.e. changes in cytoskeleton and axonal transport, which may be occurring that account for the morphological changes observed. These events are all trademarks of axonal degradation (Koike, Yang et al. 2008). Mitochondrial membrane potential (MMP) is a key indicator of mitochondrial function and can be used to assess potential mechanisms that play a role in axonal degradation

(Mazzeo, Beat et al. 2009; Perry, Norman et al. 2011). We will thus assess the effects of strain injury on MMP at the axonal level

In the present study we report the response of hippocampal axons to increasing degrees of uniaxial strain injury with respect to axonal bead formation, delayed elasticity and microtubule degradation. We report how their response to injury is further dependant on axonal diameter. These injury responses correspond to the extent of axonal degradation observed at the various strain injuries. We also reveal a threshold that exists in applied strain injury on axonal MMP response, where at lower applied strains hyperpolarization occurs whereas at higher applied strains depolarization occurs. We show that the NHE-1 inhibitor EIPA significantly attenuates these changes in MMP and resultant axonal degradation and has similar effects as CsA demonstrating a potential new DAI therapeutic.

3.2 Materials and Methods

3.2.1 Organotypic Hippocampus Slice Isolation

The brains of Sprague-Dawley rat pups (Taconic, NY) between the ages of 4 to 6 days old were removed and placed in ice cold Gey's Balanced Salt Solution (Sigma-Aldrich Corp, MO) supplemented with 10mM D-glucose (Sigma-Aldrich Corp, MO) and 3 μ M Kynurenic Acid (Sigma-Aldrich Corp, MO). The hippocampi are separated from the surrounding cortex and sliced into 400 μ m thick slices using a McIlwain Tissue Chopper (Vibratome, IL). The slices were carefully placed into PDMS (Sylgard 184, Fischer Scientific, MA) mini-wells and orientated such that the CA1 region was facing the dentate gyrus region of the adjacent slice, i.e. these regions were facing the microchannels. The well was filled with 450 μ l of serum containing media (1:1:2 of heat inactivated horse serum, Hanks Balanced Salt Solution, Basal Medium Eagle, supplemented with 0.5mM L-Glutamine, 30 μ g/ml gentamycin and 10mM HEPES, all from Invitrogen, CA), i.e. enough media to cover the exposed basement PDMS area. The cultures were placed on a rocker (approximately 1 revolution/60s) in a humidified 5% CO₂ incubator. After 24hours the media was changed to a serum free media (Neurobasal A, 1X B27, 0.5mM L-glutamine, 30 μ g/ml gentamycin and 10mM HEPES, all from Invitrogen CA). Thereafter, half of the media was changed every 48hours.

3.2.2 Strain device

Schematic representations of the strain device are shown in Figure 2.1. Figure 2.1A depicts the overall functioning of the device where two organotypic slices are placed on a flexible substrate called polydimethylsiloxane (PDMS), and over a period of time, axons extend from the periphery of the slice. The extensions of these axons are guided down PDMS microchannels where they eventually exit and connect to the adjacent hippocampal slice. Under the microchannel section of the device is a cavity, that when pressurized, deflects upwards causing the PDMS to elongate thus producing a uniaxial strain. This pneumatic pressure is produced by coupling to a pressure

injection system that consists of a syringe (Becton Dickinson, NJ), linear actuator (PS01-23x80 - Lin Mot Inc, WI), controller (E100-MT - Lin Mot Inc, WI), a pressure sensor (Honeywell International, NJ) and a high speed sampling system (USB-5132 - National Instruments Corporation, TX). The linear actuator and controller are coupled to the inlet port on the device and controlled by a visual basic program. A pressure sensor is coupled to the pneumatic cavity and attached to a high speed digitizer that is controlled by a Labview program (National Instruments Corporation, TX). The injected volume and rate of injection are varied to produce a variety of strains and rate of strain.

The device consists of two layers of PDMS. The first layer (referred to as the basement PDMS layer) is the layer on which the organotypic slices are placed and axons extend, and the second layer is the microchannel layer on which axons extending from the periphery of the organotypic hippocampal slices are guided to grow between the two slices. The basement and microchannel PDMS thicknesses are $75\pm 5\mu\text{m}$ and $71\pm 5\mu\text{m}$ respectively. The microchannel dimensions used were $50\mu\text{m}$ (microchannel width) \times $6\mu\text{m}$ (microchannel height) \times $50\mu\text{m}$ (microchannel spacing). The microchannel PDMS is cut into 22mm diameter circles with 3mm mini-wells punched at a spacing of 2mm from each other with a media access channel leading to each of the mini-wells. In order to reduce media evaporation, a semi-permeable membrane (permeable to O_2 and CO_2 but not permeable to H_2O , ALA Scientific Instruments, NY) was placed over the PDMS media barrier and sealed with an O-ring.

Three different uniaxial strains were applied to axons extending through the microchannel sections. These were approximately 10%, 25% and 45%. The time to reach maximum deflection for each of the three strains was kept constant at approximately 22ms.

3.2.3 Axonal beading analysis

Axons within a particular microchannel are analyzed for axonal beading after injury. The criteria for beading are: has to be at least one diameter larger than the surrounding axon diameter and the beading has to grow in size for multiple time points (this minimizes the inclusion of transportation of large organelles down the length of the axon which may appear to be an injury induced bead). The beading is normalized to the length of the axon within the pressure cavity section, i.e. per 100 μ m of axon length. The diameters of analyzed axons are measured at 10-15 discrete positions along the length of the axon and then averaged.

3.2.4 Delayed elasticity analysis

The delayed elastic effect, i.e. the “waves” / oscillations that occur along the length of the axon post strain injury, are normalized to 100 μ m axon length, and reported as a % increase in length. Axons are imaged before and post injury and any localized oscillation is included in the calculations. The number of oscillations along the axon is noted and normalized to the number occurring per 100 μ m. The amplitude of these oscillations is measured from the centerline of the axon before injury to the centerline of the axon post injury and normalized to the axon diameter. The diameters of analyzed axons are measured at 10-15 discrete positions along the length of the axon and then averaged.

3.2.5 Axonal degradation analysis

Between 15-20 microchannels were selected to be analyzed for a given strain experiment. These microchannels are selected on the basis of the number of axons that are within the channel and that there is no cell migration. Only the area within the pressurized section was analyzed. Phase contrast images were taken and saved using a computer interfaced inverted Olympus IX81 DSU microscope (Olympus, NJ). The microscope is controlled by SlidebookTM software (Olympus, NJ). Each microchannel is split into 11 sections which is the number of 40X objective images it

takes to traverse the pressurized area (each image is approximately 180 μ m x 180 μ m). Images were taken before applying a uniaxial strain injury and 1hr, 2hrs, 4hrs, 9hrs and 24hrs post injury. Each image position along every microchannel is saved in Slidebook™ and at each subsequent time point recalled and reimaged thus allowing for each section of axon to be compared over time. The numbers of axons entering and exiting a particular microchannel are counted before injury. If at any section along the length of the axon there is no longer a visible outline of an axon, and no mitochondrial activity (JC-1 fluorescence), this is seen as an axon that has undergone degeneration. This is normalized to the total number of axons and reported as a %.

3.2.6 Monitoring changes in mitochondrial membrane potential

The changes in axonal MMP due to applied uniaxial strains are monitored using the JC-1 dye (5,5',6,6'-tetrachloro-1,1',3,3'-tetraethylbenzimidazolylcarbocyanine iodide) (Invitrogen, CA). This dye exhibits a fluorescence shift between green (~525nm) and red (~590nm) depending on the MMP. Polarized mitochondria are marked by punctate orange-red fluorescent staining which is due to the formation of red fluorescent J-aggregates. When mitochondria depolarize, the red aggregate color is replaced by a diffuse green monomer fluorescence. Thus a depolarization is indicated by a decrease in the red/green fluorescence intensity ratio. A decrease in this fluorescence intensity ratio was thus interpreted as a decrease in MMP and an increase in this ratio an increase in MMP (Trojan, Gilman et al. 1997; Xu, Wang et al. 2001). This ratio allows for comparing changes in membrane potential between different conditions and over time. The ratio of green to red fluorescence is dependant only on the membrane potential and not on other mitochondrial changes such as size, shape and density that typically influence single component indicators. Fluorescent images were acquired using a computer interfaced inverted Olympus IX81 DSU microscope (Olympus, NJ). The microscope is controlled by Slidebook™ software (Olympus, NJ). Axons were excited using 488nm and 590nm filters and the same exposure time was used for all experiments. Axons were incubated with 2mM JC-1 for 30mins in serum free

media on a rocker. This is followed by 2 washes in serum free media for 10mins each. The cultures are allowed to equilibrate for a 90min period before taking initial images.

Between 15-20 microchannels were selected to be analyzed for a given strain experiment. These microchannels are selected on the basis of the number of axons that are within the channel and that there is no cell migration. Only the area within the pressurized section was analyzed, i.e. 2mm. Each microchannel is split into 11 sections (a 40X objective viewing area). Images were taken before applying a uniaxial strain injury, immediately after injury (0hr), and 1hr, 2hrs, 4hrs, 9hrs and 24hrs post injury. Each image position along every microchannel is saved in Slidebook™ and at each subsequent time point recalled and reimaged at both fluorescent intensities. In order to account for any changes in MMP due to temperature changes during imaging or strain injury device attachment, uninjured controls were monitored over a 24 hour period. As a positive control 10μM of carbonyl cyanide p-(trifluoromethoxy) phenylhydrazone (FCCP - a potent protonophore and uncoupler of oxidative phosphorylation) (Sigma-Aldrich Corp, MO) was added to cultures for 10mins for a controlled depolarization.

3.2.7 CsA and EIPA treated conditions

Cyclosporin A – mitochondrial permeability transition pore inhibitor

The original clinical use of cyclosporin A (CsA) is as an immunosuppressant normally reserved for organ transplants in order to reduce the effects of organ rejection (Sullivan, Sebastian et al. 2011). However, its inhibitory effect on the mitochondrial permeability transition pore (mPTP) is an important side effect and potentially another clinical use (currently undergoing late stage clinical trials). It has been shown that CsA binds to cyclophilin D, which forms part of the mPTP, and inhibits the calcineurin phosphatase pathway. The effects of CsA on MMP, using the JC-1 dye (see monitoring changes in MMP methods above), and axonal degradation (24hrs post strain injury - see axonal degradation methods above) were assessed. CsA was administered at 1μM in serum free media 1hr before strain injury until the end of the experiment.

NHE inhibitor – inhibits sodium / proton exchanger

Sodium-hydrogen exchange (NHE) inhibitors have been shown to reduce the influx of calcium into mitochondria, inhibit the mPTP and preserve the MMP after injury (Toda, Kadono et al. 2007). More specifically the NHE1 inhibitor ethylisopropyl amiloride (EIPA) was applied in this study and its effect on MMP assessed. EIPA was administered at 10 μ M in serum free media 30mins before strain injury until the end of the experiment.

3.2.8 Immunohistochemical staining

Hippocampal slices and extending axons were fixed in 4% paraformaldehyde (Sigma-Aldrich Corp, MO) for 20 minutes. The cultures were washed three times in Tris Buffered Saline (TBS) (0.5M Tris Base, 9% NaCl, pH 7.4) for 5 minutes each, blocked and permeabilized for 1hr at room temperature using 0.1% Triton-X, 1% bovine serum albumin, 10% goat serum and TBS. Primary antibodies in TBS with 1% goat serum were then added to cultures and incubated overnight at 4°C. After washing the cultures three times with TBS for 5 minutes each, secondary antibodies in TBS were added for 1 hour at room temperature. The cultures were then washed three times with TBS for 5 minutes each and stored in PBS at 4°C for imaging. Primary antibodies used were: rabbit anti-amyloid precursor protein (APP) C-terminus IgG (Millipore, CA) at 10 μ g/ml, and mouse anti-tubulin beta III IgG1 (Millipore, CA) at 10 μ g/ml. Secondary antibodies used were: goat anti-rabbit Alexa Fluor 488 IgG (Invitrogen, CA) and goat anti-mouse Alexa Fluor 647 IgG (Invitrogen, CA). Isotype controls used were: purified rabbit IgG (Invitrogen, CA) at 10 μ g/ml and purified mouse IgG1 (BD Bioscience, CA) at 10 μ g/ml.

Fluorescent images were acquired using a computer interfaced inverted Olympus IX81 DSU microscope that was controlled using SlidebookTM software (Olympus, NJ). Axons were excited using 488nm and 647nm filters and the same exposure time was used for all experiments.

3.2.9 Data Analysis

Data are represented as means \pm SE, and significance is calculated using Student's *t*-test and

P < 0.05 was regarded as significant.

3.3 Results

3.3.1 Axonal beading

In order to better understand the response of axons to the dynamic nature of a strain injury, we quantified axonal beading according to a number of different applied strain injuries. Using our strain injury model (Figure 2.1), the effects of three different uniaxial strains, i.e. 10%, 25% and 45%, are investigated in this study. These strains were selected on the basis that they represent the low, medium and high end of strains that have been shown to produce damage in TBI events (Margulies, Thibault et al. 1990; Meaney and Thibault 1990; Morrison, Meaney et al. 1998).

An example of axons that have been subjected to a uniaxial strain injury of 45% that have started to form axonal beads can be seen in Figure 3.1A (before injury and 4hrs after injury). The arrows highlight axonal beading occurring at multiple points along the axon after injury in the form of dense round dark structures. As the graph in Figure 3.1B shows, axonal beading is observed at all three applied strains. The number of axonal beads was quantified 4hour following strain injury and varies according to the applied strain. The number of beads occurring along the length of the axon is normalized per 100 μ m length. As expected, the number of axonal beads increases as the applied strain is increased, with an almost exponential increase ($R^2 = 0.98$).

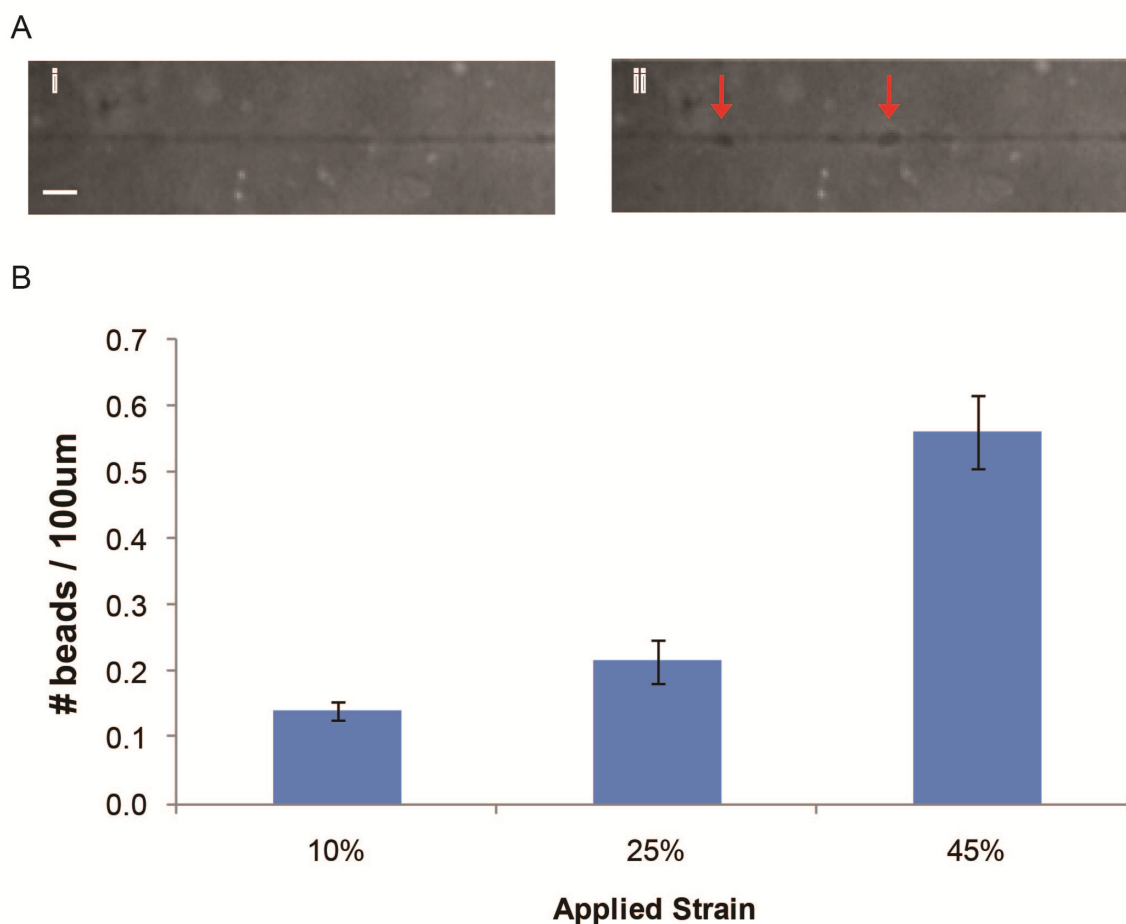


Figure 3.1. Axonal beading after uniaxial strain injury. A) Axons within a microchannel undergoing axonal beading, i) before injury, ii) 4 hours after 45% strain injury. Arrows indicate axonal beads. B) The number of beads occurring along the length of an axon is normalized per 100µm length for various applied strains, i.e. 10%, 25% and 45%. * $P < 0.05$. Scale bar, 10µm.

In addition to quantifying how axonal bead formation varied with respect to the applied strain, we investigated the effect that axonal diameter has on this response. It appears that the diameter of the axon or axon bundle plays a significant role in the response to the injury, with respect to the number of beads that form. Figure 3.2 (A-C) shows how the number of axonal beads varies with the diameter of the axon / bundle for the three different applied strains (Fig 3.2A – 10% strain, Fig 3.2B – 25% strain and Fig 3.2C – 45% strain). By grouping axon / bundle diameters into 0.4µm groups a trend emerges. For all three applied strains the lowest diameter group produces the

largest number of beads. This diameter group is generally where individual axons would be found (Westrum and Blackstad 1962). As the axon / bundle diameter increases, so the number of beads decreases. For applied strains of 10 and 25%, no beading was observed on diameters above 1.8 μ m.

We have shown that as applied strain increases so there is a corresponding increase in the number of beads that are observed along the axon length. This response is dependent on the diameter of the axon / bundle with a decrease in the number of beads as diameter increases.

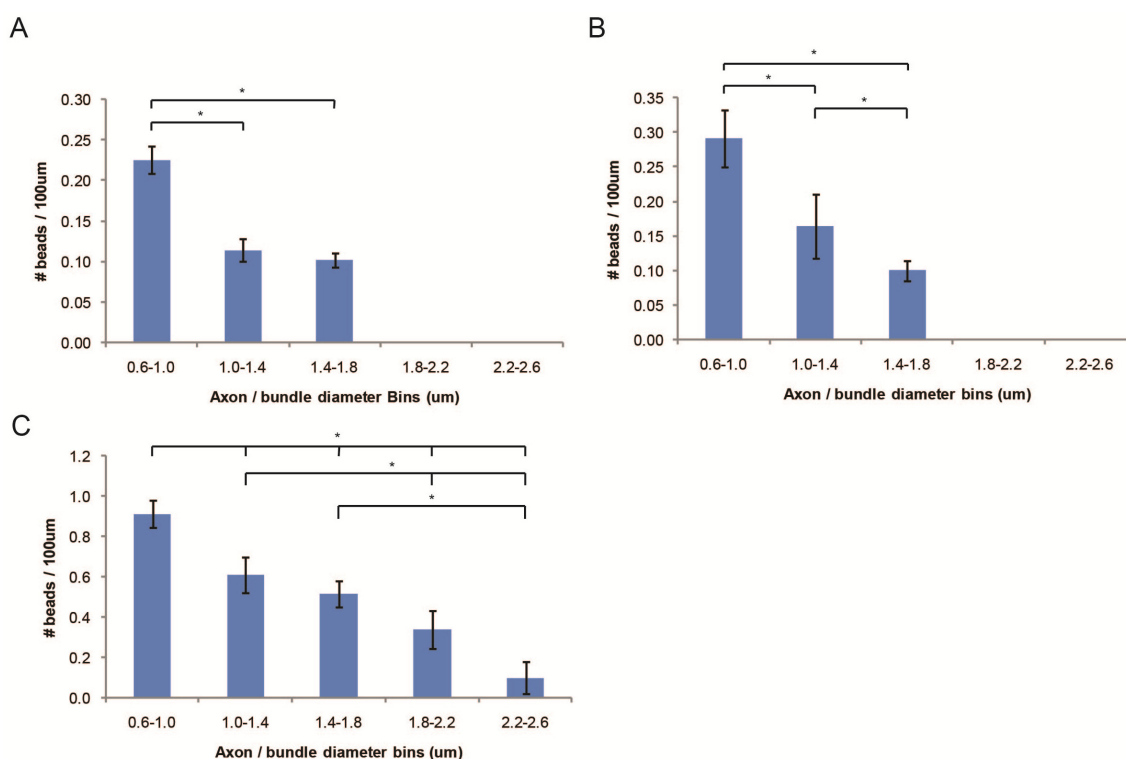


Figure 3.2. Diameter dependence of axonal beading after uniaxial strain injury. The diameter of an axon or axon bundle has been grouped together in 0.4 μ m bins from 0.6 μ m to 2.6 μ m. The number of beads occurring along the length of an axon is normalized per 100 μ m length. A) 10% applied strain, B) 25% applied strain, and C) 45% applied strain. $P < 0.05$.

3.3.2 Delayed Elasticity

The characteristic “delayed elastic” response of axons to a dynamic strain injury was also quantified. When axons are subjected to high rates of strain they have been shown to exhibit a delayed response in returning to their original length by temporarily forming “waves or oscillations” along the length of the axon (Smith, Wolf et al. 1999). These “waves” are the additional length that the axon experiences due to the applied strain injury, and over time due its elastic nature, contracts back to its original length. An example of this can be seen in Figure 3.3A (before and after a strain injury). This particular example shows an axon immediately after it has been exposed to a 45% strain injury. As the figure shows, oscillations occur at multiple points along the axon length with varying amplitudes. These oscillations result in localized increases in axonal length that when added up results in an overall increase in axonal length as compared to the original length before injury. The axons that undergo this delayed elastic response recover to their original length generally within the hour. These temporary increases in length are shown in Figure 3.3B for multiple applied strains, i.e. 10%, 25% and 45%. As the applied strain is increased, so there is a corresponding increase in this temporary elongation, i.e. ~2 %, ~4.5% and 9% when 10%, 25% and 45% strain is applied respectively. The increase in temporary length increase observed is almost proportional to the applied strain ($R^2 = 0.99$).

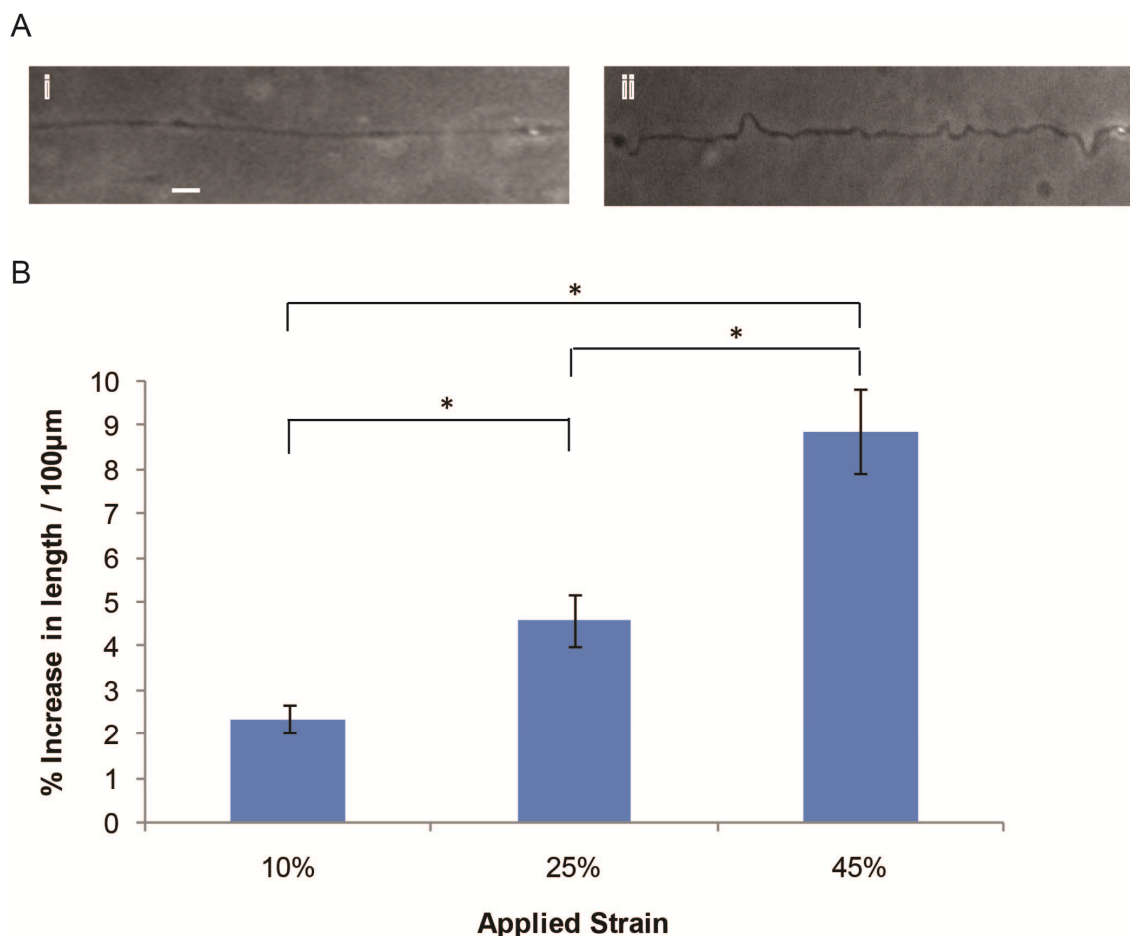


Figure 3.3. Delayed Elastic effects on axons that are strain injured. A) Example of an axon that is exposed to a 45% strain, i) before injury and ii) after injury. B) The localized increase in axon length due to delayed elasticity normalized per 100µm length for 10%, 25%, and 45% applied strain. * $P < 0.05$. Scale bar, 10µm.

We again quantified how the diameter of the axon affects the delayed elastic response to the applied strain. As observed with axonal beading, the axon / bundle diameter appears to have a significant effect on its response to an applied strain injury. By separating the axons into 0.4µm diameter bins, we can further see how diameter affects their response. Figure 3.4 shows how diameter affects different parameters within this delayed elastic effect, namely the increase in axonal length, the number of oscillations along the length of the axon (normalized to 100µm) and the amplitude of these oscillations (normalized to the axon / bundle diameter). At the lower 10%

applied strain, only axons between 1 μ m and 2 μ m experience this delayed elastic effect and we observe increases in length throughout the range of diameters (Fig 3.4A). For 25% and 45% applied strains we observe how the temporary increase in axon length following injury increases as axon / bundle diameter increases up to a peak where they then decrease. The peak in increased axon length appears to be between 2.2-2.6 μ m and 1.8-2.2 μ m for 25% and 45% applied strains respectively.

We next looked at how the number of oscillations that occur along the length of the axon may vary with axon / bundle diameter (Fig 3.4B). For the 10% applied strain there does not seem to be as significant a difference as axon / axon bundle diameter increases, however for 25% and 45% applied strains, we again see significant diameter dependence with both applied strains peaking between 1.4-2.6 μ m. The amplitude of these oscillations generally did not rely as heavily on the diameter as the other two parameters shown, i.e. apart from the higher end of the diameter spectrum (Fig 3.4C).

We have shown that as applied strain increases so there is a corresponding increase in the delayed elastic response, i.e. an increase in the temporary axon elongation. This response is dependent on the diameter of the axon with increasing diameters there is a corresponding increase in temporary elongation and the number of oscillations observed, with a decrease in oscillation amplitude.

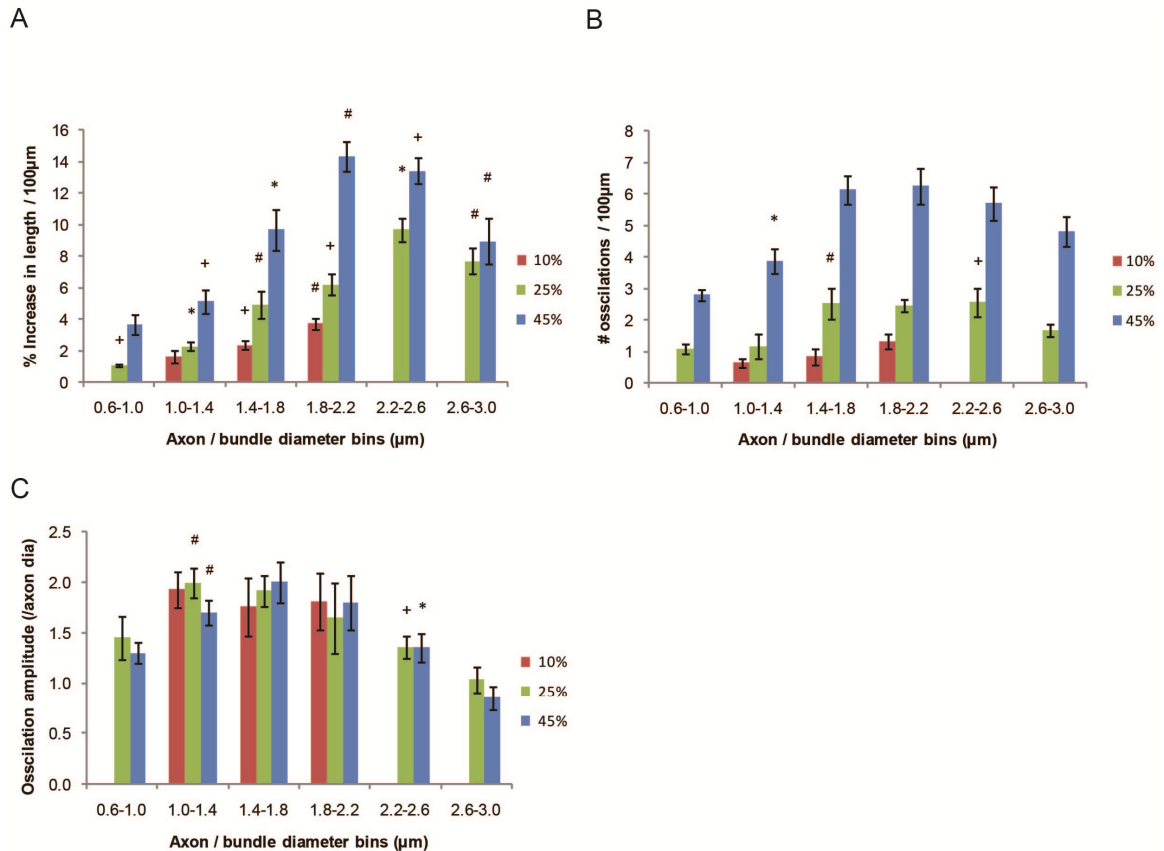


Figure 3.4. Diameter dependence for delayed elastic effects after strain injury. A) How the temporary increase in axon length varies with axon / axon bundle diameter, B) how the number of oscillations per 100μm of axon length varies with respect to axon / axon bundle diameter, and C) how the amplitude of these oscillations varies with respect to axon / axon bundle diameter. Red – 10% applied strain, green, 25% applied strain and blue – 45% applied strain. * denotes $P < 0.05$ compared to the diameter to the left and right, # denotes $P < 0.05$ compared to the diameter to the left, and + denotes $P < 0.05$ compared to the diameter to the right.

3.3.3 Cytoskeletal effects following strain injury

We next investigated some of the molecular events that may have attributed to axonal beading. Cytoskeletal components actin and microtubules form the basis for the structural integrity of the axon. Thus when an axon is subjected to a strain injury, these are the components that will resist the force and since microtubules are the stiffer of the two, they will oppose the majority of the

force (Gittes, Mickey et al. 1993; Tang-Schomer, Patel et al. 2010). If the applied force is too large, then there is a mechanical breaking that can lead to further disassembly of surrounding microtubules (Tang-Schomer, Patel et al. 2010).

Microtubules are not only structural components of the axon but also play an important role in facilitating the transport of vital proteins needed in order for the axon to function. Thus a breakdown in microtubules can lead to a disruption in axonal transport and a buildup of essential proteins, which is one of the reasons why axonal beading occurs. Figure 3.5 shows axons immunostained for β -tubulin (microtubule marker) and how microtubules breakdown over time after strain injury and how this degradation varies for different applied strains. In Fig 3.5A we see an unstrained axon with a constant level of fluorescent intensity staining along the length of the axon, even where local axonal enlargements (boutons en passant) occur (arrows). Figure 3.5B, C and D, show how microtubule degradation varies according to the applied strain, i.e. 10%, 25% and 45%, and how it varies over time, i.e. at 1hr, 4hrs and 24hrs post strain injury. For 10% applied strain, initially we see continuous fluorescence intensity staining along the axon length of with very few localized increases in intensity representing local axonal beads. By 4hrs post injury, the number and size of these beads has increased as well as some partial degradation, however by 24hrs, in the majority of cases, it appears that some beads may have decreased in size (some pockets of bright fluorescence – arrows), but no major degradation. For 25% applied strain, we see a larger number of axonal beads at 1hr post injury and by 4hrs we start to see some degradation along the length of the axon which seems to increase further by 24hrs. At the higher 45% applied strain, we see degradation occurring as early as 1hr post injury and further increasing by 4hrs with complete degradation in certain regions occurring by 24hrs post injury. We show that as both the applied strain and time after injury increases so we observe increases in both the amount of β -tubulin accumulation (beading) and degradation.

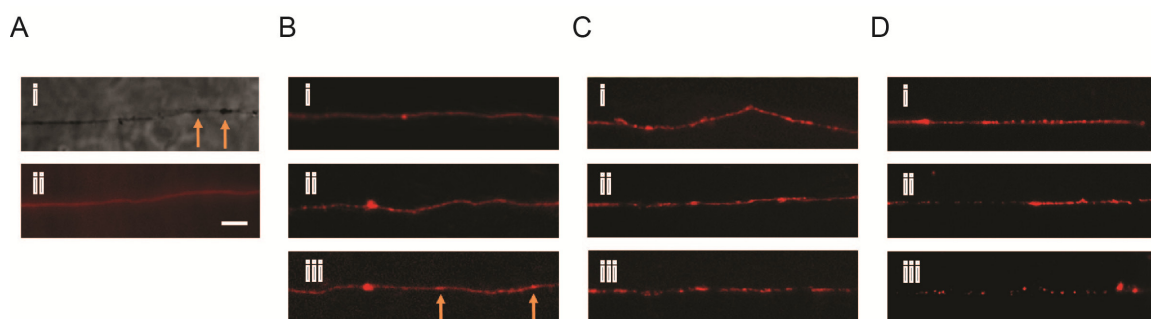


Figure 3.5. Axons stained for β -tubulin. A) Unstrained axon, i) phase contrast image, ii) β -tubulin stain, B) 10% applied strain, i) 1hr post injury, ii) 4hrs post injury, iii) 24hrs post injury, C) 25% applied strain, i) 1hr post injury, ii) 4hrs post injury, iii) 24hrs post injury, D) 45% applied strain, i) 1hr post injury, ii) 4hrs post injury, iii) 24hrs post injury. Scale bar, 10 μ m.

3.3.4 Axonal transport effects following strain injury

Another confirmation of a breakdown in axonal transport is an accumulation in certain transported proteins. Axonal transport of vesicles and organelles is carried out by motor protein driven movement along microtubules (Coleman 2005). Disruption in this axonal transport can be visualized by monitoring the transport of these vesicles and organelles. One protein that is transported along the length of axons, via vesicles, is the protein amyloid- β precursor protein (APP) (Blumbergs, Scott et al. 1994). This protein is known to be linked to fast axonal transport and therefore has been found to build up in axonal beads that form following injury. By staining for APP along the length of injured axons, we can thus further confirm the breakdown in axonal transport that occurs following a strain injury. Figure 3.6 shows APP staining in axons subjected to various strains and at various time points following injury. Figure 3.6A shows an unstrained axon (phase contrast image – Fig 3.6A i) demonstrating fairly uniform fluorescence intensity along the length of the axon (Fig 3.6A ii). Figure 3.6A iii is an enlargement of an axon segment (red box in Fig 3.6A ii) and shows the punctate staining commonly found in vesicle transport (Muresan and Muresan 2005). In the case of a 10% applied strain (Fig 3.6B), by 1hr post injury we observe an accumulation of APP (i.e. an increase in fluorescence intensity) at certain points along the length of the axon. Not all of these increases in intensity exceed the diameter of the

axon. The number of these accumulations increases by 4hrs post injury with sections showing gaps in fluorescence (i.e. an increase in distance between vesicles). By 24hrs the distance between vesicles appears to even out with some accumulations increasing in size. When 25% strain is applied (Fig 3.6C), we observe an increase in the number of accumulations by 1hr post injury, with an increase in both number and size by 4hrs, and by 24hrs, sections of no fluorescence. At the higher applied strain of 45% (Fig 3.6D), we see large sections of high concentrations of APP with sections of no fluorescence as early as 1hr post injury. By 4hrs post injury we see an increase in number and size of high concentrated areas of APP, and by 24hrs large areas of low to no fluorescence with pockets of high intensity along the length.

We again show that as both the applied strain and time after injury increases so we observe increases in the number of APP accumulation points and a decrease in the fluorescence intensity in certain regions.

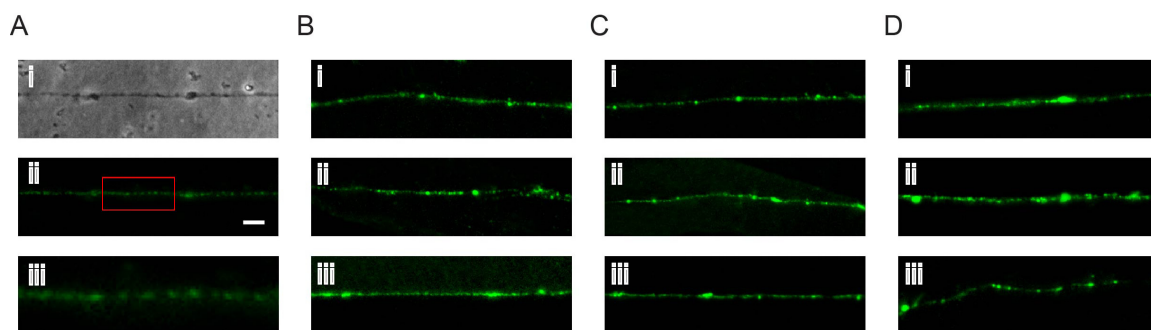


Figure 3.6. Axons stained for Amyloid- β Precursor Protein (APP). A) Unstrained axon, i) phase contrast image, ii) β -tubulin stain, iii) enlarged section of ii) (red box), B) 10% applied strain, i) 1hr post injury, ii) 4hrs post injury, iii) 24hrs post injury, C) 25% applied strain, i) 1hr post injury, ii) 4hrs post injury, iii) 24hrs post injury, D) 45% applied strain, i) 1hr post injury, ii) 4hrs post injury, iii) 24hrs post injury. Scale bar, 10 μ m.

3.3.5 Degradation

Not only is axonal beading a hallmark of DAI, but it is also a prelude to axonal degradation. The mechanical breaking of microtubules and the knock-on effect in axonal transport can ultimately lead to axonal degradation since distal portions of the axon are not receiving necessary nutrients to sustain cell function (Vargas and Barres 2007). When axonal degradation is assessed at 24hrs post strain injury, with respect to the three different applied strains, we see that the percentage of axons that undergo degradation increases with respect to the applied strain (Figure 3.7). There is almost a linear increase in degradation from 16% to 51% to 91% degradation for 10%, 25% and 45% applied strain respectively. The applied strains of 10% and 45% seem to almost represent the two ends of the spectrum, with 10% applied strain experiencing relatively minimal degradation and 45% applied strain experiencing almost complete degradation. We have shown that as applied strain increases so there is a corresponding increase in the amount of axonal degradation observed at 24hrs following injury.

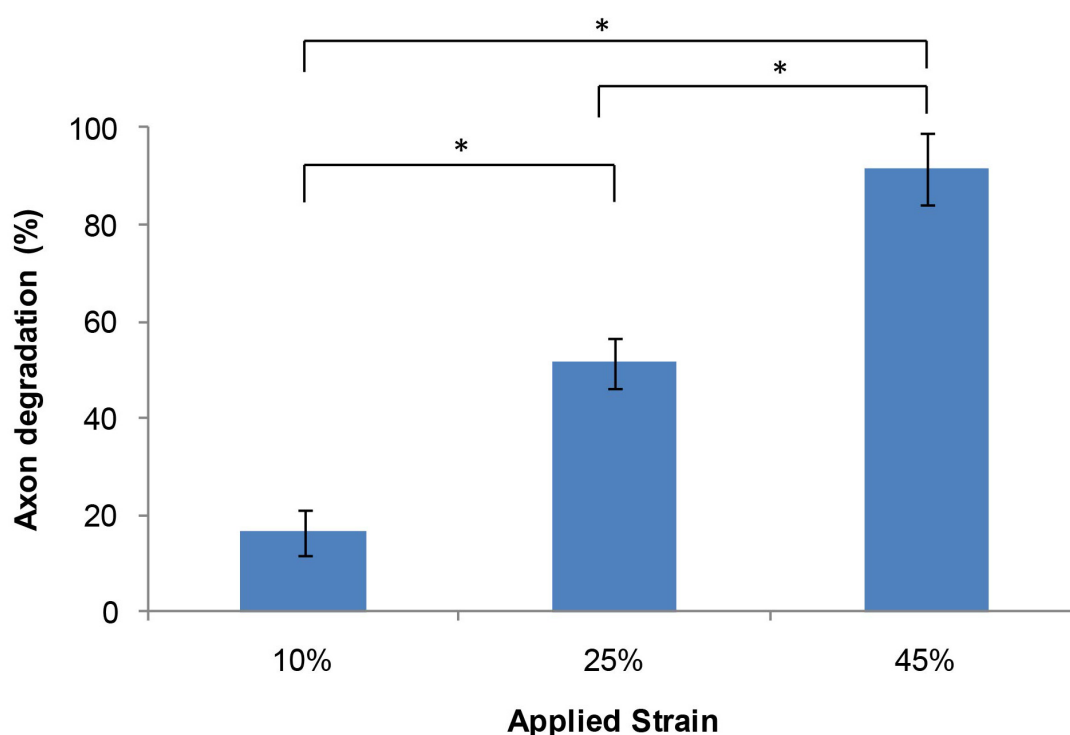


Figure 3.7. Axonal degradation assessed at 24hrs following strain injury with respect to applied strain. * $P < 0.05$.

3.3.6 Changes in mitochondrial membrane potential

Not all axonal degradation following strain injury is due to the physical breakdown in intracellular cytoskeletal structures, but also due to the influx of ions into the cell that initiate numerous intracellular pathways ultimately resulting in cell death (Morrison, Elkin et al. 2011). The influx of certain ions, particularly calcium, can lead to changes in mitochondrial function such as a collapsing of their inner membrane potential (Ahmed, Rzigalinski et al. 2000). MMP is a key indicator of mitochondrial function and can be used to assess potential mechanisms that play a role in axonal degradation (Mazzeo, Beat et al. 2009; Perry, Norman et al. 2011). This was done using the JC-1 dye that exhibits a fluorescence shift between green and red depending on the MMP. When mitochondria depolarize, there is a shift from red to green fluorescence and thus a decrease in red/green fluorescence intensity ratio.

The MMP was monitored at 11 discrete positions along the length of an axon exposed to a uniaxial strain injury and over a time course of 24 hours. The time points chosen to monitor were: before injury, immediately after injury (0hr), 1hr, 2hrs, 4hrs, 9hrs and 24hrs post injury. These membrane potentials are normalized to the membrane potential before injury, thus monitoring changes in potential following injury. To initially assess the stability of JC-1 and MMP over a 24hr period, control experiments were performed where the device went through the same process as it would for an injury except no injury was applied (Fig 3.8A). Very little change in MMP is observed over a 24hr period. A controlled depolarization was performed by adding 10 μ M of FCCP to the cultures resulting in a decrease in MMP to approximately 11% of the original fluorescence (Fig 3.8A). Figure 3.8 B-D shows how the MMP varies both along the axon length and over time for the three different applied strains of 10%, 25% and 45%. When a 10% strain is applied (Fig 3.8B) we initially see no significant change in membrane potential immediately following injury, which is consistent along the full length of the microchannel. By one hour post injury we start to observe an increase in membrane potential at the two ends of the pressure cavity, i.e. in the regions of low applied strain (positions 1-3 and 9-11). The membrane potential in these two regions continues to increase incrementally until 24hrs post injury. In the central

region (positions 4-8), over the first 4hrs post injury there are small increases. However by 9hrs post injury we observe a significant increase in membrane potential in this region, corresponding to the region in which maximal strain is experienced. By 24hrs we see a further small increase in potential. When a 25% strain is applied (Fig 3.8C) an overall similar trend is observed, however there is initially a very slight decrease in membrane potential at the outer regions (positions 1 and 10-11). Over the first 4hrs post injury we observe a slight increase in membrane potential at positions 2-9. By 9hrs post injury we observe a large increase in membrane potential particularly in the central region. By 24hrs post injury the increase in fluorescence ratio is almost 4 times the membrane potential seen before injury. When a 45% strain is applied (Fig 3.8D), we appear to have exceeded a threshold of injury and observe a dramatic decrease in membrane potential. The region of maximal decrease again corresponds to the central region where maximal strain is experienced. This decrease is observed immediately following injury and further incremental decreases are observed until 24hrs after injury.

We have shown that there appears to be a threshold of applied strain that determines either hyperpolarization or depolarization of MMP. At lower applied strains (10% and 25%) we observe an increase in MMP whereas for 45% applied strain there is a decrease in MMP.

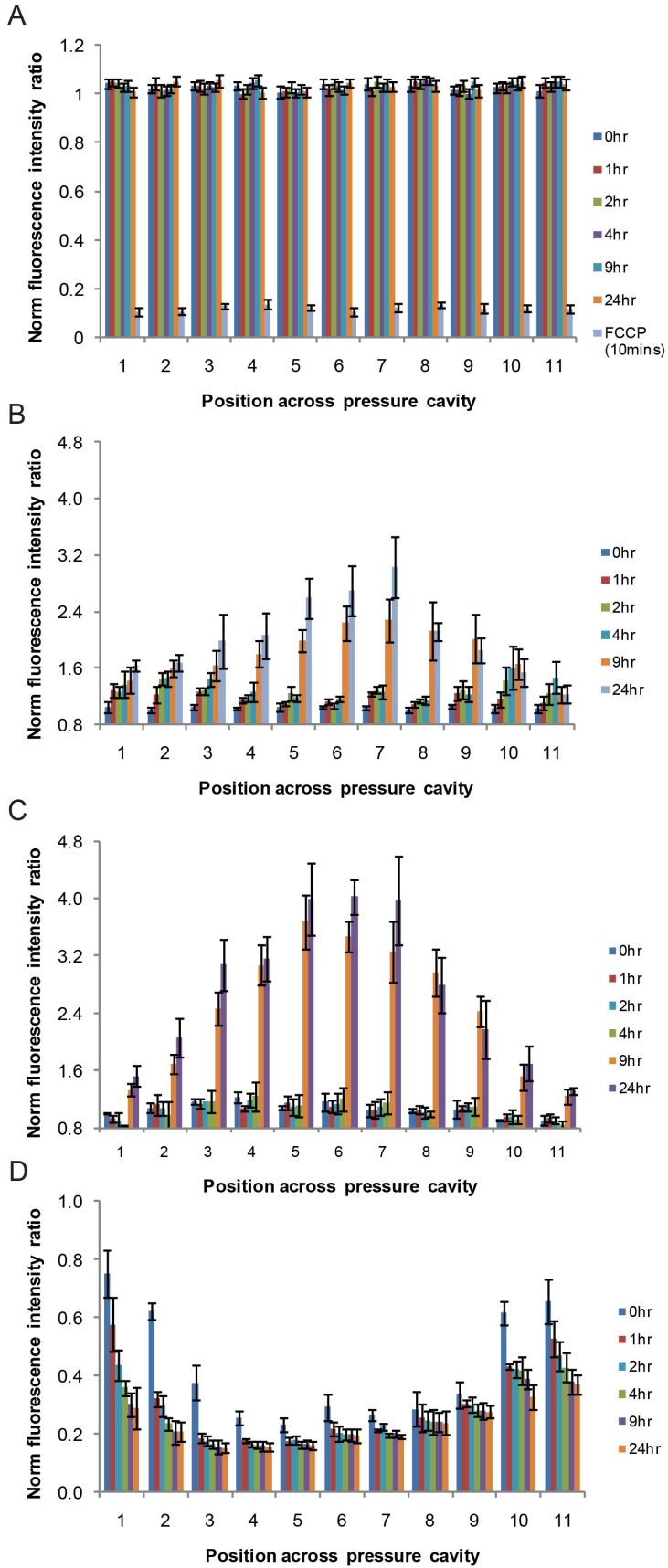


Figure 3.8. Monitoring mitochondrial membrane potential changes over a 24hr period through the use of the JC-1 dye. Mitochondrial membrane potential changes are normalized to their potential before injury and assessed at 11 discrete sections along the axons and 6 time points, i.e. immediately following injury (0hr), 1hr, 2hrs, 4hrs, 9hrs and 24hrs post injury. A) Uninjured control and addition of FCCP (10mins). Changes in mitochondrial membrane potential after applying a uniaxial strain injury, B) 10% applied strain, C) 25% applied strain, and D) 45% applied strain.

3.3.7 Mitochondrial numbers

In addition to the JC-1 dye allowing us to observe changes in MMP, it also allows us to monitor mitochondrial numbers. What was interesting to note, was that there was an increase in the number of mitochondria observed for the 25% applied strain condition (Table 2). This was the only condition that a significant increase in the number of mitochondria was observed as compared to before injury. As shown in the table, a 2.1 fold increase in the number was observed in the central portion (Positions 4-7) of the device with small increases towards the two outer edges (Positions 1 and 11), with only the outer edges being significant as compared to the central region.

Table 2. Increase in the number of mitochondria by 24hrs after 25% applied strain as compared to before injury. All positions were significant as compared to before injury, and positions 1,2 and 11 are significant compared to positions 4-7, $P < 0.05$

Position across pressure cavity											
	1	2	3	4	5	6	7	8	9	10	11
Fold increase	*	*									*
	3.9±0.5	3.1±0.4	2.8±0.5	2.1±0.4	2.2±0.4	2.1±0.4	2.4±0.3	2.4±0.6	2.4±0.7	2.8±0.5	3.3±0.5

3.3.8 Addition of EIPA and CsA

The mitochondrial membrane potential (MMP) that exists across the mitochondrial inner-membrane controls ATP synthesis, mitochondrial calcium buffering, the generation of reactive oxygen species (ROS), and opening of the mitochondrial permeability transition pore (mPTP), all fundamental processes during normal mitochondrial function (Nicholls and Budd 2000).

Disrupting any one of these functions can lead to cell death. With mitochondria playing a significant role in cell death determination, we looked towards mechanisms that could maintain their integrity following injury. Sodium-hydrogen exchange (NHE1) inhibitors have been shown to reduce the influx of calcium into mitochondria, inhibit the mPTP and preserve the MMP after injury (Teshima, Akao et al. 2003; Toda, Kadono et al. 2007). We applied the NHE1 inhibitor ethylisopropyl amiloride (EIPA) in this study and its effect on MMP was evaluated (Figure 3.9). The effects of EIPA were compared to the well studied mPTP inhibitor cyclosporine A (CsA) (Figure 3.10).

Figure 3.9 shows the MMP response to three applied uniaxial strains of 10%, 25% and 45%. When a 10% strain is applied we see an initial increase in membrane potential immediately following injury in the central region (positions 4-9) (Fig 3.9A). This membrane potential again peaks in the central region corresponding to the region in which maximal strain is experienced. This increase continues to increase over time reaching a maximum at 24hrs. The maximal MMP is however significantly lower than that observed in non-treated conditions (Fig 3.8B). When a 25% strain is applied we again observe an initial increase in MMP immediately following injury in the central region (positions 4-9). There are incremental increases to 4hrs post injury where there is a large increase by 9hrs post injury and a leveling off by 24hrs post injury. The maximal increase in membrane potential, i.e. in the central region, is again significantly less than that observed in non-treated conditions (Fig 3.8C). When a 45% strain is applied, we observe no significant change in membrane potential immediately following injury (Fig 3.9C). This is dramatically different to the large drop off in membrane potential seen in non-treated conditions

(Fig 3.8D). By 1hr post injury there is a decrease in membrane potential, with a steady drop off over a 24hr period.

We have shown that exposure to EIPA results in a reduction in both the amount of MMP hyperpolarization at lower applied strains (10% and 25%) and the amount of MMP depolarization observed at 45% applied strain.

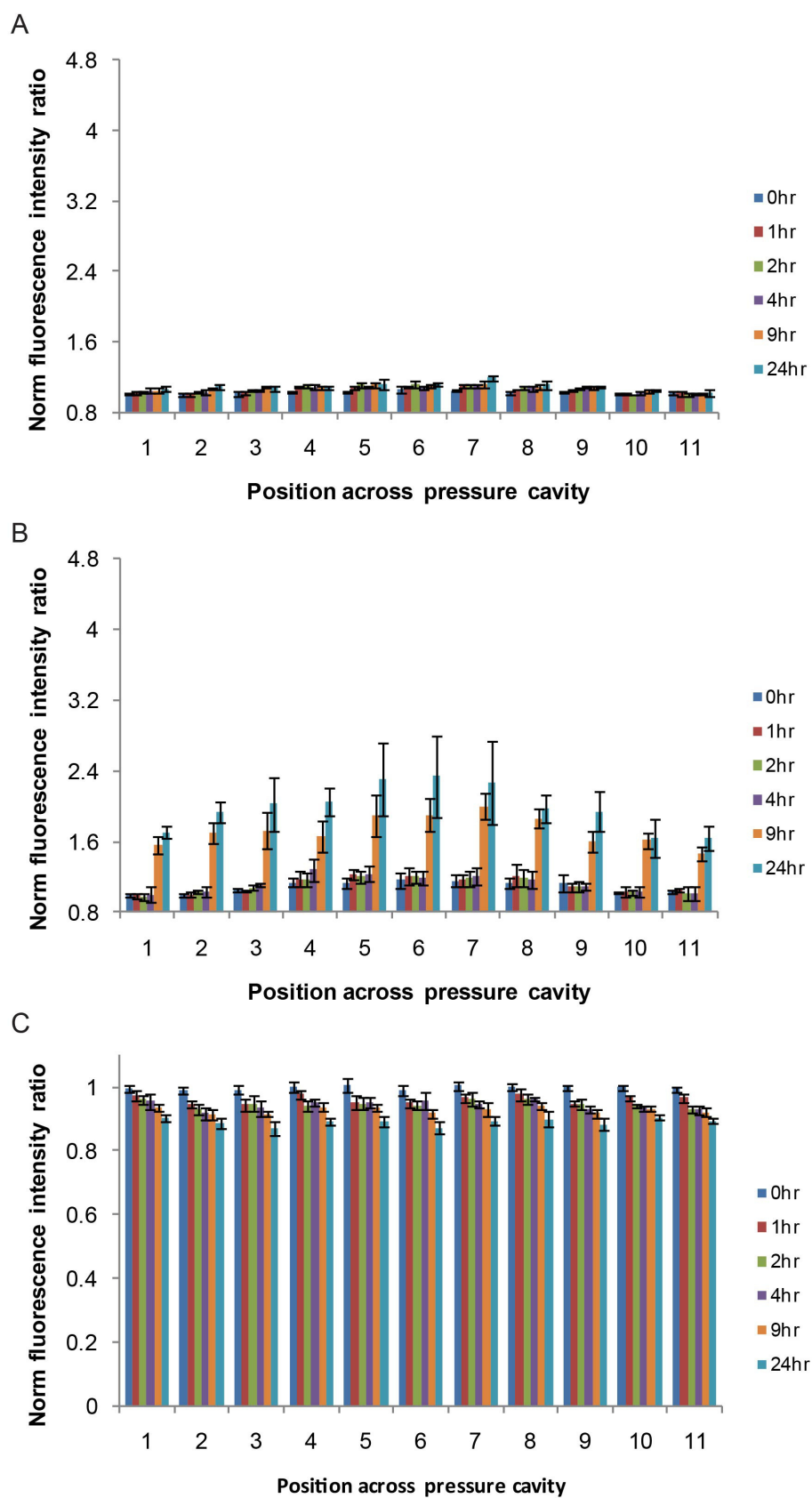


Figure 3.9. Monitoring mitochondrial membrane potential changes over a 24hr period after applying the NHE-1 inhibitor EIPA and a uniaxial strain injury. Mitochondrial membrane potential changes are normalized to their potential before injury and assessed at 11 discrete sections along the axons and 6 time points, i.e. immediately following injury (0hr), 1hr, 2hrs, 4hrs, 9hrs and 24hrs post injury. A) 10% applied strain, B) 25% applied strain, and C) 45% applied strain.

We wanted to compare the novel use of EIPA against another therapeutic that attenuates mitochondrial dysfunction. We thus applied the mPTP inhibitor cyclosporin A (CsA) that is currently in late stage clinical trials, to our cultures (Sullivan, Sebastian et al. 2011).

The mPTP is calcium activated, highly regulated, and is responsible for allowing the release of non-specific solutes of less than 1500Da in molecular weight some of which are attributed to initiating cell death (Lifshitz, Sullivan et al. 2004). We applied CsA prior to injury and monitored changes in MMP. Figure 3.10 shows the MMP responses to three applied uniaxial strains, 10%, 25% and 45% after application of CsA. When a 10% strain is applied we observe a slight decrease in membrane potential at the two outer regions of the pressure cavity (positions 1-2 and 10-11) rising to a slight peak around the central region (positions 3-9) slightly above the original membrane potential (Fig 3.10A). These values steadily decrease over a 24hr period. Around the central region these final values are slightly below original membrane potentials, whereas at the two ends of the pressure cavity we observe more of a decrease in membrane potential. The peak values around the central region are significantly less than those seen in the EIPA treated and non-treated conditions (Fig 3.9A and 3.8B). When a 25% strain is applied we observe an initial increase in membrane potential immediately following injury with a peak in the central portion of the cavity (Fig 3.10B). Thereafter the membrane potential steadily decreases until 4hr post injury however by 9hrs post injury we see an increase in membrane potential back to values seen immediately following injury. By 24hrs post injury, there is generally a further increase in membrane potential although not significantly. The maximum membrane potentials observed are significantly less than those for EIPA treated and non-treated conditions (Fig 3.9B and 3.8C).

When a 45% strain is applied, we observe a decrease in membrane potential immediately following injury that is significantly lower than membrane potentials prior to injury (Fig 3.10C). This initial decrease in membrane potential peaks in the central region corresponding to maximal applied strain (positions 4-7). This decrease is significantly less than that observed in the non-treated condition but significantly more than that for the EIPA treated condition (Fig 3.9C and 3.8D). There is generally a steady decrease in membrane potential over the 24hr period with the final values being similar to those observed for the EIPA treated condition however significantly higher than those observed for the non-treated condition.

We have shown that the exposure to CsA results in a MMP that initially hyperpolarizes and then steadily depolarizes over 24hrs at lower applied strains (10% and 25%) and a decrease in the amount of depolarization observed at 45% applied strain.

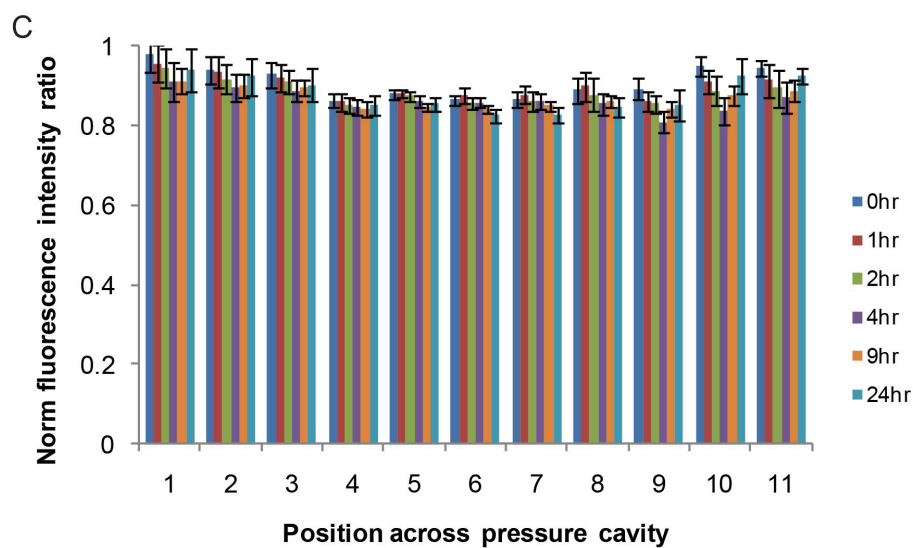
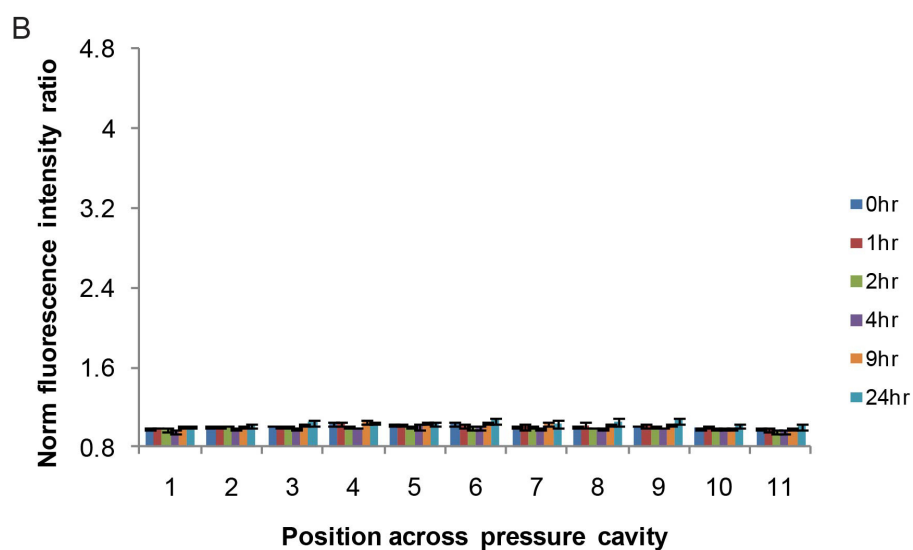
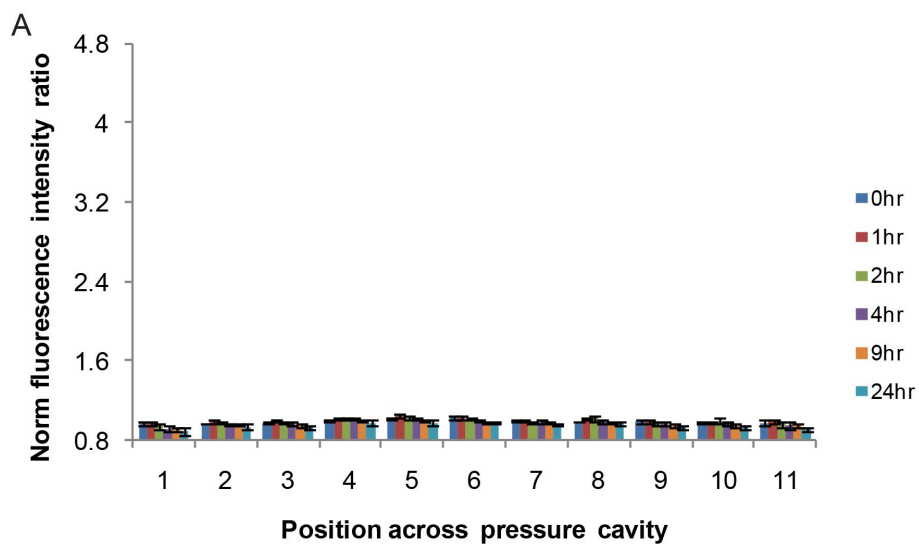


Figure 3.10. Monitoring mitochondrial membrane potential changes over a 24hr period after applying the mPTP inhibitor Cyclosporin A and a uniaxial strain injury. Mitochondrial membrane potential changes are normalized to their potential before injury and assessed at 11 discrete sections along the axons and 6 time points, i.e. immediately following injury (0hr), 1hr, 2hrs, 4hrs, 9hrs and 24hrs post injury. A) 10% applied strain, B) 25% applied strain, and C) 45% applied strain.

The ultimate assessment of treating uniaxially strained axons with EIPA and CsA are observing what effects they have on axonal degradation. As before, axonal degradation is assessed at 24hrs post injury for all three applied strains (Figure 3.11). For the 10% applied strain we observe no significant change in degradation from both the EIPA and CsA treated conditions. However for both the 25% and 45% applied strain conditions, we observe significant decreases in axonal degradation for both the EIPA and CsA treated conditions, but no significance between the EIPA and CsA treated conditions.

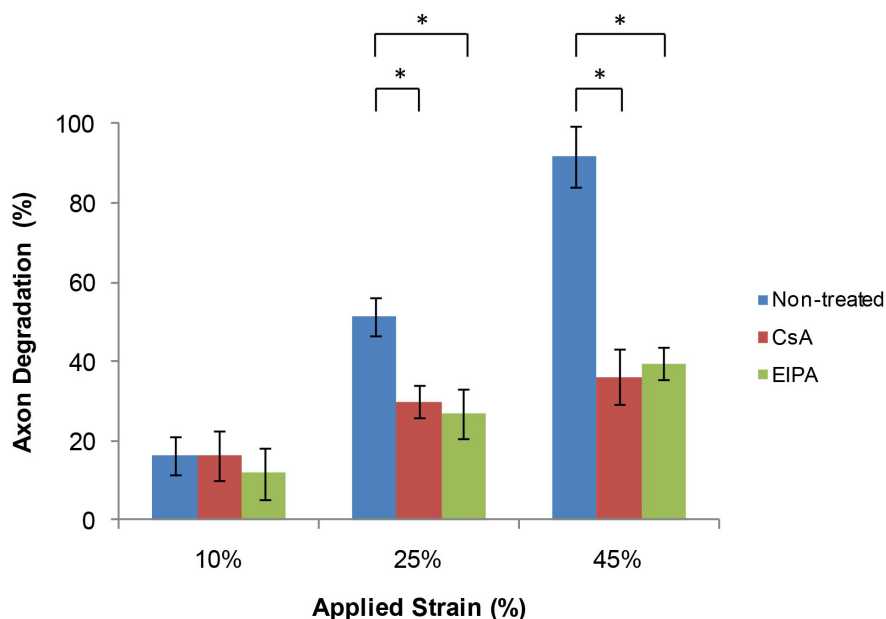








Figure 3.11. Axonal degradation assessed at 24hrs post injury after treatment with EIPA and cyclosporine A. Degradation is assessed for three uniaxial strains, i.e. 10%, 25% and 45%.

* $P < 0.05$.

An overall summary of the changes in axonal response to strain injury are shown in Table 3.

Table 3. Summary of axonal response to 10%, 25% and 45% applied strain injuries. +

denotes varying levels of increase in a parameter, — denotes varying levels of decrease in a parameter, 0 denotes no change and line shapes denote the slope of a change in parameter.

		10%	25%	45%
Beading	overall	+	++	+++
	diameter dependence			
DE	overall	+	++	+++
	diameter dependence			
β-tubulin degradation/accumulation		+	++	+++
APP accumulation		+	++	+++
Axonal degradation		+	++	+++
JC-1	MMP monitoring	++	+++	— — —
	mitochondrial # increase	0	++	0
	Effects of EIPA on MMP	—	—	— —
	Effects of CsA on MMP	—	—	— —
Axonal degradation after EIPA / CsA		0	—	— —

3.4 Discussion

We have shown that after the application of a uniaxial strain injury there are a number of parameters that affect an axons response to injury. Looking at two of the classic physical responses to strain injury of axonal beading and delayed elasticity we observe that they are both strain and diameter dependant. As applied strain is increased there is a corresponding increase in the number of beads that occur and transient increase in axonal length. An increase in diameter results in a decrease in the number of beads occurring along the axon length for all three applied strains. On the other hand an increase in diameter results in a transient increase in length and increase in the number of oscillations along the length of the injured axon. We next delved into a few of the molecular events that may play a role in axonal beading, namely strain effects on microtubules and axonal transport. We found that a breakdown in microtubules was dependant on both the amount of applied strain and the time after injury, i.e. increases were observed for both. This cytoskeletal breakdown resulted in a buildup of axonal transport products in the form of localized concentrations of APP at axonal beadings and an increase in the distance between APP containing vesicles. The ultimate result of this injury effects is axonal degradation which is seen to increase as applied strain is increased. The effect of strain injury on mitochondrial membrane function was investigated and found that a potential threshold exists between 25% and 45% strain that results in either a dramatic decrease in membrane potential (i.e. ~45%) or an increase in membrane potential (i.e. below 45%). The addition of the NHE1 inhibitor resulted in mitigating the drop in membrane potential at higher strains but also inhibited the increase in membrane potential at lower strains. This was similarly seen with the addition of CsA, with both resulting in a decrease in overall axonal degradation at 25% and 45% applied strains.

Axonal beading is one of the first observable responses to injury and is due to a buildup in transport proteins owing to a breakdown in axonal cytoskeleton (Gentleman, Nash et al. 1993; Sievers, Platt et al. 2003; Tang-Schomer, Johnson et al. 2011). This response is observed both *in vivo* and *in vitro* (Sieg, Wahle et al. 1999; Smith 2000; Nakayama, Aoki et al. 2001; Kilinc, Gallo et al. 2008). Multiple beads are observed to form along the length of a given axon due to the fact that not all microtubules are damaged at the same point along an axon (Tang-Schomer, Patel et al. 2010). Our results show that as the degree of applied strain injury increases, there is almost an exponential increase in the number of axonal beadings that occur along the length of the axon. This relationship corresponds to both the APP accumulation and the axonal degradation at 24hrs post injury observed for the various strain injuries. These results are slightly less than half that seen in a fluid shear induced injury (45 dyn/cm^2 with 20 ms onset time at 1hr post injury) (Kilinc, Gallo et al. 2008). However in their injury model they observe pores forming in the plasma membrane following injury (for molecules $\geq 480\text{Da}$), whereas we do not (for molecules $\geq 622\text{Da}$ - data not shown) demonstrating that the two injury models could be inherently different. Our permeability results are consistent with other uniaxial strain injury models (Smith, Wolf et al. 1999).

Not only does applied strain dictate axonal response to injury but the diameter of the axon or axonal bundle seems to play a significant role in this response, i.e. as diameter increases the number of beads decreases. The number of microtubules found within an axon is dependent on the axon diameter, i.e. as the diameter of the axon increases so does the number of microtubules (Rochlin, Wickline et al. 1996). Therefore as the diameter of the axon or axon bundle increases there are more microtubules across which the load is distributed. Therefore a greater load distribution potentially results in

less microtubules being damaged during injury and consequently less beads forming. This would be true for any applied injury level.

The range of diameters observed in our model correlate with those detected *in vivo* in rat hippocampii (0.1 μ m – 2.8 μ m, with average below 1 μ m) (Wyss, Swanson et al. 1980), which could be either single axons (with varying diameters) or multiple axons bundling together. In addition to observing individual axons, we also observe axons forming bundles as they clearly come together near the start of a microchannel and proceeded to stay together for the duration of the channel. The fact that the average axon diameter is below 1 μ m implies that the diameters observed in our study were probably bundles of multiple axons. Bundle formation is prevalent in a number of regions within the brain that are frequently involved in TBI, such as: the corpus collosum, anterior commissure, corticospinal tract, optic nerve and the fornix-fimbria that connects the hippocampus with the cortex (Westrum and Blackstad 1962; Tate and Bigler 2000; Meythaler, Peduzzi et al. 2001; Chen, Sun et al. 2004; Wilde, Bigler et al. 2006; Matsukawa, Shinoda et al. 2011; Wang, Hamm et al. 2011). *In vivo* studies using a fluid percussion injury model have shown that small caliber and unmyelinated axons can be even more susceptible to TBI, particularly from a functional point of view, than larger caliber and myelinated axons, i.e. electrophysiologically (Reeves, Phillips et al. 2005).

The viscoelastic response of axons to strain injury (commonly referred to as “delayed elastic effect”) is hypothesized to be due to the breakdown and subsequent misalignment in microtubules following injury (Smith, Wolf et al. 1999; Tang-Schomer, Patel et al. 2010). Misalignment within the bundle results in them not being able to slide freely over one another thus delaying the typical elastic response observed during

normal brain accelerations (Tang-Schomer, Patel et al. 2010). When this response is quantified we observe an increase that corresponds to the applied strain. There is however a large shift in axon length increase between 25% and 45% applied strain which may correspond to the threshold observed when changes in MMP are monitored. This delayed increase in axon length may be activating mechanosensitive ion channels for longer periods thus further exacerbating pathological responses (Wolf, Stys et al. 2001; Hemphill, Dabiri et al. 2011).

An increase in the applied strain may result in potentially more microtubules being damaged and misaligned and resisting the return to the axon's original length. As mentioned above, the larger the diameter the more microtubules available to resist the load, potentially decreasing the number of damaged microtubules. However each axon is connected to an adjacent axon through potential integrin binding (Van Vactor 1998) so if microtubules in a particular axon are damaged and that axon undergoes the viscoelastic response observed then since it is bound to an adjacent axon it will affect both axons return to their original length. This resistive viscoelastic force seems to be fairly substantial since we and others observe that it takes ~50minutes for an axon to return to its original length (Smith, Wolf et al. 1999; Tang-Schomer, Patel et al. 2010). So if very few axons within a particular bundle are affected, it may have an effect on the whole bundle. This is assuming that the binding between axons is sound. However, if this binding is not very secure, then we observe in some cases "bundle unraveling" (although infrequently). This is where an axon (or multiple axons) within a bundle that may not have been securely bound to the rest of the bundle elastically returns to its original length whereas the rest of the bundle remains in the transient elongated length (Dolle, Morrison et al. 2012).

The increases in length observed in this study are larger than those observed using other injury models (Smith, Wolf et al. 1999; Tang-Schomer, Patel et al. 2010). In these models, the diameters of their axons were not explicitly stated, but from their published images, their axon diameters appear to be in the order of 0.6-1.0 μ m in diameter, i.e. single or small bundle axons. If that is the case, that brings our results slightly above theirs. In their model they state that they do not observe primary axotomy at strain levels below 65%, however in our model we observe primary axotomy occurring at 45% applied strain demonstrating differences in the models (Dolle, Morrison et al. 2012). The increase in length that we observe as diameter increases corresponds to the increase seen in the number of oscillations along the axon length. As expected, larger diameter bundles exhibit the viscoelastic response at higher applied strains, whereas a much narrower range of diameter is affected at 10% applied strain. Along sections of axon that we observe “delayed elasticity” we noticed an increase in the number of axonal beads forming. Thus the increase in applied strain, the number of axonal beads, the delayed elastic effect and the resulting axonal degradation all appear to correlate to each other.

When we investigated the molecular events that may account for the formation of axonal beading we found that through β -Tubulin immunostaining, strain injured axons show a progressive loss in microtubules with respect to time and applied strain. An interesting observation was that at 24hours after applying a strain of 10% there were spots of bright β -tubulin staining that were however not larger than the diameter of the axon as typically seen within a few hours following injury. This could be either a much delayed response to injury through the initiation of an axonal bead, or possibly a former axonal bead that has decreased in size. Tang-Schomer and colleagues observe complete microtubule

depolymerization, i.e. no “rescuing” of microtubules following injury, which implies that we are not observing a decrease in bead diameter. The delayed bead formation could be due to lipid peroxidation induced microtubule degradation (which will be discussed later).

This breakdown in microtubules was confirmed with immunostaining for APP. APP is used as a tool in detecting axonal injuries due to the fact that it is transported in vesicles by fast anterograde axonal transport and therefore accumulates at points of transport disruptions (Leclercq, Stephenson et al. 2002). APP accumulations have been detected in humans as early as 2 hours following injury (McKenzie, McLellan et al. 1996).

Axonal beading is a characteristic of axonal degradation (Koike, Yang et al. 2008). The onset of axon degradation has been observed to occur within 24 hours in young rats and several days in humans following injury (Miledi and Slater 1970; Lubinska 1977; Chaudhry, Glass et al. 1992). The classical first stages of degradation include the breakdown of the cytoskeleton due to a trauma (as in our case), the activation of calpain or both (Vargas and Barres 2007; Vosler, Brennan et al. 2008). Calpain (calcium dependant proteases with papain-like activity) activation results in the cleavage of many proteins, in particular α -spectrin (cytoskeletal protein) and activation of mitochondrial-associated apoptosis pathways (Vosler, Brennan et al. 2008). This activation has been shown to occur within 15-30 minutes after injury resulting in rapid axonal degradation (Buki, Okonkwo et al. 2000). Axonal fragmentation is observed in acute axonal degeneration that occurs in a relatively short period of time (Kerschensteiner, Schwab et al. 2005). The majority of the degradation observed in our model occurs within 24 hours after strain injury, and is consistent with other similar models (Tang-Schomer, Patel et al.

2010). The extent of degradation observed in this study correlate to microtubule breakdown and APP accumulation.

As we have shown, the diameter of the axon / bundle has a major influence on its response to an applied strain injury and therefore influences the degree of axonal degradation. As the diameter increases, we observe acceleration in the time it takes for axonal degradation to occur. An example of this, is at diameters less than $\sim 1.4\mu\text{m}$ the majority of axonal degradation takes 24hrs, however in diameters larger than $\sim 1.4\mu\text{m}$, the majority of axonal degradation occurs within 4hrs, i.e. after a 45% strain injury (data not shown). This may be a reason why it is rare to find bundles of more than 6 individual axons in the hippocampus (Westrum and Blackstad 1962).

In order to better characterize the response of an axon to an applied strain, we investigated the effects on mitochondrial function. One of the reasons why we looked specifically at mitochondria is due to the fact that changes in the health of a cell can generally be assessed by observing changes in mitochondrial function (Mazzeo, Beat et al. 2009; Perry, Norman et al. 2011). The MMP that exists across the mitochondrial inner-membrane controls ATP synthesis, mitochondrial calcium buffering and the generation of ROS, all fundamental processes during normal mitochondrial function (Nicholls and Budd 2000). Disrupting any one of these functions can lead to cell death. Thus monitoring MMP is a key indicator of mitochondrial function and can be used to assess potential mechanisms that play a role in axonal degradation (Perry, Norman et al. 2011). Disruptions in the MMP could be in the form of either a decrease (depolarization – reduction in ATP and opening of the mPTP) or increase (hyperpolarization – generation of ROS) in potential both of which can lead to

detrimental effects on the cell (Sullivan, Thompson et al. 1999; Poppe, Reimertz et al. 2001). Low ATP levels can initiate necrosis, opening of the mPTP can initiate apoptosis and excessive ROS generation can lead to damage of lipids, proteins, DNA and membranes.

It appears that there is an applied strain threshold ($25\% < \text{threshold} < 45\%$), below which there is a delayed MMP hyperpolarization and above which an immediate and sustained depolarization. Immediately following injury there is no significant change in MMP for applied strains below the threshold however above the threshold we observe MMP depolarization almost to the level seen after application of the uncoupler FCCP. This initial response threshold to strain injury is similar to results seen in an *in vitro* biaxial strain injury model where no change in MMP was observed for mild (31% strain) and moderate (38% strain) injuries, however a severe injury (54% strain) resulted in a significant (32%) decrease in MMP by 15mins and maintained over 24hours (Ahmed, Rzigalinski et al. 2000). The decrease in membrane potential was not quite as dramatic as observed in our model, however their model employs dissociated embryonic day17 neurons that cover an elastic substrate and the *whole-cell* MMP was measured.

Observing whole-cell MMPs may be misleading due to the averaged values being derived from very different intensity distributions (Diaz, Setzu et al. 1999). Our model concentrates on observing individual mitochondrial changes within extended axons averaged over a short distance and therefore may be much larger. Decreases in MMP of $>60\%$ have been observed in astrocytes subjected to *in vitro* fluid percussion injury (Jayakumar, Rao et al. 2008). These initial MMP changes correspond to calcium threshold concentrations observed within mitochondria, which when exceeded, results in the collapse of the MMP and an opening of the mPTP (Bernardi and Petronilli 1996).

Large increases in intracellular calcium are observed immediately following uniaxial strain injury to neurons and is dependent on the degree of applied strain (Lusardi, Rangan et al. 2004).

The MMP hyperpolarization observed for strains below the threshold is maximum in the central region of the pressure cavity corresponding to the area of peak strains. One reason for the increase in MMP could be an increase in ATP production in response to injury. Endothelial cells exposed to a shear stress of 10dynes/cm² exhibit a 30% increase in MMP with a corresponding 70% increase in intracellular ATP (Kudo, Morigaki et al. 2000). ATP is not only used in cellular metabolism but as a signaling molecule where its release into the extracellular space has been shown to stimulate surrounding astrocytes to restore function (Rathbone, Middlemiss et al. 1999) and activate microglia to mediate inflammatory responses (Fields and Stevens 2000). However this does not necessarily imply that there is an increase in production, but could rather be a release in current stores of intracellular ATP.

In a biaxial strain injury model it was shown that at mild, moderate and severe biaxial strains, no change in ATP levels were observed, even though at the severe strain injury level there was a significant decrease in MMP (Ahmed, Rzigalinski et al. 2000). This demonstrates that the reasons for observing increases in MMP may vary for different cell types and that this increase is not synonymous with enhanced mitochondrial activity, i.e. ATP synthesis (Diaz, Setzu et al. 1999; Xu, Wang et al. 2001). In contrast, isolated brain mitochondria show a modest depolarization in MMP when ATP production is increased (Komary, Tretter et al. 2010).

Another more likely reason for observing increases in MMP is due to the inhibition of electron transport machinery. These could include the Inhibition of F_0F_1 -ATPase or adenine nucleotide translocase (ANT) (Komary, Tretter et al. 2010). Inhibition of F_0F_1 -ATPase results in a buildup of hydrogen ions in the mitochondrial inner-membrane space resulting in an increase in MMP (Suzuki, Ueno et al. 2002). In a cortical contusion model of traumatic brain injury, F_0F_1 ATPase was oxidized resulting in it being inactivated (Opii, Nukala et al. 2007). ANT is an ADP/ATP antiporter that exchanges ADP for ATP across the inner mitochondrial membrane (i.e. ADP^{3-} into the matrix and ATP^{4-} out normally reduces part of the electrochemical gradient) therefore inhibiting this function will result in an increase in the MMP (Belzacq, Vieira et al. 2003). A number of factors have been shown to inhibit ANT such as Bax (Belzacq, Vieira et al. 2003), which has been shown to increase in response to a controlled cortical impact (CCI) injury (Wennersten, Holmin et al. 2003) and calcium (inhibition of ANT appears to be calcium concentration dependant, i.e. only at lower pathological concentrations (Komary, Tretter et al. 2010)).

The MMP hyperpolarization-depolarization trend has been observed when isolated mitochondria from the cortex were exposed to various levels of calcium (Komary, Tretter et al. 2010). At low pathological levels of calcium a significant hyperpolarization is observed, whereas complete depolarization occurred at higher pathological calcium levels. Almost a two fold increase in MMP has been observed within 16 hours of rat hippocampal neurons being exposed to staurosporine (calcium dependant induction of cell death in neurons (Prehn, Jordan et al. 1997)), and similar to our results, a fourfold increase in MMP in D283 medulloblastoma cells within three hours (Poppe, Reimertz et

al. 2001). A fourfold increase in MMP would relate to an increase in $\sim 35\text{mV}$, i.e. using the Nernst equation for cationic indicators (Nicholls and Budd 2000).

In T-cells, epithelial cells, and neurons hyperpolarization can be an early indicator of apoptotic initiated cell death (Poppe, Reimertz et al. 2001; Gergely, Niland et al. 2002; Giovannini, Matarrese et al. 2002). However this mitochondrial initiated apoptosis would probably be independent of those requiring the opening of the mPTP due to the fact that this pore is inhibited by high concentrations of protons (Bernardi 1996). One of the end results of a high MMP is the production of ROS (Korshunov, Skulachev et al. 1997; Piacentini, Farrace et al. 2002). A two-fold increase in MMP resulted in a near two-fold increase in ROS in isolated brain mitochondria (Komary, Tretter et al. 2010). These ROS include superoxide (O_2^-) and hydrogen peroxide (H_2O_2) and have been shown to increase after TBI resulting in damage to lipids, proteins and nucleic acids (Lewen, Matz et al. 2000; Hall, Vaishnav et al. 2010). In a relatively short period of time oxidative stress has detrimental effects on both lipid membranes (within an hour) and nucleic acids (within 6hrs) (Ishihara, Minami et al. 2000; Deng, Thompson et al. 2007). Free radical induced membrane lipid peroxidation (LP) is particularly prevalent and hazardous in the central nervous system due to the high content of lipids that are susceptible to LP (Hall, Vaishnav et al. 2010). LP disrupts the normal architecture of the membrane making it more permeable to ions and inhibits both plasma-membrane and endoplasmic-reticulum Ca^{2+} -ATPase thereby decreasing calcium extrusion from the cytosol (Mattson 1998). In a CCI model of TBI, oxidative damage to the cytoskeleton was observed to peak at 24hrs post injury (Deng, Thompson et al. 2007). One of the end products of LP (4-hydroxynonenal – 4HNE) has also been shown to disrupt microtubules (Neely, Sidell et al. 1999). Thus LP could be another mechanism that results in some of the axonal

beading we observe, i.e. in addition to the initial strain induced primary injury (Roediger and Armati 2003; Kilinc, Gallo et al. 2009).

When we apply a 45% strain we observe almost complete depolarization within a relatively short period of time. Sufficiently high calcium concentrations within mitochondria have been shown to initiate the opening of the mPTP (Hansson, Mansson et al. 2004) that results in free passage of protons across the inner membrane leading to MMP depolarization (Leung and Halestrap 2008). MMP depolarization results in a decrease in ATP production as observed in a biaxial strain injury model (Geddes, LaPlaca et al. 2003). Necrosis induced cell death is very much ATP concentration dependant with >90% of cell death in low ATP cells attributed to necrosis (Leist, Single et al. 1997). Since we are observing axonal degradation occurring over a relatively short period of time (<24hrs), this probably excludes apoptosis as playing a significant role (Pike, Zhao et al. 2000).

We thus hypothesize that we may be observing a calcium concentration dependant effect on MMP where at relatively low levels of applied strain (10% and 25%) hyperpolarization occurs whereas at higher levels of applied strain (45%) depolarization occurs. We further hypothesize that MMP hyperpolarization is generating excessive amounts of ROS and that depolarization results in an opening of the mPTP and the initiation of necrotic and apoptotic pathways. Both of which may play a significant role in the axonal degeneration observed.

Using the MMP dye JC-1 we were able to detect changes in mitochondrial numbers along the length of axons. We observed a significant increase in the number of

mitochondria along the length of axons only when the intermediate 25% strain was applied. This could be due to a number of possible reasons: 1) it could be a buildup in mitochondria due to a breakdown in axonal transport (Maxwell 1996; Kilinc, Gallo et al. 2008). Since we observe a breakdown in microtubules this certainly could be a factor. 2) Mitochondrial biogenesis or fission. Due to the fact that it appears to take more than 24hrs for mitochondrial biogenesis to complete, this may not be what we are observing (Rasbach and Schnellmann 2007). Mitochondrial fission on the other hand seems to act on a much shorter time scale where a threefold increase in mitochondrial number was seen within 3hrs after an oxidative stress injury in axons due to hyperglycemia (Vincent, Edwards et al. 2010). 3) An injury response recruiting mitochondria to areas of injury. Axonal transport of mitochondria appears to be very much dependent on the calcium concentration within the cytoplasm (Chang, Niescier et al. 2011). At high levels of intracellular calcium, mitochondrial motility is severely inhibited. Thus the mitochondrial injury response may be a passive one, i.e. not initiated through activation of a specific signaling pathway but due to environmental conditions (elevated calcium concentrations) that immediately affect the motility of the mitochondria. This results in mitochondria stopping in areas of high calcium concentrations, i.e. areas where energy requirements are high and calcium buffering is needed. Mitochondrial transport is independent of matrix calcium concentration or the MMP (Yi, Weaver et al. 2004).

We suspect that it is a combination of mitochondrial fission and calcium dependant transport inhibition. The 10% applied strain injury is probably sufficiently low enough that it does not induce fission and the intracellular calcium concentration is probably not elevated enough to impede mitochondrial motility thereby maintaining a random number of mitochondria along the length of the axon. In the 45% applied strain condition we

observe significant MMP depolarization implying that sufficiently high calcium levels are probably being experienced which would result in motility being close to zero. If the mPTP opened, the outer membrane would probably have ruptured therefore making it difficult for mitochondrial fission to occur.

This strain injury device was used to not only better understand axonal responses to various strain injuries but was also used to test potential therapeutics that may reduce the devastating effects of DAI. This is particularly important due to the fact that there is still no reliable treatment protocol for TBI victims, despite the fact that over the last 25 years there have been over 20 agents that have reached phase III in clinical trials (Maas, Stocchetti et al. 2008). We suspected that the changes in MMP observed for the various applied strains was playing a significant role in the observed axonal degradation and thus looked at molecules that could attenuate these effects. The sodium-hydrogen exchanger (NHE) is a counter-transport system that couples the extrusion of protons to the influx of sodium (regulating cell pH and volume) (Masereel, Pochet et al. 2003). A byproduct of an influx of sodium into the cell is the activation of $\text{Na}^+/\text{Ca}^{2+}$ channels leading to an increase in intracellular calcium resulting in an increase in mitochondrial calcium. Thus inhibiting NHE-1 decreases both intracellular and mitochondrial calcium (Toda, Kadono et al. 2007) and lowering MMP by reducing the amount of protons entering the mitochondrial matrix (Ruiz-Meana, Garcia-Dorado et al. 2003). Certain NHE-1 inhibitors have also been shown to also inhibit mPTP opening. When EIPA (NHE-1 inhibitor) was added to our cultures before injury we observed a significant decrease in MMP hyperpolarization at 10% and 25% applied strains with significantly less depolarization at 45% applied strain.

We hypothesize that at 10% and 25% applied strains the addition of EIPA is resulting in a decrease in mitochondrial calcium and protons entering the matrix thus lowering the MMP and at 45% applied strain it is inhibiting opening of the mPTP thus decreasing MMP depolarization. We show that the addition of EIPA results in a significant reduction in axonal degradation revealing how considerable an effect reducing MMP hyperpolarization / depolarization can have on axonal degradation.

We believe this is the first time that EIPA / a NHE inhibitor has been used to reduce the effects of traumatic axonal injury. NHE inhibitors are currently being investigated for their effects on reducing epileptic seizures since higher intracellular pH inhibits neuronal excitability (Ali, Ahmad et al. 2008). TBI induced epilepsy is the most common form of acquired epilepsy with as many as 50% of severe TBI victims succumbing, NHE inhibitors could therefore have a dual function of inhibiting epileptogenesis and reducing axonal death. The current study has provided us with preliminary data on the effects of EIPA on DAI. We therefore plan to investigate the therapeutic window in which EIPA could be administered following a strain injury. With the delayed response in significant changes in MMP observed for lower strains we believe that a window does exist, however for higher strains, that remains to be seen.

We wanted to compare the results we observed with the addition of EIPA to a well known inhibitor of mitochondrial dysfunction, CsA. In addition to being a potent immunosuppressive, CsA inhibits the opening of the mPTP (Sullivan, Rabchevsky et al. 2005). The addition of CsA resulted in significant decrease in the amount of MMP hyperpolarization and depolarization as compared to non-treated conditions. CsA induced reduction in MMP hyperpolarization back to basal levels has been shown in

other injury models (Xu, Wang et al. 2001). This could be due to a combination of factors such as: 1) the fact that CsA has been shown to be a weak calcium ionophore which would result in an increase in intracellular calcium to levels high enough that could result in a slight MMP depolarization (Vereb, Panyi et al. 1990), 2) CsA inhibition of ANT (which is how it inhibits the mPTP) through CypD may interfere with the calcium dependant inhibition of ANT, and / or 3) mPTP has been shown to “flicker” open during normal conditions, thus CsA could be blocking calcium influx through the mPTP resulting in a decrease in overall mitochondrial calcium concentration. The well documented inhibition of mPTP would account for the decrease in MMP depolarization. EIPA appears to inhibit mPTP to similar levels as that of CsA, as we see slight differences at 24hrs between the two conditions. This level of mPTP inhibition has been observed using a similar NHE-1 inhibitor Cariporide (Villa-Abrille, Cingolani et al. 2011). So in addition to the benefit of potentially reducing intracellular calcium and matrix proton concentrations, EIPA appears to have a similar inhibitory effect on the mPTP within hippocampal axons as does CsA.

In summary, we have demonstrated that not only does the magnitude of an applied strain have an effect on the response to injury, so does the axon / bundle diameter. These diameter effects influence axonal beading, delayed elastic response and axonal degradation. At low applied strains, ROS generation, as a result of MMP hyperpolarization, may play a significant role in axonal degradation whereas at higher strains, opening of the mPTP may play a significant role. When these effects are partially inhibited by EIPA and CsA, the amount of axonal degradation is significantly reduced. The inhibitory effects of EIPA on axonal degradation highlight an additional potential therapeutic for traumatic axonal strain injury.

3.5 References:

- Ahmed, S. M., B. A. Rzigalinski, et al. (2000). "Stretch-induced injury alters mitochondrial membrane potential and cellular ATP in cultured astrocytes and neurons." J Neurochem **74**(5): 1951-1960.
- Ali, A., F. J. Ahmad, et al. (2008). "Seizures and sodium hydrogen exchangers: potential of sodium hydrogen exchanger inhibitors as novel anticonvulsants." CNS Neurol Disord Drug Targets **7**(4): 343-347.
- Belzacq, A. S., H. L. Vieira, et al. (2003). "Bcl-2 and Bax modulate adenine nucleotide translocase activity." Cancer Res **63**(2): 541-546.
- Berdichevsky, Y., H. Sabolek, et al. (2009). "Microfluidics and multielectrode array-compatible organotypic slice culture method." J Neurosci Methods **178**(1): 59-64.
- Bernardi, P. (1996). "The permeability transition pore. Control points of a cyclosporin A-sensitive mitochondrial channel involved in cell death." Biochim Biophys Acta **1275**(1-2): 5-9.
- Bernardi, P. and V. Petronilli (1996). "The permeability transition pore as a mitochondrial calcium release channel: a critical appraisal." J Bioenerg Biomembr **28**(2): 131-138.
- Blumbergs, P. C., G. Scott, et al. (1994). "Staining of amyloid precursor protein to study axonal damage in mild head injury." Lancet **344**(8929): 1055-1056.
- Buki, A., D. O. Okonkwo, et al. (2000). "Cytochrome c release and caspase activation in traumatic axonal injury." J Neurosci **20**(8): 2825-2834.
- Chang, K. T., R. F. Niescier, et al. (2011). "Mitochondrial matrix Ca²⁺ as an intrinsic signal regulating mitochondrial motility in axons." Proc Natl Acad Sci U S A **108**(37): 15456-15461.

- Chaudhry, V., J. D. Glass, et al. (1992). "Wallerian degeneration in peripheral nerve disease." Neurol Clin **10**(3): 613-627.
- Chen, Z. Y., C. Sun, et al. (2004). "Abnormal hippocampal axon bundling in EphB receptor mutant mice." J Neurosci **24**(10): 2366-2374.
- Coleman, M. (2005). "Axon degeneration mechanisms: commonality amid diversity." Nat Rev Neurosci **6**(11): 889-898.
- Coronado, V. G., L. Xu, et al. (2011). "Surveillance for traumatic brain injury-related deaths--United States, 1997-2007." MMWR Surveill Summ **60**(5): 1-32.
- Deng, Y., B. M. Thompson, et al. (2007). "Temporal relationship of peroxynitrite-induced oxidative damage, calpain-mediated cytoskeletal degradation and neurodegeneration after traumatic brain injury." Exp Neurol **205**(1): 154-165.
- Diaz, G., M. D. Setzu, et al. (1999). "Subcellular heterogeneity of mitochondrial membrane potential: relationship with organelle distribution and intercellular contacts in normal, hypoxic and apoptotic cells." J Cell Sci **112 (Pt 7)**: 1077-1084.
- Dolle, J. P., B. r. Morrison, et al. (2012). "Characterization of organotypic uniaxial strain injury model." in preparation.
- Fields, R. D. and B. Stevens (2000). "ATP: an extracellular signaling molecule between neurons and glia." Trends Neurosci **23**(12): 625-633.
- Geddes, D. M., M. C. LaPlaca, et al. (2003). "Susceptibility of hippocampal neurons to mechanically induced injury." Exp Neurol **184**(1): 420-427.
- Gennarelli, T. and D. Meaney (1996). "Mechanisms of primary head injury." In: Wiekens B, editor. Neurosurgery. Volume II II: 2611-2621.
- Gennarelli, T. A., L. E. Thibault, et al. (1989). "Axonal injury in the optic nerve: a model simulating diffuse axonal injury in the brain." J Neurosurg **71**(2): 244-253.

- Gentleman, S. M., M. J. Nash, et al. (1993). "Beta-amyloid precursor protein (beta APP) as a marker for axonal injury after head injury." Neurosci Lett **160**(2): 139-144.
- Gergely, P., Jr., B. Niland, et al. (2002). "Persistent mitochondrial hyperpolarization, increased reactive oxygen intermediate production, and cytoplasmic alkalinization characterize altered IL-10 signaling in patients with systemic lupus erythematosus." J Immunol **169**(2): 1092-1101.
- Giovannini, C., P. Matarrese, et al. (2002). "Mitochondria hyperpolarization is an early event in oxidized low-density lipoprotein-induced apoptosis in Caco-2 intestinal cells." FEBS Lett **523**(1-3): 200-206.
- Gittes, F., B. Mickey, et al. (1993). "Flexural rigidity of microtubules and actin filaments measured from thermal fluctuations in shape." J Cell Biol **120**(4): 923-934.
- Hall, E. D., R. A. Vaishnav, et al. (2010). "Antioxidant therapies for traumatic brain injury." Neurotherapeutics **7**(1): 51-61.
- Hansson, M. J., R. Mansson, et al. (2004). "Brain-derived respiring mitochondria exhibit homogeneous, complete and cyclosporin-sensitive permeability transition." J Neurochem **89**(3): 715-729.
- Hemphill, M. A., B. E. Dabiri, et al. (2011). "A possible role for integrin signaling in diffuse axonal injury." PLoS One **6**(7): e22899.
- Ishihara, I., Y. Minami, et al. (2000). "Activation of calpain precedes morphological alterations during hydrogen peroxide-induced apoptosis in neuronally differentiated mouse embryonal carcinoma P19 cell line." Neurosci Lett **279**(2): 97-100.
- Jayakumar, A. R., K. V. Rao, et al. (2008). "Trauma-induced cell swelling in cultured astrocytes." J Neuropathol Exp Neurol **67**(5): 417-427.

- Kerschensteiner, M., M. E. Schwab, et al. (2005). "In vivo imaging of axonal degeneration and regeneration in the injured spinal cord." Nat Med **11**(5): 572-577.
- Kilinc, D., G. Gallo, et al. (2008). "Mechanically-induced membrane poration causes axonal beading and localized cytoskeletal damage." Exp Neurol **212**(2): 422-430.
- Kilinc, D., G. Gallo, et al. (2009). "Mechanical membrane injury induces axonal beading through localized activation of calpain." Exp Neurol **219**(2): 553-561.
- Koike, T., Y. Yang, et al. (2008). "Axon & dendrite degeneration: its mechanisms and protective experimental paradigms." Neurochem Int **52**(4-5): 751-760.
- Komary, Z., L. Tretter, et al. (2010). "Membrane potential-related effect of calcium on reactive oxygen species generation in isolated brain mitochondria." Biochim Biophys Acta **1797**(6-7): 922-928.
- Korshunov, S. S., V. P. Skulachev, et al. (1997). "High protonic potential actuates a mechanism of production of reactive oxygen species in mitochondria." FEBS Lett **416**(1): 15-18.
- Kudo, S., R. Morigaki, et al. (2000). "Shear-stress effect on mitochondrial membrane potential and albumin uptake in cultured endothelial cells." Biochem Biophys Res Commun **270**(2): 616-621.
- Leclercq, P. D., M. S. Stephenson, et al. (2002). "Simple morphometry of axonal swellings cannot be used in isolation for dating lesions after traumatic brain injury." J Neurotrauma **19**(10): 1183-1192.
- Leist, M., B. Single, et al. (1997). "Intracellular adenosine triphosphate (ATP) concentration: a switch in the decision between apoptosis and necrosis." J Exp Med **185**(8): 1481-1486.

- Leung, A. W. and A. P. Halestrap (2008). "Recent progress in elucidating the molecular mechanism of the mitochondrial permeability transition pore." Biochim Biophys Acta **1777**(7-8): 946-952.
- Lewen, A., P. Matz, et al. (2000). "Free radical pathways in CNS injury." J Neurotrauma **17**(10): 871-890.
- Lifshitz, J., P. G. Sullivan, et al. (2004). "Mitochondrial damage and dysfunction in traumatic brain injury." Mitochondrion **4**(5-6): 705-713.
- Lubinska, L. (1977). "Early course of Wallerian degeneration in myelinated fibres of the rat phrenic nerve." Brain Res **130**(1): 47-63.
- Lusardi, T. A., J. Rangan, et al. (2004). "A device to study the initiation and propagation of calcium transients in cultured neurons after mechanical stretch." Ann Biomed Eng **32**(11): 1546-1558.
- Maas, A. I., N. Stocchetti, et al. (2008). "Moderate and severe traumatic brain injury in adults." Lancet Neurol **7**(8): 728-741.
- Margulies, S. S., L. E. Thibault, et al. (1990). "Physical model simulations of brain injury in the primate." J Biomech **23**(8): 823-836.
- Masereel, B., L. Pochet, et al. (2003). "An overview of inhibitors of Na(+)/H(+) exchanger." Eur J Med Chem **38**(6): 547-554.
- Matsukawa, H., M. Shinoda, et al. (2011). "Genu of corpus callosum as a prognostic factor in diffuse axonal injury." J Neurosurg **115**(5): 1019-1024.
- Mattson, M. P. (1998). "Modification of ion homeostasis by lipid peroxidation: roles in neuronal degeneration and adaptive plasticity." Trends Neurosci **21**(2): 53-57.
- Maxwell, W. L. (1996). "Histopathological changes at central nodes of Ranvier after stretch-injury." Microsc Res Tech **34**(6): 522-535.

- Mazzeo, A. T., A. Beat, et al. (2009). "The role of mitochondrial transition pore, and its modulation, in traumatic brain injury and delayed neurodegeneration after TBI." Exp Neurol **218**(2): 363-370.
- McKenzie, K. J., D. R. McLellan, et al. (1996). "Is beta-APP a marker of axonal damage in short-surviving head injury?" Acta Neuropathol **92**(6): 608-613.
- Meaney, D. F. and L. E. Thibault (1990). "Physical model studies of cortical brain deformation in response to high strain rate inertial loading." In: International Conference on the Biomechanics of Impacts. Lyon, France: IRCOBI: 215- 224.
- Meythaler, J. M., J. D. Peduzzi, et al. (2001). "Current concepts: diffuse axonal injury-associated traumatic brain injury." Arch Phys Med Rehabil **82**(10): 1461-1471.
- Miledi, R. and C. R. Slater (1970). "On the degeneration of rat neuromuscular junctions after nerve section." J Physiol **207**(2): 507-528.
- Morrison, B., 3rd, B. S. Elkin, et al. (2011). "In vitro models of traumatic brain injury." Annu Rev Biomed Eng **13**: 91-126.
- Morrison, B., 3rd, D. F. Meaney, et al. (1998). "Mechanical characterization of an in vitro device designed to quantitatively injure living brain tissue." Ann Biomed Eng **26**(3): 381-390.
- Muresan, Z. and V. Muresan (2005). "Coordinated transport of phosphorylated amyloid-beta precursor protein and c-Jun NH2-terminal kinase-interacting protein-1." J Cell Biol **171**(4): 615-625.
- Nakayama, Y., Y. Aoki, et al. (2001). "Studies on the mechanisms responsible for the formation of focal swellings on neuronal processes using a novel in vitro model of axonal injury." J Neurotrauma **18**(5): 545-554.

- Neely, M. D., K. R. Sidell, et al. (1999). "The lipid peroxidation product 4-hydroxynonenal inhibits neurite outgrowth, disrupts neuronal microtubules, and modifies cellular tubulin." J Neurochem **72**(6): 2323-2333.
- Nicholls, D. G. and S. L. Budd (2000). "Mitochondria and neuronal survival." Physiol Rev **80**(1): 315-360.
- Opii, W. O., V. N. Nukala, et al. (2007). "Proteomic identification of oxidized mitochondrial proteins following experimental traumatic brain injury." J Neurotrauma **24**(5): 772-789.
- Perry, S. W., J. P. Norman, et al. (2011). "Mitochondrial membrane potential probes and the proton gradient: a practical usage guide." Biotechniques **50**(2): 98-115.
- Piacentini, M., M. G. Farrace, et al. (2002). "Transglutaminase overexpression sensitizes neuronal cell lines to apoptosis by increasing mitochondrial membrane potential and cellular oxidative stress." J Neurochem **81**(5): 1061-1072.
- Pike, B. R., X. Zhao, et al. (2000). "Stretch injury causes calpain and caspase-3 activation and necrotic and apoptotic cell death in septo-hippocampal cell cultures." J Neurotrauma **17**(4): 283-298.
- Poppe, M., C. Reimertz, et al. (2001). "Dissipation of potassium and proton gradients inhibits mitochondrial hyperpolarization and cytochrome c release during neural apoptosis." J Neurosci **21**(13): 4551-4563.
- Povlishock, J. T. and C. W. Christman (1995). "The pathobiology of traumatically induced axonal injury in animals and humans: a review of current thoughts." J Neurotrauma **12**(4): 555-564.
- Prehn, J. H., J. Jordan, et al. (1997). "Ca²⁺ and reactive oxygen species in staurosporine-induced neuronal apoptosis." J Neurochem **68**(4): 1679-1685.

- Rasbach, K. A. and R. G. Schnellmann (2007). "Signaling of mitochondrial biogenesis following oxidant injury." J Biol Chem **282**(4): 2355-2362.
- Rathbone, M. P., P. J. Middlemiss, et al. (1999). "Trophic effects of purines in neurons and glial cells." Prog Neurobiol **59**(6): 663-690.
- Rochlin, M. W., K. M. Wickline, et al. (1996). "Microtubule stability decreases axon elongation but not axoplasm production." J Neurosci **16**(10): 3236-3246.
- Roediger, B. and P. J. Armati (2003). "Oxidative stress induces axonal beading in cultured human brain tissue." Neurobiol Dis **13**(3): 222-229.
- Ruiz-Meana, M., D. Garcia-Dorado, et al. (2003). "Cariporide preserves mitochondrial proton gradient and delays ATP depletion in cardiomyocytes during ischemic conditions." Am J Physiol Heart Circ Physiol **285**(3): H999-1006.
- Sieg, F., P. Wahle, et al. (1999). "Cellular reactivity to mechanical axonal injury in an organotypic in vitro model of neurotrauma." J Neurotrauma **16**(12): 1197-1213.
- Sievers, C., N. Platt, et al. (2003). "Neurites undergoing Wallerian degeneration show an apoptotic-like process with Annexin V positive staining and loss of mitochondrial membrane potential." Neurosci Res **46**(2): 161-169.
- Smith, D. H., X. H. Chen, et al. (1999). "Accumulation of amyloid beta and tau and the formation of neurofilament inclusions following diffuse brain injury in the pig." J Neuropathol Exp Neurol **58**(9): 982-992.
- Smith, D. H., Meaney, D.F (2000). "Axonal Damage in Traumatic Brain Injury." Neuroscientist **6**(6): 483-495.
- Smith, D. H., J. A. Wolf, et al. (1999). "High tolerance and delayed elastic response of cultured axons to dynamic stretch injury." J Neurosci **19**(11): 4263-4269.

- Sullivan, P. G., A. G. Rabchevsky, et al. (2005). "Mitochondrial permeability transition in CNS trauma: cause or effect of neuronal cell death?" J Neurosci Res **79**(1-2): 231-239.
- Sullivan, P. G., A. H. Sebastian, et al. (2011). "Therapeutic window analysis of the neuroprotective effects of cyclosporine A after traumatic brain injury." J Neurotrauma **28**(2): 311-318.
- Sullivan, P. G., M. B. Thompson, et al. (1999). "Cyclosporin A attenuates acute mitochondrial dysfunction following traumatic brain injury." Exp Neurol **160**(1): 226-234.
- Suzuki, T., H. Ueno, et al. (2002). "F(0) of ATP synthase is a rotary proton channel. Obligatory coupling of proton translocation with rotation of c-subunit ring." J Biol Chem **277**(15): 13281-13285.
- Tang-Schomer, M. D., V. E. Johnson, et al. (2011). "Partial interruption of axonal transport due to microtubule breakage accounts for the formation of periodic varicosities after traumatic axonal injury." Exp Neurol.
- Tang-Schomer, M. D., A. R. Patel, et al. (2010). "Mechanical breaking of microtubules in axons during dynamic stretch injury underlies delayed elasticity, microtubule disassembly, and axon degeneration." FASEB J **24**(5): 1401-1410.
- Tate, D. F. and E. D. Bigler (2000). "Fornix and hippocampal atrophy in traumatic brain injury." Learn Mem **7**(6): 442-446.
- Teshima, Y., M. Akao, et al. (2003). "Cariporide (HOE642), a selective Na⁺-H⁺ exchange inhibitor, inhibits the mitochondrial death pathway." Circulation **108**(18): 2275-2281.

- Toda, T., T. Kadono, et al. (2007). "Na⁺/H⁺ exchanger inhibitor cariporide attenuates the mitochondrial Ca²⁺ overload and PTP opening." Am J Physiol Heart Circ Physiol **293**(6): H3517-3523.
- Troyan, M. B., V. R. Gilman, et al. (1997). "Mitochondrial membrane potential changes in osteoblasts treated with parathyroid hormone and estradiol." Exp Cell Res **233**(2): 274-280.
- Van Vactor, D. (1998). "Adhesion and signaling in axonal fasciculation." Curr Opin Neurobiol **8**(1): 80-86.
- Vargas, M. E. and B. A. Barres (2007). "Why is Wallerian degeneration in the CNS so slow?" Annu Rev Neurosci **30**: 153-179.
- Vereb, G., Jr., G. Panyi, et al. (1990). "Effect of cyclosporin A on the membrane potential and Ca²⁺ level of human lymphoid cell lines and mouse thymocytes." Biochim Biophys Acta **1019**(2): 159-165.
- Villa-Abrille, M. C., E. Cingolani, et al. (2011). "Silencing of cardiac mitochondrial NHE1 prevents mitochondrial permeability transition pore opening." Am J Physiol Heart Circ Physiol **300**(4): H1237-1251.
- Vincent, A. M., J. L. Edwards, et al. (2010). "Mitochondrial biogenesis and fission in axons in cell culture and animal models of diabetic neuropathy." Acta Neuropathol **120**(4): 477-489.
- Vosler, P. S., C. S. Brennan, et al. (2008). "Calpain-mediated signaling mechanisms in neuronal injury and neurodegeneration." Mol Neurobiol **38**(1): 78-100.
- Wang, J., R. J. Hamm, et al. (2011). "Traumatic axonal injury in the optic nerve: evidence for axonal swelling, disconnection, dieback, and reorganization." J Neurotrauma **28**(7): 1185-1198.

- Wennersten, A., S. Holmin, et al. (2003). "Characterization of Bax and Bcl-2 in apoptosis after experimental traumatic brain injury in the rat." Acta Neuropathol **105**(3): 281-288.
- Westrum, L. E. and T. W. Blackstad (1962). "An electron microscopic study of the stratum radiatum of the rat hippocampus (regio superior, CA 1) with particular emphasis on synaptology." J Comp Neurol **119**: 281-309.
- Wilde, E. A., E. D. Bigler, et al. (2006). "Vulnerability of the anterior commissure in moderate to severe pediatric traumatic brain injury." J Child Neurol **21**(9): 769-776.
- Wolf, J. A., P. K. Stys, et al. (2001). "Traumatic axonal injury induces calcium influx modulated by tetrodotoxin-sensitive sodium channels." J Neurosci **21**(6): 1923-1930.
- Wyss, J. M., L. W. Swanson, et al. (1980). "The organization of the fimbria, dorsal fornix and ventral hippocampal commissure in the rat." Anat Embryol (Berl) **158**(3): 303-316.
- Xu, M., Y. Wang, et al. (2001). "Mitochondrial K(ATP) channel activation reduces anoxic injury by restoring mitochondrial membrane potential." Am J Physiol Heart Circ Physiol **281**(3): H1295-1303.
- Yi, M., D. Weaver, et al. (2004). "Control of mitochondrial motility and distribution by the calcium signal: a homeostatic circuit." J Cell Biol **167**(4): 661-672.

Chapter 4

4.1 Conclusions

Developing a more physiologically relevant model that maintains the three dimensional tissue architecture found in vivo with the ability of visualizing individual axons and their response to a uniaxial strain injury could prove to be a useful tool. This model was developed and characterized to produce accurate and reproducible strains and strain rates that are found to occur in typical traumatic brain injury events. Results obtained validated the fidelity of the model and were comparable to those seen in vivo and other in vitro injury models. We can conclude that: 1) the response to uniaxial strain is very much dependant on the axon / bundle diameter. The smaller the diameter the more beading along the length of axon and the less increase in length observed during delayed elastic events. 2) The response of microtubules to uniaxial strain is dependent on the applied strain and the applied strain field. The most microtubule degradation was observed in the region of peak strains and the least degradation in the regions of low strain. The higher the strain the more microtubule degradation and the more breakdown in axonal transport observed. 3) The amount of degradation corresponds to the degree of applied injury with an increase in degradation as applied strain injury increases. 4) The mitochondrial membrane potential response is proportional to the applied strain field. That is, the peak response is observed in the region of peak strain. 5) There is a threshold that exists in the response of axonal mitochondrial membrane potential with respect to the applied strain. Beyond the threshold immediate depolarization occurs and below which delayed hyperpolarization occurs. 6) Attenuating both mitochondrial membrane potential hyperpolarization and depolarization through the addition of cyclosporin A and the NHE-1 inhibitor EIPA, results in a significant decrease in axonal degradation. 7) Mitochondrial dysfunction plays a major role in axonal degradation

observed. 8) EIPA may have similar inhibitory effects on the mitochondrial permeability transition pore as cyclosporin A. 9) These results highlight EIPA as a potential new therapeutic for attenuating axonal degradation following strain injury.

4.2 Future Studies

We have successfully developed a device that is capable of generating uniaxial strains to axons that extend from the periphery of hippocampal organotypic slices that are maintained in culture for extended periods of time. With this model, researchers working in the field of traumatic brain injury will be able to monitor morphologic, molecular and functional changes in response to injury in real-time and long-term

We demonstrated that the response of an axon to a uniaxial strain injury is dependent on its diameter. We however did not confirm if the axon / bundles observed were individual large bore axons or bundles of small bore axons. This could be confirmed accomplished by fixing samples after injury and taking TEM images of cross sections through the axons.

We also demonstrated that at lower applied strains, hyperpolarization of the mitochondrial membrane potential occurs. We hypothesize that this is due to a calcium concentration dependent effect which inhibits the electron transport chain. Specific mechanisms for this hyperpolarization could be investigated.

The preliminary findings that we observed with the application of EIPA were using a single dose and applied before injury. A more detailed investigation determining the

optimal dose of EIPA and the optimal therapeutic window after injury should also be done.

The system could also be used to explore other known drugs to further test both the fidelity of the system as well as the potential mechanism of the drug action.

Although the current study was done using hippocampal slices obtained from rat pups, this could be extended to mouse pups thus opening up the world of transgenic mice and the vast array of molecular reporters that accompany them. In particular, the link between traumatic brain injury and neurodegenerative diseases such as Alzheimer's and epilepsy are gaining interest. With respect to Alzheimer's disease (AD), mitochondrial dysfunction appears to be an early event in the pathological progression of the disease (Hauptmann, Scherping et al. 2009). Our device could potentially be capable of monitoring mitochondrial changes in axons extending from transgenic AD slices. With respect to injury induced epilepsy, changes in action potential propagation following injury could elucidate potential therapeutics that could alleviate some of these problems. This would be done by incorporating multiple electrode arrays into the device, i.e. initially placing electrodes underneath the organotypic slices, and monitoring functional changes (Figure 4.1). Eventually electrodes could be placed within the microchannels and the action potentials within individual axons / bundles could be monitored (i.e. when stretchable electrodes are capable of withstanding large deformations).

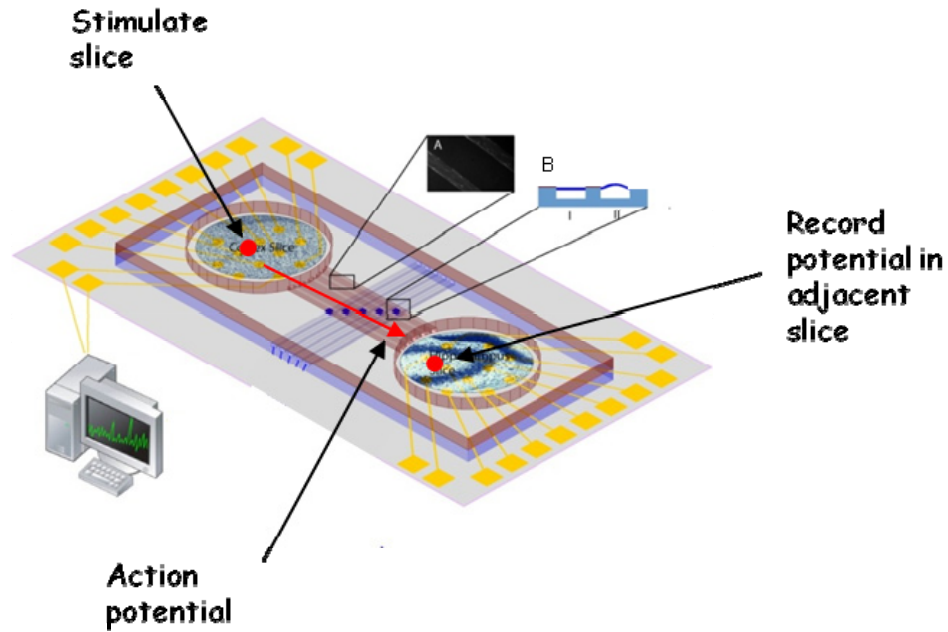


Figure 4.1. Schematic of a device incorporating multiple electrode arrays. The ability of axons to transmit action potentials are monitored electrophysiologically via an integrated multiple electrode array. A inset: Axons connecting two organotypic brain slices are guided by PDMS microchannels. B Inset: i) axons before injury, ii) axons during applied strain injury.

The current strain injury device monitors changes in unmyelinated axons extending from organotypic slices. This device could be modified to incorporate oligodendrocytes thus allowing axons to be myelinated and thus assessing the protective effects of myelin on strain injury (Figure 4.2).



Figure 4.2. Schematic of a potential device that allows for the incorporation of oligodendrocytes. A) Isometric view of proposed device showing different PDMS layers on a glass coverslip. B) Detailed view of central microchannel portion of the device, showing long channels connecting two mini-wells and oligodendrocyte inlet ports (channels and ports not to scale).